

A Reproduced Copy
OF

N83-36109

Reproduced for NASA

by the

NASA Scientific and Technical Information Facility

LIBRARY COPY

DEC 10 1986

LANGLEY RESEARCH CENTER
LIBRARY, NASA
HAMPTON, VIRGINIA



COLLEGE
ENGINEERING



POLYTECHNIC
INSTITUTE
STATE
UNIVERSITY



(NASA-TM-85429) CHARACTERISTICS OF THERMALLY-INDUCED TRANSVERSE CRACKS IN GRAPHITE EPOXY COMPOSITE LAMINATES (NASA)
139 p HC A07/MF A01 CSCL 11D 63/24 15224
883-36109 Unclas

College of Engineering
Virginia Polytechnic Institute and State University
Blacksburg, VA 24061

VPI-E-83-23

June, 1983

Characteristics of Thermally-Induced
Transverse Cracks in Graphite-Epoxy
Composite Laminates

Daniel S. Adams¹

David E. Bowles²

Carl T. Herakovich³

Department of Engineering Science & Mechanics

Interim Report 33
The NASA-Virginia Tech Composites Program

NASA Cooperative Agreement NCC1-15

Prepared for: Environmental Effects Branch
National Aeronautics & Space Administration
Langley Research Center
Hampton, VA 23665

¹Graduate student

²Materials Engineer, Materials Division, NASA-Langley

³Professor of Engineering Science & Mechanics

BIBLIOGRAPHIC DATA SHEET		1. Report No. VPI-E-83-23	2.	3. Recipient's Accession No.	
4. Title and Subtitle				5. Report Date	
CHARACTERISTICS OF THERMALLY-INDUCED TRANSVERSE CRACKS IN GRAPHITE-EPOXY COMPOSITE LAMINATES				June 1983	
7. Author(s)				8. Performing Organization Rept. No.	
D. S. Adams, D. E. Bowles, C. T. Herakovich				VPI-E-83-23	
9. Performing Organization Name and Address				10. Project/Task/Work Unit No.	
Virginia Polytechnic Institute & State University Engineering Science & Mechanics Blacksburg, Virginia 24061				11. Contract/Grant No.	
				CA NCC1-15	
12. Sponsoring Organization Name and Address				13. Type of Report & Period Covered	
National Aeronautics & Space Administration Langley Research Center Hampton, Virginia 23665				14.	
15. Supplementary Notes					
16. Abstracts					
<p>The characteristics of thermally-induced transverse cracks in T300/5208 graphite-epoxy cross-ply and quasi-isotropic laminates were investigated both experimentally and analytically. The formation of transverse cracks and the subsequent crack spacing present during cool-down to -250°F (116K) and thermal cycling between 250 and -250°F (116 and 394K) was investigated. The state of stress in the vicinity of a transverse crack and the influence of transverse cracking on the laminate coefficient of thermal expansion (CTE) was predicted using a generalized plane strain finite element analysis and a modified shear-lag analysis.</p> <p>It is shown that a majority of the cross-ply laminates experienced transverse cracking during the initial cool-down to -250°F whereas the quasi-isotropic laminates remained uncracked. All cross-ply laminates and the [0/±45/90]_s quasi-isotropic laminate exhibited transverse cracking following 20 thermal cycles. The uniformity of crack spacing increased with an increasing number of thermal cycles. The cross-ply laminates exhibit a rather sharp drop in CTE at crack densities less than 50 cracks/in. (19.7 cracks/cm whereas the quasi-isotropic laminate exhibit a smaller decrease in CTE. The in situ transverse strength of the 90° layers was more than 1.9 times greater than the transverse strength of the unidirectional 90° material for all laminates investigated.</p>					
17. Key Words and Document Analysis. 17a. Descriptors					
composite materials, thermal stresses, damage, thermal expansion, finite elements, experiment, cryogenic					
17b. Identifiers/Open-Ended Terms					
17c. COSATI Field/Group					
18. Availability Statement				19. Security Class (This Report)	
Distribution Unlimited				UNCLASSIFIED	
				20. Security Class (This Page)	
				21. No. of Pages	
				124	
				22. Price	

ACKNOWLEDGEMENTS

This work was supported by the NASA-Virginia Tech Composites Program, NASA Cooperative Agreement NCC1-15. The authors wish to thank Professors Michael W. Hyer and J. N. Reddy for helpful discussions. A special thanks is extended to Ms. Connie Callison for typing this manuscript.

TABLE OF CONTENTS

	<u>Page</u>
ACKNOWLEDGEMENTS.....	iii
LIST OF TABLES.....	vi
LIST OF FIGURES.....	vii
 CHAPTER	
1. INTRODUCTION.....	1
2. LITERATURE REVIEW.....	4
2.1 Parameters Affecting Transverse Cracking Under Mechanical Loading.....	4
2.2 Thermally Induced Transverse Cracking.....	5
2.3 Thermal Cycling.....	7
2.4 Transverse Crack Spacing Theories.....	8
2.5 Prediction of Transverse Cracking Effects on the CTE.....	10
3. ANALYTICAL STUDIES.....	12
3.1 General Formulation.....	13
3.1.1 Assumptions.....	13
3.1.2 Temperature Dependence of Material Properties.....	16
3.1.3 In Situ Transverse Strength of 90° Layers.....	16
3.1.4 Failure Criteria for Transverse Cracking.....	18
3.1.5 Stress Free Temperature.....	18
3.2 Initiation of Transverse Cracks.....	19
3.2.1 Formulation.....	19
3.2.2 Determination of Crack Initiation Temperatures.....	22
3.3 Stresses in the Vicinity of a Transverse Crack.....	25
3.3.1 Finite Element Analysis.....	27
3.3.2 Modified Shear-Lag Analysis.....	33
3.3.3 Analysis of $[0_2/90_2]_5$ Laminate.....	41

3.4	Influence of Transverse Cracking on Laminate CTE.....	49
4.	EXPERIMENTAL PROGRAM.....	55
4.1	Material Specification.....	55
4.2	Specimen Preparation.....	56
4.3	Equipment.....	58
4.4	Initial Thermal Cycle Tests.....	62
4.5	Thermal Cycling Tests.....	64
5.	EXPERIMENTAL RESULTS AND OBSERVATIONS.....	65
5.1	Initial Thermal Cycle Test Results.....	67
5.2	Cyclic Thermal Test Results.....	78
5.2.1	Cross-Ply Laminates.....	78
5.2.2	Quasi-Isotropic Laminates.....	85
5.3	Correlation with Analytical Studies.....	85
5.3.1	Determination of In Situ Transverse Strength.....	85
5.3.2	Crack Spacing in $[0_2/90_2]_5$ Laminate.....	88
5.4	Observations.....	91
6.	CONCLUSIONS.....	96
	REFERENCES.....	98
	APPENDIX	
A	T300/5208 Graphite-Epoxy Properties.....	102
B	Constrained Displacement Finite Element Solutions.....	112
C	CLFE2DC Input Data Sequence.....	121

LIST OF TABLES

<u>Table</u>		<u>Page</u>
1	Fiber Volume of Test Panels.....	57
2	Temperature of Initial Transverse Cracking.....	68
3	Transverse Crack Density Versus Temperature.....	77
4	Transverse Crack Density Versus Number of Thermal Cycles..	79
A.1	Material Property Coefficients for T300/5208 Graphite-Epoxy.....	103

LIST OF FIGURES

<u>Figure</u>	<u>Page</u>
1 Transverse Cracking in a $[0/90_3]_s$ Laminate.....	2
2 Transverse Cracking in Cross-Ply Laminate Configurations.....	14
3 Transverse Cracking in Quasi-Isotropic Laminate Configurations.....	15
4 Laminate Geometry.....	20
5 Temperature of Initial Transverse Cracking in Cross-Ply Laminates as a Function of the In Situ Transverse Tensile Strength.....	24
6 Initial Equilibrium Crack Spacing Model.....	26
7 Boundary Conditions on Modeled Region for Determining Initial Equilibrium Transverse Crack Spacing.....	29
8 Modeled Region for Multiple Transverse Cracking.....	31
9 Three Crack Spacing Mesh for Confirming Boundary Conditions.....	32
10 272 Element x 306 Node Finite Element Mesh.....	34
11 Modified Shear-Lag Analysis Model.....	36
12 Free Body Diagram of 90° Layer for Modified Shear-Lag Analysis.....	37
13 σ_2 Stress in the 90° Layer of a $[0_2/90_2]_s$ Laminate in the Vicinity of a Transverse Crack.....	42
14 τ_{xy} Stress Along $0^\circ/90^\circ$ Interface ($\frac{z}{T} = 1.0$) in a $[0_2/90_2]_s$ Laminate in the Vicinity of a Transverse Crack.....	44
15 σ_2 Stress Gradients in 90° Layer of a $[0_2/90_2]_s$ Laminate in the Vicinity of a Transverse Crack.....	45
16 σ_2 Stress at Midplane Between Transverse Cracks ($y=B$) in $[0_2/90_2]_s$ Laminate.....	48
17 CTE as a Function of Crack Density in Cross-Ply Laminates.....	51

18	Percent Retention of CTE in Cross-Ply Laminates.....	52
19	Percent Retention of CTE in Quasi-Isotropic Laminates.....	53
20	Thermal Cycling Specimen.....	59
21	Experimental Equipment.....	60
22	Interior View of Environmental Chamber.....	61
23	Transverse Cracking in a $[0_2/90_2]_S$ Laminate.....	63
24	Outer 90° Layer Damage Present Prior to Testing in Quasi-Isotropic Laminates.....	66
25	Temperature of Initial Transverse Cracking in 90° Layer of $[0_n/90_m]_S$ Laminates.....	69
26	Temperature of Initial Transverse Cracking in 90° Layers of $[90_n/0_m]_S$ Laminates.....	70
27	Warping of $[90_3/0]_S$ Laminate Specimens 1, 2, and 3 Due to Thermal Loading.....	72
28	Transverse Cracking and Delamination in $[90_3/0]_S$ Laminate (Specimen 2).....	73
29	Fiber Breakage in Adjacent 0° Layer of $[90_3/0]_S$ Laminate (Specimen 2).....	74
30	Location of Test Specimens in $[0_2/90]_S$ and $[90_3/0]_S$ Laminate Panel.....	75
31	Cycle Thermal Test Results for $[0_n/90_m]_S$ Cross-Ply Laminates.....	80
32	Cyclic Thermal Test Results for $[90_n/0_m]_S$ Cross-Ply Laminates.....	82
33	Comparison of $[0_3/90]_S$ and $[90/0_3]_S$ Laminate Cyclic Thermal Test Results.....	83
34	In Situ Transverse Strength of 90° Layers in Cross-Ply Laminates.....	87
35	Transverse Cracking During Thermal Loading in $[0_2/90_2]_S$ Laminate.....	89

Chapter 1

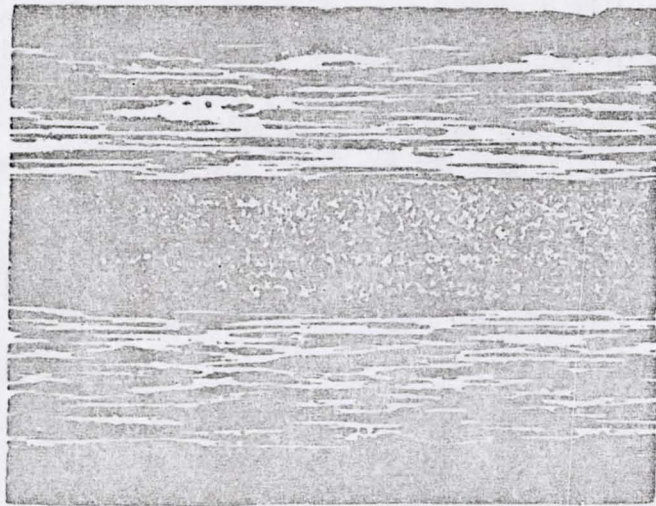
INTRODUCTION

Advanced composite materials are currently being considered for use in a number of applications where the dimensional stability of the structure is of primary importance. Such applications include several space structures: communication antennae, telescopes, solar reflectors, satellite power systems, and a space operations center. These materials are leading candidates due to their high specific stiffness and low coefficient of thermal expansion (CTE) in the fiber direction. Graphite fibers actually contract when heated (near room temperature) resulting in a small, negative CTE in the fiber direction of a unidirectional lamina. In contrast, the CTE perpendicular to the fibers is a rather large, positive value comparable to that of aluminum. The CTE of a composite laminate may be tailored by selecting the appropriate orientation of the individual layers of the laminate.

In the extremely cold space environment in which these materials are to be used, large thermal stresses may develop due to the mismatch in the CTE of adjacent plies at different orientations. When the in-plane normal stress, σ_2 , becomes sufficiently large, transverse cracks result. Such cracks run parallel to the fibers in planes approximately perpendicular to the midplane of the ply in which they occur, and form at quite even intervals (Fig. 1).

Although transverse cracking may not significantly alter the structural integrity of a laminate, the CTE may be changed enough to render the laminate unacceptable for dimensional stability critical applica-

ORIGINAL PAGE IS
OF POOR QUALITY



75X

Fig. 1. Transverse Cracking in a $[0/90_3]_s$ Laminate.

tions. Therefore, an understanding of transverse cracking effects on the laminate CTE is essential for such applications.

The purpose of this investigation was to study the characteristics of thermally-induced transverse cracks, both experimentally and analytically. Specific emphasis was placed on determining the state of stress in the vicinity of a transverse crack, the temperature at which transverse cracks form and the subsequent crack density present, the occurrence of additional transverse cracking under increased thermal load and thermal cycling, and the effects of transverse cracks on the laminate CTE.

Chapter 2

LITERATURE REVIEW

The presence of transverse cracking in composite laminates has been a topic of interest for several years. While many studies have focused on the parameters affecting the development of transverse cracking, only recently has its effects on laminate behavior received much attention. This chapter presents a brief review of studies involving transverse cracking in composite laminates.

2.1 Parameters Affecting Transverse Cracking Under Mechanical Loading

Although often assumed to be a ply failure, transverse cracking has been shown by Bailey and Parvizi [1] to initiate as localized debondings at the fiber-matrix interface in glass-epoxy laminates. Under increasing mechanical load, the debondings linked up to form tiny cracks a few fiber diameters in length. These in turn linked up to form transverse cracks. Bailey et al. [2] reported that for graphite-epoxy and glass-epoxy cross-ply laminates (i.e., laminates with fibers alternating between 0° and 90° orientations), formation of transverse cracks occurred instantaneously in thick transverse layers. In thinner transverse layers, however, tiny cracks formed, but did not propagate through the entire layer until higher strain levels were achieved or did not propagate at all prior to final failure. Several authors [3, 4, 5] have noted that transverse crack density increases with increasing transverse layer thickness. Bailey et al. [2] also reported the occurrence of interlaminar delaminations at the $0^\circ/90^\circ$ interface of glass-epoxy cross-

ply laminates. Such delaminations were found to occur after the onset of transverse cracking but prior to final fracture. They did not observe delaminations in graphite-epoxy cross-ply laminates. Crossman and Wang [5] studied $[\pm 25/90_n]$ graphite-epoxy laminates and found that transverse cracking was completely suppressed for transverse layer thicknesses of 0.010 in. (0.026 cm) and below (two plies). Interlaminar delaminations were the only form of damage present prior to final failure for these laminates. For transverse layers thicker than 0.021 in. (0.053 cm), or four plies, transverse cracking occurred first, followed by delamination. Parvizi et al. [6] found transverse cracking completely suppressed in glass-epoxy cross-ply laminates with a transverse layer thickness under 0.006 in. (0.015 cm), or one ply.

Reifsnider and Highsmith [7] observed that transverse crack spacing in graphite-epoxy laminates decreased with increasing strain until a particular characteristic spacing developed at which no further cracking occurred. Kriz et al. [8] concluded that this minimum crack spacing was independent of such factors as load history and environmental effects, but dependent only upon the lamina and laminate properties as well as the stacking sequence.

2.2 Thermally-Induced Transverse Cracking

In addition to mechanically applied loads, transverse cracking may result from pure thermal loading. Several authors [4, 9-13] have discussed the thermal stresses due to curing at elevated temperatures and factors affecting the magnitude of the residual stresses. Spain [9]

discussed several factors influencing thermally-induced cracking including resin shrinkage during cure, resin coefficient of thermal expansion, curing temperature, and ply orientation. Bowles [14] studied the effects of transverse cracks on the thermal response of quasi-isotropic graphite-epoxy laminates using mechanically cracked specimens. The laminate CTE was found to decrease with increasing crack density. A twenty-five percent decrease in CTE was reported at the highest crack density 52 cracks/in. (2.05 cracks/mm).

Mills et al. [4] studied transverse cracking in graphite-polyimide cross-ply and quasi-isotropic laminates under five types of thermal loading and room temperature tensile loading. It was determined that transverse crack density and the load to initiate transverse cracks are functions of the type of loading and the laminate configuration; cross-ply laminates were generally found to exhibit higher crack densities than quasi-isotropic laminates under thermal loading. Casswell [15] investigated transverse cracking due to thermal loading in graphite-epoxy cross-ply laminates. Transverse cracking was present in all laminates after the initial cool-down to -250°F (116K), the crack density increasing as the volume percentage of the transverse layer decreased from seventy-five to twenty-five percent. Since the thermal stresses in the transverse layer (at a given thermal load) increase as the volume percentage decreases, however, this result may not be attributed solely to transverse layer thickness. Under a cyclic type of thermal loading in which specimens were cooled in 25°F (14K) increments to -250°F (116K), but returned to room temperature for examination after

each cooling increment, transverse crack density was found to increase with increasing thermal load.

2.3 Thermal Cycling

Camahort et al. [16] thermally cycled unidirectional and $[0_4/\pm 40/\pm 70]_S$ (a low CTE configuration) graphite-epoxy specimens twenty-five times between -322 and 212°F (76 and 373K) to determine the effects on mechanical and thermal properties. Cyclic loading resulted in a six to thirteen percent decrease in the transverse tensile modulus, a very small increase in the transverse tensile strength and a significant decrease in the CTE of the $[0_4/\pm 40/\pm 70]_S$ laminate. The unidirectional laminate was affected very little by the cyclic loading. Fahmy and Cunningham [17] thermally cycled selected graphite-epoxy laminates between -58 and 302°F (223 and 423K). Mechanical and thermal properties were evaluated after 10, 100, 1000, and 5000 cycles. Cyclic loading was found to reduce the CTE by as much as one-third of its original value. Degradation of mechanical properties occurred largely in the first ten cycles. Berman [18] thermally cycled composite sandwich structures composed of G/70/934 graphite-epoxy laminates on aluminum honeycomb core between -250 and 150°F (116 and 339K). Transverse cracks were first reported after 50 cycles and increased in number until 3000 cycles, beyond which only widening of existing cracks occurred. Tensile and flexural properties remained virtually unchanged after 15,000 cycles. The laminate CTE, however, decreased significantly, mainly in the first 3,000 cycles.

Although all three studies [16-18] investigated the influence of thermal cycling on the mechanical and thermal laminate properties, none correlated these results with the amount of transverse cracking present.

2.4 Transverse Crack Spacing Theories

A transverse crack spacing theory for cross-ply laminates using a modified shear-lag analysis was developed by Garrett and Bailey [3] and improved by Parvizi and Bailey [19]. In this theory, a linear elastic laminate analysis is used to predict the first transverse crack formed under tensile loading. When the transverse ply cracks, the load it carried is transferred to the adjacent longitudinal plies at the plane of the crack. The theory assumes that load is transferred back into the transverse ply via shear stress at an exponentially decreasing rate while moving away from the crack. A maximum stress theory is used to predict failure. An envelope of permissible crack spacings based on a random position of the first crack and a specimen of any given length is predicted as a function of applied stress. A comparison of experimental results with theoretical predictions for graphite-epoxy cross-ply laminates by Bailey et al. [2] showed good correlation. Parvizi and Bailey [19] reported an even better correlation with glass-epoxy cross-ply laminates. Neither study included the residual thermal stresses due to cooling when predicting crack spacing. Mills et al. [4] applied the same theory to graphite-polyimide cross-ply laminates and extended the theory for use with quasi-isotropic laminates. Residual stresses were

predicted with laminate analysis using stress and temperature dependent material properties. Residual stress was added to mechanically applied stress when plotting the experimental results. The correlation reported for quasi-isotropic laminates was somewhat better than for cross-ply laminates. Plunkett [20], using data from Ref. [19], reported that the modified shear lag analysis predicts crack density well for thicker transverse layers e.g., 0.16 in. (0.4 cm), but begins to over predict crack density as the transverse layer thickness decreases.

Stevens and Lupton [21] proposed a theory based on the assumption that crack spacing is inversely proportional to applied stress. The correlation with experimental data for glass-epoxy cross-ply laminates was quite good. Parvizi and Bailey [19] noted a similar correlation, also for glass-epoxy cross-ply laminates, but only over an intermediate range of crack spacing. They also noted that the modified shear-lag analysis predicts such an inverse proportionality over an intermediate range of crack spacing.

Wang and Crossman [22] and Crossman et al. [23] extended the energy release rate theory of Rybicki et al. [24] to predict transverse cracking. For a given laminate, a nondimensional available strain energy release rate function is determined. This function is reported to be quite complicated, being dependent on the crack location and geometry, stacking sequence, lamina properties and thicknesses, and applied loads [23]. Both studies used the finite element method with a crack closure procedure to calculate the available strain energy release rate function. This procedure involves extending a crack by a small, finite

amount and computing the work required to close the extension introduced [22]. This work may be thought of as that which is available to extend a crack. The strain energy release rate required for crack extension is determined experimentally by monitoring a slow, stable crack extension. A comparison of the available and required strain energy release rates determines whether additional cracking will occur at a given value of applied stress. Transverse crack spacing is predicted by placing two cracks at a distance most energetically favorable for a given stress. Residual curing stresses are accounted for in the theory by adding their effects into the predicted available strain energy release rate. Comparisons with experimental results for graphite-epoxy $[\pm 25/90_2]_5$ and $[\pm 25/90_3]_5$ laminates showed good correlations [23].

2.5 Prediction of Transverse Cracking Effects on the CTE

Bowles [14] used a classical lamination theory analysis with reduced transverse stiffness, E_2 , in the cracked layer to predict the effect of transverse cracking on the laminate CTE. A finite element analysis was used to determine the relationship between crack density and reduction in laminate transverse stiffness. Classical lamination theory was then used to determine the reduction in E_2 of the cracked layer needed to produce the same reduction in laminate transverse stiffness. A master curve, independent of laminate configuration, for the reduction in E_2 as a function of crack density was constructed and used in conjunction with a classical lamination theory analysis to predict changes in the laminate CTE due to transverse cracks. Predictions were

in good agreement with experimental data for quasi-isotropic graphite-epoxy laminates.

Chapter 3

ANALYTICAL STUDIES

In this chapter, the characteristics of transverse cracking are studied analytically. The study is begun by attempting to predict the temperature at which transverse cracks initially form in a laminate. Next, the state of stress in the vicinity of a transverse crack is investigated and the initial equilibrium crack spacing predicted. The formation of additional transverse cracking under increasing thermal load is then investigated. Finally, the influence of transverse cracking on the laminate CTE is studied. Classical lamination theory, a modified shear-lag analysis, and a generalized plane strain finite element analysis are used in making these determinations.

A total of ten laminates were selected for analysis and experimental correlation. Six were cross-ply laminate configurations; $[0/90_3]_S$, $[0_2/90_2]_S$, $[0_3/90]_S$, $[90/0_3]_S$, $[90_2/0_2]_S$, and $[90_3/0]_S$. The remaining four were quasi-isotropic laminate configurations; $[0/\pm 45/90]_S$, $[0/45/90/-45]_S$, $[90/\mp 45/0]_S$, and $[90/-45/0/45]_S$. These laminates were selected to study the effects of 90° layer thickness and adjacent constraints on both the formation of transverse cracks and the laminate CTE. The material chosen for this investigation was T300/5208 graphite-epoxy.

3.1 General Formulation

3.1.1 Assumptions

To render the study of transverse cracking under thermal loading and its effects on the laminate CTE tractable, the following assumptions are made:

1. Individual layers are homogeneous, orthotropic materials.
2. The laminates are infinite plates in the x and y directions (Figs. 2 and 3).
3. Transverse cracks occur only in the 90° layers.
4. Transverse cracks occur at evenly spaced intervals and extend completely through the laminate.

As will be seen in the following sections, these assumptions allow for a generalized plane strain analysis of transverse cracking using a two dimensional, repeating unit cell.

As shown in Figs. 2 and 3, two perpendicular series of cracks may be present in different layers of both the cross-ply and quasi-isotropic laminates. To study characteristics of one series of transverse cracks, the analysis is limited to a region between two cracks (perpendicular to the first series) and at a sufficient distance from each such that any effects of these cracks may be neglected. A 3-D analysis would be required to study the interaction between the two series of transverse cracks.

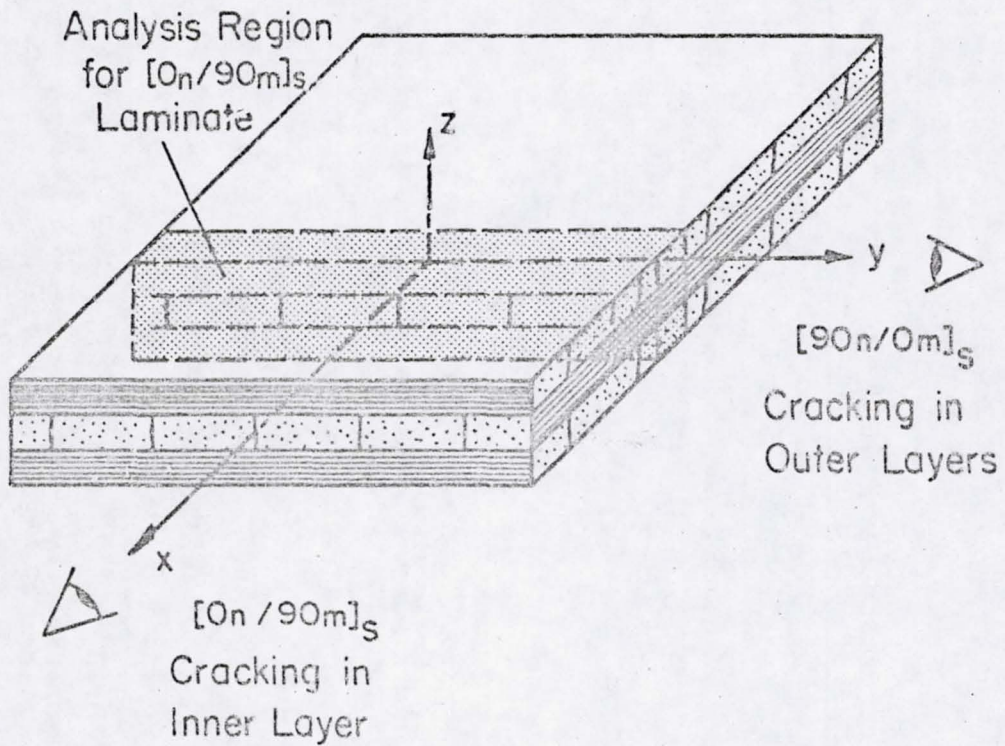
ORIGINAL PAGE IS
OF POOR QUALITY

Fig. 2. Transverse Cracking in Cross-Ply Laminate Configurations.

ORIGINAL PAGE IS
OF POOR QUALITY

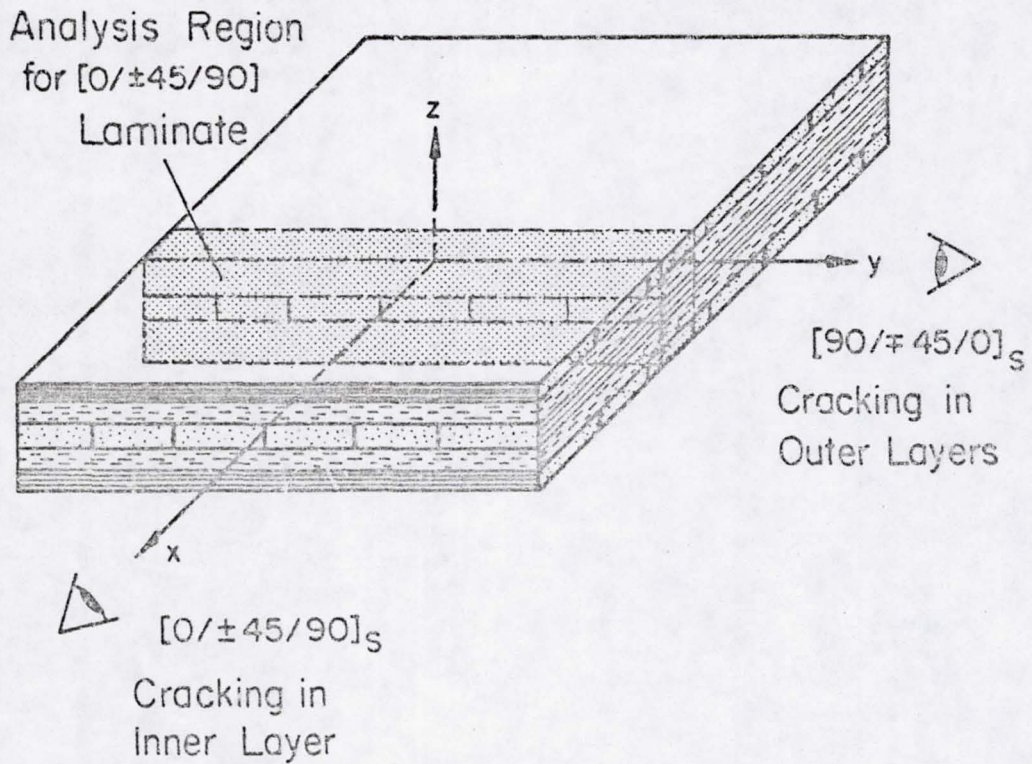


Fig. 3. Transverse Cracking in Quasi-Isotropic Laminate Configurations.

3.1.2 Temperature Dependence of Material Properties

In an application where the analysis is performed over a large temperature range, temperature dependent material properties should be used. In this analysis the mechanical, thermal, and strength properties used are second order least squares curve fits to available data on T300/5208 graphite-epoxy. Mechanical and strength property data is taken from reference [26], in which all tests were performed on specimens made from the same prepreg material used in the experimental portion of this study. Data for the transverse Young's modulus, E_2 , at -250°F (116K) is taken from reference [27]. Thermal property data is taken from references [28-31]. Temperature dependence is present in all mechanical, strength and thermal properties but to various degrees (Appendix A). A constant value for the out-of-plane shear modulus, G_{23} , and the minor Poisson's ratio, ν_{23} , from reference [32] is used in the generalized plane strain finite element analysis. Coefficients of the least squares curve fits as well as the graphical representation of the data and material properties are presented in Appendix A.

3.1.3 In Situ Transverse Strength of 90° Layers

The transverse strength of a layer in a multidirectional laminate (in situ strength) has been shown to be appreciably greater than the transverse strength determined from a unidirectional tensile coupon. Chamis and Sullivan [33] studied angleplied and quasi-isotropic laminates to determine the in situ strength of the various layers. The laminates were mechanically loaded to fracture at which point the stress

state of the individual layers were predicted by a classical lamination theory analysis. These layer stresses were input into a tensor polynomial failure criteria and the in situ strengths determined. For AS/3501 graphite-epoxy, the in situ transverse strength was reported to be three times greater than the uniaxial strength. Flagg and Kural [33] studied $[0_2/90_n]_s$, $[\pm 30/90_n]_s$, and $[\pm 60/90_n]_s$, $n = 1, 2, 3, 4$, T300/934 graphite-epoxy laminates to determine the in situ transverse strength of the 90° layers. Specimens were incrementally loaded and examined for transverse cracking after each increment. The laminate load at the onset of transverse cracking in the 90° layer was determined and the in situ strength of the 90° layers predicted using a classical lamination theory analysis. The ratios of the in situ strength of the 90° layers to the uniaxial strength reported were 2.48 for the $[0_2/90_2]_s$, 2.21 for the $[\pm 30/90]_s$, and 1.96 for the $[\pm 60/90]_s$ laminate. As the thickness of the 90° layer increased, the in situ strength in the three types of laminates was lower and closer to the strength of a unidirectional 90° coupon.

In this study, the effects of the in situ transverse strength of the 90° layers on the predicted temperature of initial transverse cracking are investigated (section 3.2.2). Determinations of the in situ transverse strengths for the thermally loaded specimens studied experimentally are presented in section 5.3.1.

3.1.4 Failure Criteria for Transverse Cracking

A maximum normal stress failure criteria is used to predict the occurrence of transverse cracking. Under this criteria, a crack is assumed to occur when the transverse normal stress, σ_2 , exceeds the in situ transverse strength, σ_2^{ult} , of the material. The maximum normal stress criteria has been applied to the formation of transverse cracks by several other authors [3, 8, 19, 20]. Upon formation, transverse cracks are assumed to span the entire thickness of the 90° layer.

3.1.5 Stress Free Temperature

The temperature at which bonding occurs in a laminate during cool down from cure is known as the stress free temperature (SFT). The SFT is used as a basis for computing the residual thermal stresses during cooling. Although often assumed to be the curing temperature, the SFT has been chosen as a lower temperature by some authors. Tsai [35] proposed using an unsymmetric [$\pm\theta$] laminate which warps upon cooling to determine the SFT, which is taken to be the temperature at which the laminate flattens upon reheating. Pagano and Hahn [36] used this technique on T300/5208 graphite-epoxy and determined the SFT to be between 250 and 300°F (394 and 422K). A value of 250°F was chosen for their analysis. Bowles [37], used the same technique on T300/5208 graphite-epoxy specimens made from the same prepreg material used in the experimental portion of this study. The SFT was determined to be near 350°F. A value of 350°F is therefore chosen for this investigation.

3.2 Initiation of Transverse Cracks

3.2.1 Formulation

A classical lamination theory analysis is used to predict the initial temperature at which transverse cracks form under thermal load. A brief summary of the stress-strain-temperature relations for an arbitrary laminate are given following the method of Hahn and Pagano [11]. A more detailed development of classical lamination theory is available in reference [38].

The standard laminate configuration used is shown in Fig. 4. Assuming the superposition of strains, the total strain in the k th layer, ϵ , is given as the sum of the mechanical strain, ϵ^m , and thermal strain, ϵ^T

$$\{\epsilon(T)\}^k = \{\epsilon^m(T)\}^k + \{\epsilon^T(T)\}^k \quad (3.1)$$

where

$$\{\epsilon^T(T)\}^k = \int_{SF}^T \{\alpha(\tau)\}^k d\tau \quad (3.2)$$

and

$$\begin{aligned} T_{SF} &= \text{stress free temperature} \\ T &= \text{temperature of interest} \\ \{\alpha(\tau)\}^k &= \text{temperature dependent CTE} \\ &\quad \text{of the } k\text{th layer} \end{aligned}$$

The stress strain relations for the k th layer in the laminate coordinate system are given as

ORIGINAL PAGE IS
OF POOR QUALITY

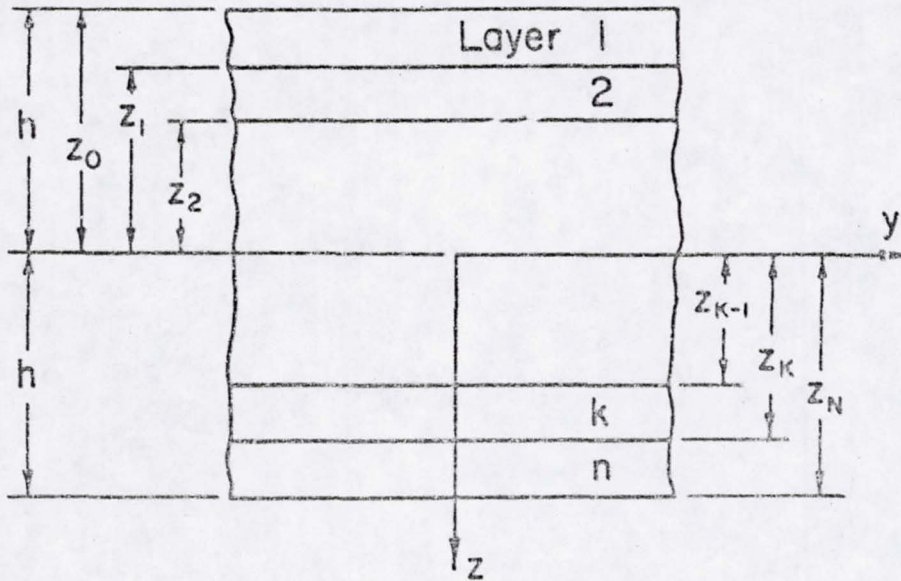


Fig. 4. Laminate Geometry.

$$\{\sigma(T)\}^k = [\bar{Q}(T)]^k \{\varepsilon^m(T)\}^k \quad (3.3)$$

Substituting (3.1) and (3.2) into (3.3) gives

$$\{\sigma(T)\}^k = [\bar{Q}(T)]^k \left(\{\varepsilon(T)\}^k - \int_{T_{SF}}^T \{\alpha(\tau)\}^k d\tau \right) \quad (3.4)$$

Equation (3.4) shows that the inclusion of temperature dependent material properties requires a knowledge of the elastic properties, $[\bar{Q}(T)]^k$, at the temperature of interest and the thermal properties, $\{\alpha(T)\}^k$, as a function of temperature between the stress free temperature and the temperature of interest. Expressing the total strain, $\{\varepsilon(T)\}^k$, in terms of the laminate midplane strains, $\{\varepsilon_0(T)\}$, and curvatures, $\{\kappa(T)\}$, gives

$$\{\sigma(T)\}^k = [\bar{Q}(T)]^k \left(\{\varepsilon_0(T)\} + z^k \{\kappa(T)\} - \int_{T_{SF}}^T \{\alpha(\tau)\}^k d\tau \right) \quad (3.5)$$

Integrating through the thickness of the laminate yields

$$\begin{Bmatrix} N(T) + N^T(T) \\ M(T) + M^T(T) \end{Bmatrix} = \begin{bmatrix} A(T) & B(T) \\ B(T) & D(T) \end{bmatrix} \begin{Bmatrix} \varepsilon_0(T) \\ \kappa(T) \end{Bmatrix} \quad (3.6)$$

where

$$(N^T(T), M^T(T)) = \int_{-h}^h [\bar{Q}(T)]^k \int_{T_{SF}}^T \{\alpha(\tau)\}^k d\tau (1, z) dz$$

$$([A], [B], [D]) = \int_{-h}^h [\bar{Q}(T)]^k (1, z, z^2) dz$$

Equation (3.6) relates the applied inplane forces and moments to the midplane strains and curvatures. Under pure thermal loading, $N(T) = M(T) = 0$ and Eqn. (3.6) is inverted, giving the laminate response under a given thermal load

$$\begin{Bmatrix} \epsilon_0(T) \\ \kappa(T) \end{Bmatrix} = \begin{bmatrix} A(T) & B(T) \\ B(T) & D(T) \end{bmatrix}^{-1} \begin{Bmatrix} N^T(T) \\ M^T(T) \end{Bmatrix} \quad (3.7)$$

The stresses in a particular layer are determined by substituting the values for $\epsilon_0(T)$ and $\kappa(T)$ into Eqn. (3.5).

3.2.2 Determination of Crack Initiation Temperatures

Since both the stress and uniaxial strength vary with temperature, a trial and error procedure is used to determine the temperature of initial cracking. A value for the in situ strength is selected in terms of a multiple of the uniaxial strength (i.e., $\sigma_2^{ult} = C\sigma_t(T)$, where C is a constant). A temperature is selected and the stress and in situ strength are calculated. If not equal, another temperature is estimated and the procedure repeated until the temperature at which $\sigma_2 = \sigma_2^{ult}$ has been predicted to within 1°F.

Since the stresses predicted in symmetric laminates with a classical lamination theory analysis are independent of stacking sequence, only three analyses need to be performed to represent all ten laminates of interest; one for the $[0/90_3]_s$ and $[90_3/0]_s$ laminates, another for the $[0_3/90]_s$ and $[90/0_3]_s$ laminates, and a third for the $[0_2/90_2]_s$, $[90_2/0_2]_s$ and the four quasi-isotropic laminates (since σ_2 in the 90° layers of a $[0_2/90_2]_s$, $[90_2/0_2]_s$, and quasi-isotropic laminates are identical).

The predicted temperatures at which transverse cracks initially form in the three groups of laminates are shown in Fig. 5 for four values of the in situ transverse strength. As the percentage of the 90° layer in the cross-ply laminates decreases, the thermal load needed to produce transverse cracking at a given in situ strength decreases. This result is expected, since the corresponding increase in the percentage of 0° layer produces a greater constraint on the 90° layer and therefore a higher transverse tensile stress, σ_2 , in the 90° layer at a given thermal load. Increasing the in situ strength results in more than a linear increase in the thermal load required to produce cracking, a result of the temperature dependent material properties. For the case where the in situ strength of the 90° layer is taken as the uniaxial strength of the material ($\sigma_2^{ult} = Y_t(T)$), transverse cracking is predicted to be present in all laminates at room temperature. However, as will be shown in Chapter 5, this was not the case. All laminates were determined to be free of transverse cracks at room temperature, indicating an in situ strength greater than the unidirectional strength, $Y_t(T)$.

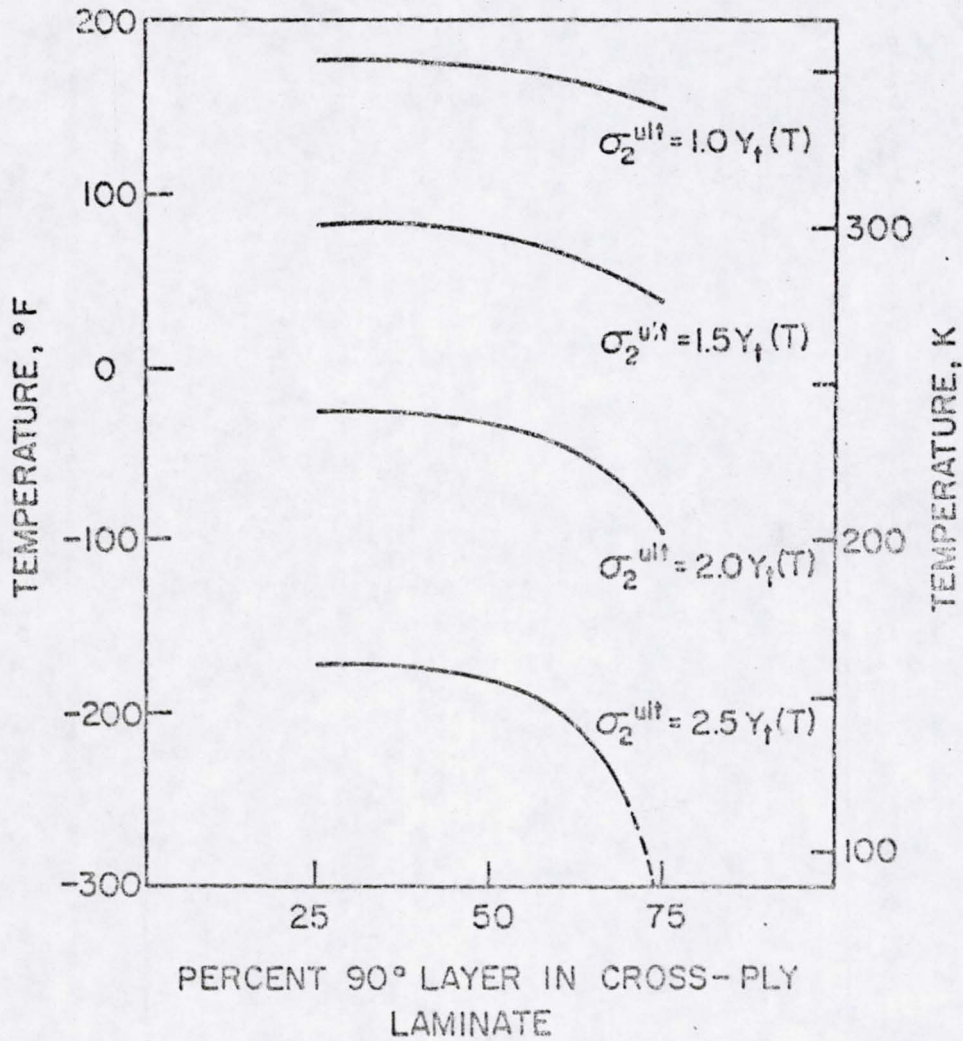
ORIGINAL PAGE IS
OF POOR QUALITY

Fig. 5. Temperature of Initial Transverse Cracking in Cross-Ply Laminates as a Function of the In Situ Transverse Strength.

3.3 Stresses in the Vicinity of a Transverse Crack

Once the thermal load required to produce transverse cracking is determined using classical lamination theory, an understanding of the state of stress in the 90° layer in the vicinity of a transverse crack is necessary to predict the equilibrium crack spacing present and the additional thermal load required to produce additional transverse cracking. To study the stress state, a single transverse crack is assumed to form in the 90° layer of the laminate at the initial cracking temperature (determined by classical lamination theory) as shown in Fig. 6. At the plane of the crack ($y=0$), the transverse normal stress, σ_2 , in the 90° layer is zero. Moving away from the crack in the 90° layer (increasing y), stress is transferred back into the cracked 90° layer via shear stresses at the interfaces with adjacent layers. At some distance from the crack plane, σ_2 reaches the in situ transverse strength of the layer and another crack is formed. This distance will be called the initial equilibrium transverse crack spacing. Transverse cracks are assumed to form periodically across the 90° layer at this spacing (Fig. 2 and 3). Thus, the task of determining the initial equilibrium crack spacing becomes one of determining the transverse normal stress in the 90° layer in the vicinity of an existing transverse crack as a function of temperature.

In this study, a generalized plane strain finite element analysis is used to determine the state of stress. Results are compared to those predicted with a modified shear-lag analysis. The $[0_2/90_2]_S$ cross-ply laminate is chosen for this investigation as being representative and

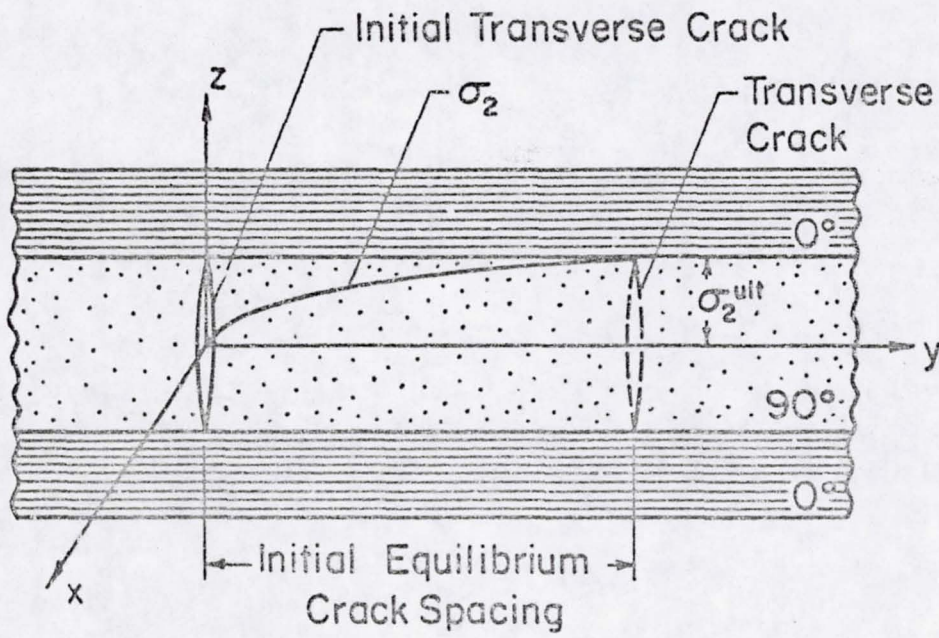
ORIGINAL PAGE IS
OF POOR QUALITY

Fig. 6. Initial Equilibrium Crack Spacing Model.

because it was found to be well behaved experimentally (see Chapter 5). A brief description of the finite element and modified shear-lag analysis methods are presented in the following sections.

3.3.1 Finite Element Analysis

Stresses and strains are assumed to be independent of the out-of-plane x coordinate (Fig. 6) allowing for a generalized plane strain finite element analysis. In such an analysis, a constant value of the x direction strain, ϵ_{xx} , is assumed and the displacement field is of the form

$$\begin{aligned} u(x,y,z) &= U(y,z) + \epsilon_{xx} \cdot x \\ v(x,y,z) &= V(y,z) \\ w(x,y,z) &= W(y,z) \end{aligned} \quad (3.9)$$

where U , V , and W are the unknown nodal displacements. In the case of pure thermal loading, ϵ_{xx} is the free laminate thermal strain due to cool down from the SFT and is determined from a classical lamination theory analysis of the thermally loaded laminate in the uncracked state. Although ϵ_{xx} may not be constant throughout the laminate in the presence of transverse cracks, Bowles [25] found that reductions predicted in ϵ_{xx} due to transverse cracks had a negligible effect on the y - z plane behavior and therefore the constant, classical lamination theory value could be assumed.

The finite element program employed was a modified version of a generalized plane strain program for laminated composites. Four node isoparametric, quadrilateral elements were used to model the region of interest. A complete description of the finite element formulation is given by the program author in reference [39].

The modeled region is chosen to extend a sufficient distance from the crack plane to where stresses and strains are not influenced by the presence of the crack and converge to those predicted by classical lamination theory. For the $[0_2/90_2]_s$ laminate, this distance was determined to be 0.20 in. (0.51 cm). Since the laminates considered in this study are symmetric, only one-half of the laminate is modeled.

The displacement boundary conditions for the modeled region (Fig. 7) are:

$$U(0,z) = 0 \quad (3.10)$$

$$U(B,z) = 0 \quad T < z < H$$

$$V(0,z) = 0$$

$$V(B,z) = V^* \text{ (constrained), } T < z < H$$

$$W(y,0) = 0$$

The U and V boundary conditions at the line $y=0$ satisfy the Kirchhoff assumption that normals to the laminate midplane remain normal to the midplane under uniform thermal loading. The condition $U(B,z) = 0$,

$T < z < H$ was verified by modeling a larger portion of the laminate and examining the U displacements in the interior of the grid where this condition is prescribed. A description of this procedure is given later in this section.

ORIGINAL PAGE IS
OF POOR QUALITY

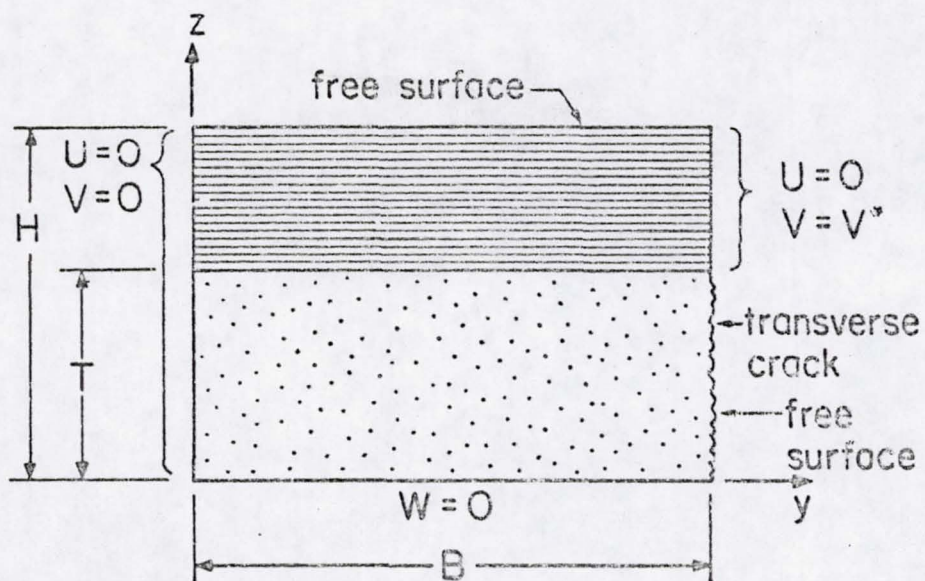


Fig. 7. Boundary Conditions on Modeled Region for Determining Initial Equilibrium Transverse Crack Spacing.

The condition $V(B,z) = V^*$, $T < z < H$ accounts for the symmetry about the transverse crack plane while allowing for free thermal strain. With this condition, the line $y=B$, $T < z < H$, is allowed to translate in the y direction, but is constrained to remain straight and vertical. The free thermal displacement, V^* , is unknown and must be solved for in the analysis. This constraint boundary condition requires a modification to the standard finite element formulation. As illustrated in Appendix B, this constrained displacement formulation may be handled by a systematic modification of the global stiffness matrix and global force vector resulting in a system of equations with fewer unknowns than the unconstrained set.

The boundary condition $W(y,0) = 0$ enforces the laminate symmetry about its midplane when modeling only the top half of the laminate.

The modeled region used to study the state of stress in the presence of a series of transverse cracks at a uniform crack spacing is shown in Fig. 8. Since a line of symmetry exists at the midplane between existing cracks ($y=0$), only one-half of the crack spacing is modeled. It is noted that the boundary conditions on the modeled region are the same as those used in determining the initial equilibrium crack spacing (Fig. 7) although the reason for employing some are different. The condition $V(0,z) = 0$ previously invoked to satisfy Kirchhoff's hypothesis now enforces the line of symmetry at the midplane between cracks. The conditions $U(0,z) = 0$ and $U(B,z) = 0$, $T < z < H$ were determined by modeling three crack spacings (Fig. 9) and examining the U displacements at these locations in the interior of the mesh. It was

ORIGINAL PAGE IS
OF POOR QUALITY

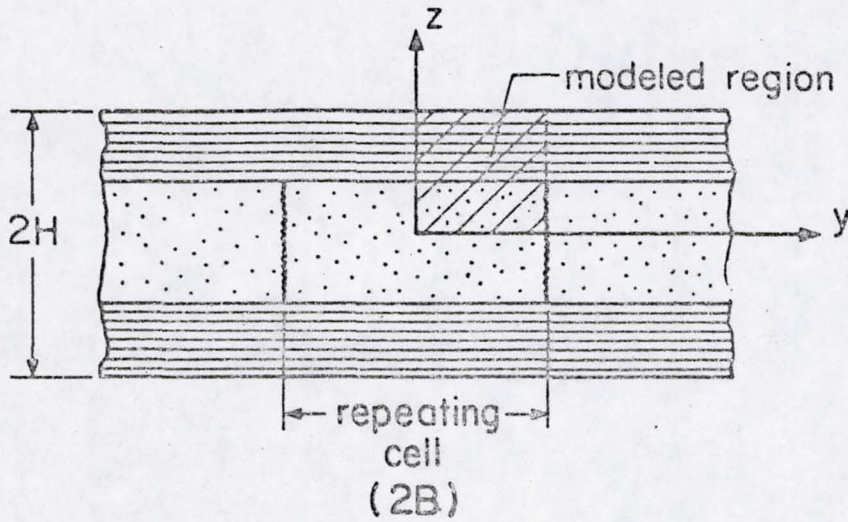


Fig. 8. Modeled Region for Multiple Transverse Cracking.

ORIGINAL PAGE IS
OF POOR QUALITY

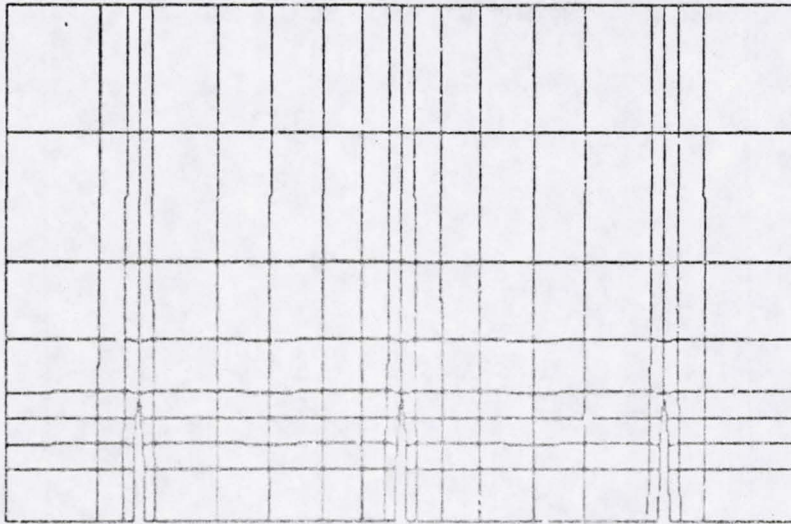


Fig. 9. Three Crack Spacing Mesh for Confirming Boundary Conditions (Shown in Deformed State for $[0_3/90]_5$ Laminate).

determined that although the U displacements are non-zero in the interior of the modeled region for the quasi-isotropic laminates, they converge to zero at $y=0$ and $y=B$, $T < z < H$ for all laminates investigated in this study. The remaining boundary conditions are invoked for the same reasons as in determining the initial equilibrium crack spacing.

The length of the modeled region, B , may be varied to produce different crack spacings by changing the y -direction mesh scale factor. Some caution must be exercised, however, to ensure that the element aspect ratios do not become so large as to produce an inaccurate solution.

A 272 element, 306 node (918 degrees of freedom) finite element mesh (Fig. 10) composed of four node isoparametric quadrilateral elements is used to model the region of interest. Four elements are used through the thickness of each ply and the element widths varied along the length of the mesh to allow for a greater number of elements near the transverse crack.

Results of the finite element analyses are presented and compared to predictions made with a modified shear-lag analysis following a brief description of the latter.

3.3.2 Modified Shear-Lag Analysis

The modified shear-lag analysis has been used by several authors [2, 3, 4, 8, 20] to predict transverse crack density as a function of the applied load. A brief description of the theory is presented here

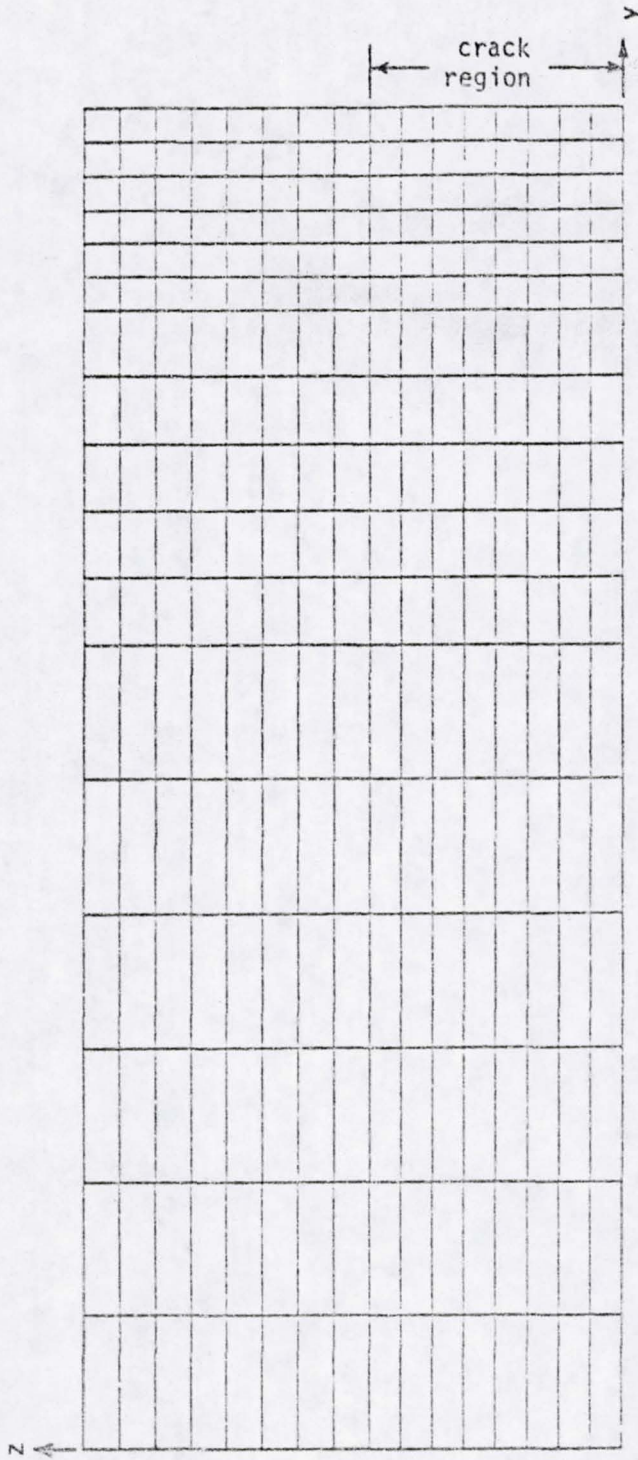


Fig. 10. 272 Element X 306 Node Finite Element Mesh.

as used in the analysis of transverse cracking under thermal loading. A complete development of the theory is presented in reference [4].

The theory presented is for a $[0_n/90_m]_s$ cross-ply laminate as shown in Fig. 11. When transverse crack forms, all thermal stresses at the crack plane ($y=0$) are relieved. Due to the mismatch in coefficients of thermal expansion between the 0° and 90° layers, stresses develop in the laminate via shear stress between the layers. The shear stress is assumed to be proportional to the difference in average elastic displacements of the 0° and 90° layers

$$\frac{\tau_{xy}}{D} = H(v_{90} - v_0) \quad (3.11)$$

where D is the 90° layer half-thickness (Fig. 11) and H is a constant. From a force balance on the 90° layer (Fig. 12),

$$\tau_{xy} = D \frac{d\sigma_2}{dy} \quad (3.12)$$

Substituting (3.12) into (3.11) gives the differential equation for σ_2

$$\frac{d\sigma_2}{dy} = H(v_{90} - v_0) \quad (3.13)$$

Differentiating and using the relations

$$\frac{dv_0}{dy} = \frac{\sigma_1}{E_1} \quad (3.14)$$

and

ORIGINAL PAGE IS
OF POOR QUALITY

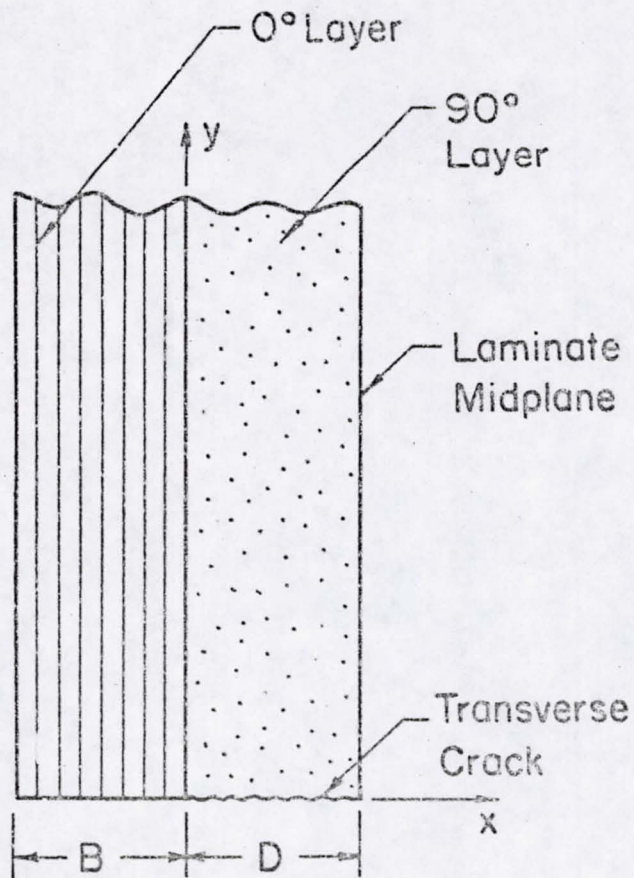


Fig. 11. Modified Shear-Lag Analysis Model.

ORIGINAL PAGE IS
OF POOR QUALITY

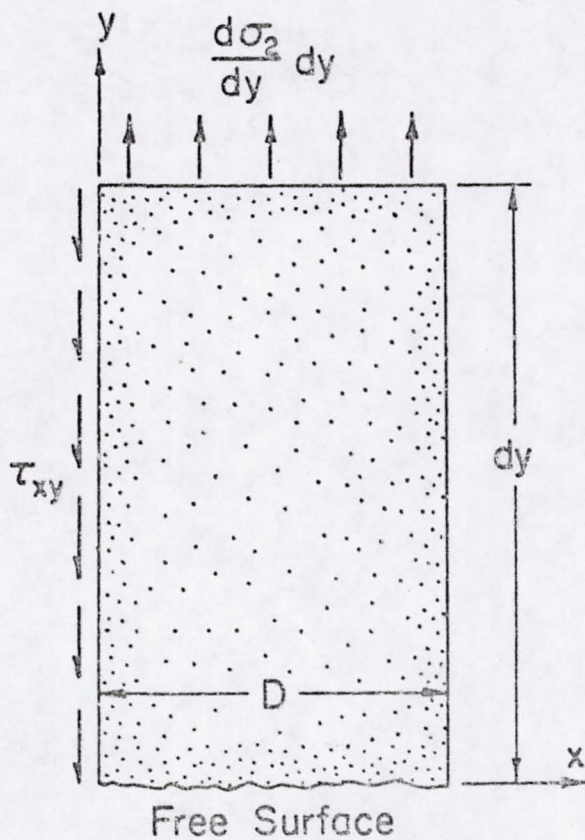


Fig. 12. Free Body Diagram of 90° Layer for Modified Shear-Lag Analysis.

$$\frac{dv_{90}}{dy} = \frac{\sigma_2}{E_2} \quad (3.15)$$

where E_1 = Young's modulus of the 0° layer

E_2 = Young's modulus of the 90° layer

gives

$$\frac{d^2\sigma_2}{dy^2} = H \left(\frac{\sigma_2}{E_2} - \frac{\sigma_1}{E_1} \right) \quad (3.16)$$

Substituting the relations

$$\sigma_1 = -\frac{\sigma_2 D}{B} \quad (3.17)$$

and

$$E_c = \frac{E_1 B + E_2 D}{B + D}$$

where E_c = Young's modulus of the composite

B = 0° layer thickness (3.18)

into (3.16) gives a second-order differential equation for σ_2 of the form

$$\frac{d^2\sigma_2}{dy^2} = \phi \sigma_2 \quad (3.19)$$

where

$$\frac{HE_c(B+D)}{E_1 E_2 B} \quad (3.20)$$

The constant, H , is determined by using the relation

$$\frac{dv}{dx} = \frac{\tau_{xy}}{G_{12}} \quad (3.21)$$

where G_{12} = shear modulus of 90° layer

Integrating (3.21) from the $0/90$ interface ($v = v_0$) to the laminate midplane ($v = v_{90}$) gives

$$v_{90} - v_0 = \frac{\tau_{xy} D}{G_{12}} \quad (3.22)$$

Substituting (3.22) into (3.11) and solving for H yields

$$H = \frac{G_{12}}{D^2} \quad (3.23)$$

Substituting (3.23) into (3.20) gives

$$\phi = \frac{E_c G_{12}}{E_1 E_2} \frac{B+D}{BD^2} \quad (3.24)$$

Invoking the boundary conditions

$$\sigma_2 \Big|_{y=0} = 0 \quad (3.25)$$

$$\sigma_2 \Big|_{\text{large } y} = \sigma_2^{\text{ult}}$$

gives a solution to (3.19) of the form

$$\sigma_2(y) = \sigma_2^{ult} (1 - \exp(-\phi^{1/2} y)) \quad (3.26)$$

The shear stress at the interface between adjacent layers is found by substituting (3.26) into (3.12)

$$\tau_{xy}(y) = D\sigma_2^{ult} \phi^{1/2} \exp(-\phi^{1/2} y) \quad (3.27)$$

To determine σ_2 in the 90° layer between two existing cracks at a given thermal load, the shear stresses due to the two cracks are summed. If the spacing between cracks is S , the shear stress is given by

$$\tau_{xy}(y) = D\sigma_2^T \phi^{1/2} [\exp(-\phi^{1/2} y) - \exp(\phi^{1/2} (y-S))] \quad (3.28)$$

where σ_2^T is the 90° layer thermal stress at the given thermal load in the absence of transverse cracks. Substituting (3.28) into (3.12) and integrating between 0 and y gives the desired expression for $\sigma_2(y)$

$$\sigma_2(y) = \sigma_2^T [1 + \exp(-\phi^{1/2} S) - \exp(-\phi^{1/2} y) - \exp(\phi^{1/2} (y-S))] \quad (3.29)$$

Since σ_2 is maximum at the midpoint between existing cracks ($y = S/2$), the next crack will form at this point when σ_2 reaches σ_2^{ult} . Therefore, setting $\sigma_2 = \sigma_2^{ult}$ at $y = S/2$ in (3.29) and solving for σ_2^T gives an expression for σ_2^T needed to produce additional transverse cracking

$$\sigma_2^T = \sigma_2^{\text{ult}} [1 + \exp(-\phi^{1/2} S) - 2\exp(-\phi^{1/2} \frac{S}{2})]^{-1} \quad (3.30)$$

The thermal load corresponding to σ_2^T may then be determined using a classical lamination theory analysis.

3.3.3 Analysis of $[0_2/90_2]_s$ Laminate

As previously mentioned, the $[0_2/90_2]_s$ laminate is chosen to investigate the state of stress about a transverse crack. For this analysis, the temperature of initial transverse cracking is taken as the experimentally determined value of -200°F (144K). The experimental procedure followed in making this determination is presented in the following two chapters. Using classical lamination theory, the transverse normal stress, σ_2 , predicted in the 90° ply at -200°F is 11.59 ksi (79.91 MPa) which corresponds to an in-situ transverse strength of $2.55 Y_t(T)$.

The transverse stress, σ_2 , in the 90° layer in the vicinity of a transverse crack as predicted by the finite element and modified shear-lag analyses are shown in Fig. 13. Finite element results are presented at four locations through the thickness of the 90° layer since a through the thickness gradient is predicted whereas a single representation is given for the shear-lag prediction which is independent of position through the layer thickness. A comparison of the two analyses shows that the shear-lag analysis predicts the rebuilding of stress in the 90° layer to occur in a shorter distance than does the finite element analysis for the majority of the thickness of the layer. Since a mathemati-

ORIGINAL PAGE IS
OF POOR QUALITY

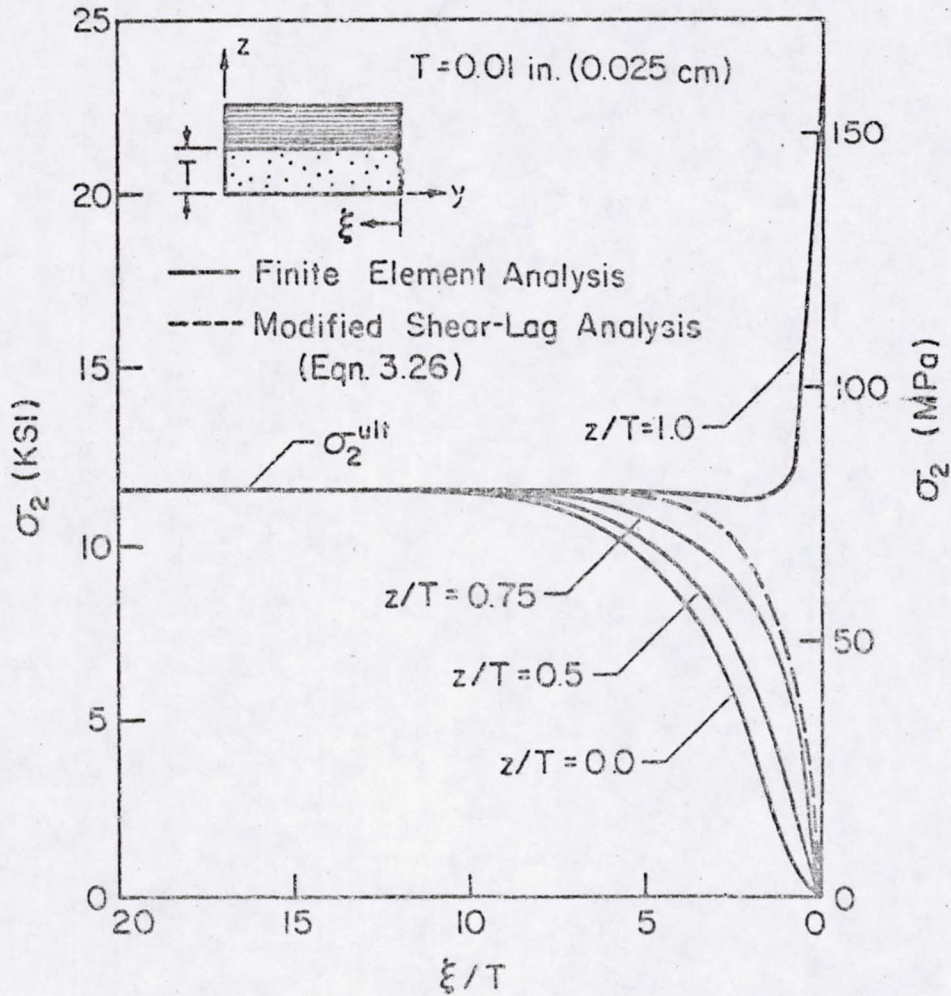


Fig. 13. σ_2 Stress in the 90° Layer of a $[0_2/90_2]_s$ Laminate in the Vicinity of a Transverse Crack (-200°F).

cal singularity exists at the tip of the transverse crack in the finite element analysis, σ_2 near the crack tip is greater than the shear-lag analysis predictions. Similarly, the shear stress, τ_{xy} , predicted along the $0^\circ/90^\circ$ interface is greater in the finite element analysis than in the shear-lag analysis (Fig. 14). The shape of the curves for both σ_2 and τ_{xy} are similar for the two analyses and suggest that a major portion of the stress is recovered in the cracked 90° layer in less than 0.05 in. ($\frac{E}{T} = 5$), but that a much greater distance is required for σ_2 to attain σ_2^{ult} for a major portion of the layer thickness.

The through the thickness gradients in σ_2 predicted with the finite element analysis are shown in Fig. 15 at several distances from the transverse crack. The gradient in σ_2 is seen to be most pronounced near the transverse crack, decreasing in magnitude with distance from the crack plane. As a result of this gradient, material near the $0^\circ/90^\circ$ interface is at the highest level of σ_2 and therefore is of primary interest for purposes of predicting the location of the next transverse crack.

Since the predicted distance at which σ_2 attains its uncracked value, σ_2^{ult} , in the finite element analysis is dependent upon the location through the 90° layer thickness, an assumption must be made to determine the equilibrium transverse crack spacing. If a crack is assumed to occur when σ_2 first reaches σ_2^{ult} at any point in the 90° layer (disregarding the singularity, i.e., $z/T < 0.875$ for the mesh used) the equilibrium crack spacing predicted by the finite element analysis is 0.09 in. ($\frac{E}{T} = 9$), corresponding to a crack density of 11.1

ORIGINAL PAGE IS
OF POOR QUALITY

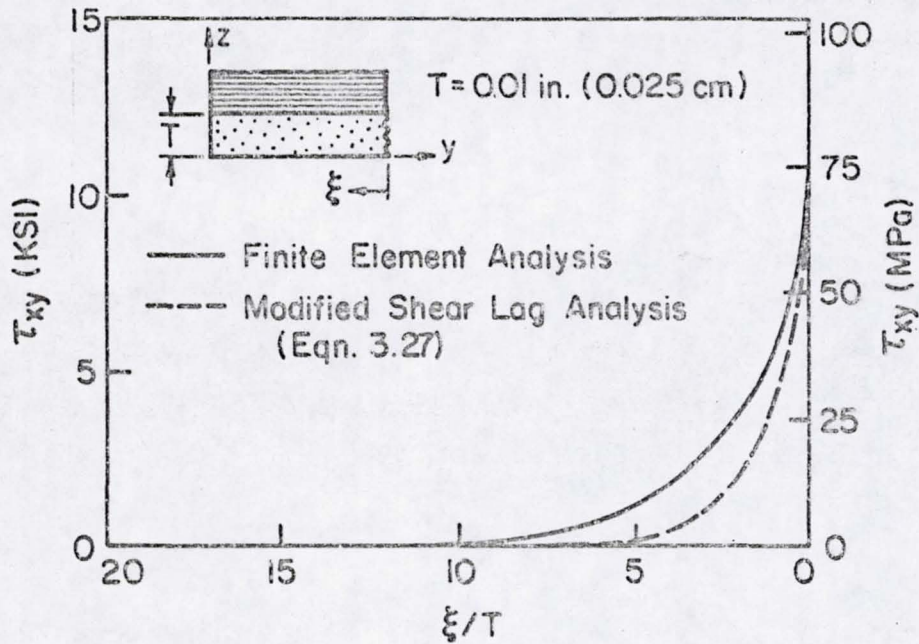


Fig. 14. τ_{xy} Stress Along $0^\circ/90^\circ$ Interface ($\frac{z}{T} = 1.0$) in a $[0_2/90_2]_S$ Laminate in the Vicinity of a Transverse Crack (-200°F).

ORIGINAL PAGE IS
OF POOR QUALITY

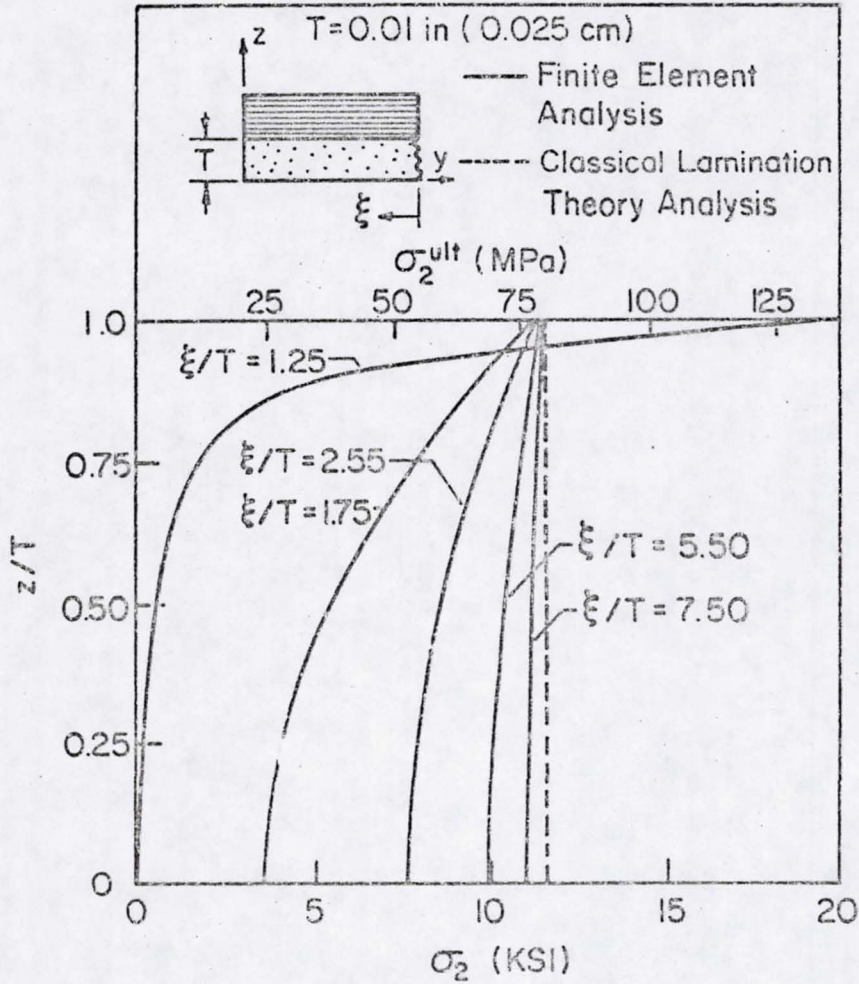


Fig. 15. σ_2 Stress Gradients in 90° Layer of $[0_2/90_2]_s$ Laminate in the Vicinity of a Transverse Crack (-200°F).

cracks/in. (4.4 cracks/cm). If, however, a crack is assumed to occur when σ_2 throughout the entire thickness of the 90° layer reaches σ_2^{ult} , the predicted crack spacing becomes 0.13 in. ($\frac{\xi}{T} = 13$) corresponding to a crack density of 7.7 cracks/in. (3.0 cracks/cm). This represents a 44% difference in predicted crack spacing between these two limiting cases.

In the modified shear-lag analysis, σ_2 approaches σ_2^{ult} asymptotically and therefore a limiting percentage of the in situ strength must be chosen to predict a finite crack spacing. Assuming that a transverse crack occurs when σ_2 reaches 99% of σ_2^{ult} , the predicted equilibrium crack spacing is 0.056 in. ($\frac{\xi}{T} = 5.6$) corresponding to 17.9 cracks/in. (7.0 cracks/cm). If a value of 99.9% of σ_2^{ult} is used, the predicted crack spacing is increased 50% to 0.084 in. ($\frac{\xi}{T} = 8.4$), a crack density of 11.9 cracks/in. (4.7 cracks/cm). A good correlation exists between the two analyses when assuming crack formation occurs when σ_2 first reaches σ_2^{ult} in the 90° layer of the finite element analysis (disregarding the singularity) and using 99.9% of σ_2^{ult} in the modified shear-lag analysis (9.0 $\frac{\xi}{T}$ and 8.4 $\frac{\xi}{T}$ crack spacing, respectively). At the temperature of initial transverse cracking (-200°F), no further transverse cracking will occur beyond the equilibrium crack spacing in either analysis since σ_2 is less than σ_2^{ult} throughout the 90° layer.

Knowing the initial equilibrium crack spacing, the next task is to determine the additional thermal load needed to produce further transverse cracking. The location of the next cracks are assumed to be at the midplane between existing cracks since σ_2 increases with distance

from each transverse crack and is greatest at these planes. Thus the task of determining the thermal load required to produce additional transverse cracking becomes one of determining the temperature at which σ_2 at the midplane between existing cracks reaches the in situ transverse tensile strength, σ_2^{ult} .

The σ_2 stress in the 90° layer of the $[0_2/90_2]_5$ laminate at the midplane between two existing cracks ($y=b$) is shown in Fig. 16 for three crack spacings. As might be expected, the through the thickness gradient predicted by the finite element analysis increases in magnitude as the crack spacing decreases. At the initial equilibrium crack spacing ($\frac{2B}{T} = 9$), the laminate midplane ($\frac{z}{T} = 0.0$) is at a 34% lower value of σ_2 than the $0^\circ/90^\circ$ interface ($\frac{z}{T} = 1.0$). Assuming that failure occurs when σ_2 first reaches σ_2^{ult} at any point in the 90° layer, a large percentage of the layer thickness is well below σ_2^{ult} at the midplane between cracks ($y=B$). The shear-lag analysis predictions are seen to correlate well with the finite element analysis predictions near the $0^\circ/90^\circ$ interface.

For predicting additional transverse cracking under increased thermal loading, an initial equilibrium crack spacing of 0.09 in. (0.23 cm), or $2B/T = 9$, is assumed to be present in the $[0_2/90_2]_5$ laminate at -200°F . In the finite element analysis, additional cracking is assumed to occur at the temperature at which σ_2 first attains σ_2^{ult} at a point in the midplane between existing cracks. Because of the temperature dependent material properties, an iterative procedure is required to determine this temperature. For the $[0_2/90_2]_5$ laminate, this tempera-

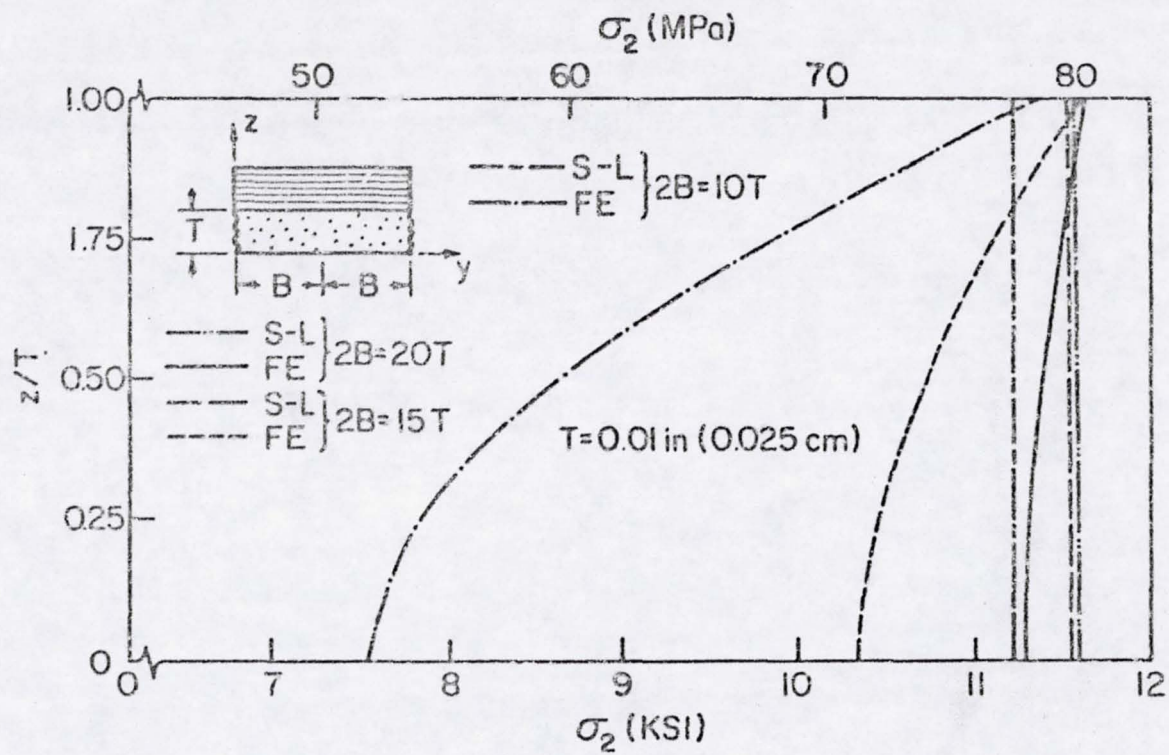


Fig. 16. σ_2 Stress at Midplane Between Transverse Cracks ($y = B$) in $[0_2/90_2]_5$ Laminate (-200°F).

ture is predicted as -235°F (125K). The crack spacing is thus reduced to one-half the initial equilibrium crack spacing, or 0.045 in. ($\frac{2B}{T} = 4.5$, or 0.11 cm) which corresponds to a crack density of 22.2 cracks/in. (8.7 cracks/cm). In the modified shear-lag analysis, Eqn. (3.30) along with a classical lamination theory analysis are used to predict the temperature at which σ_2 attains σ_2^{ult} at the midplane between existing cracks and additional cracking occurs. This temperature is predicted as -225°F (130K), 10°F higher than with the finite element analysis. Neither analysis predicts any further transverse cracking prior to -250°F , the lowest temperature used in the experimental portion of this investigation.

3.4 Influence of Transverse Cracking on Laminate CTE

A generalized plane strain finite element analysis is used to determine the influence of transverse cracks on the CTE for the ten laminates listed at the beginning of the chapter. Cracks are assumed to be present at even intervals and the resulting modeled region and boundary conditions are identical to those used in determining the initial equilibrium crack spacing (Fig. 7). To determine the laminate CTE, the modeled region is subjected to a uniform temperature change (taken to be $\Delta T = -1^{\circ}\text{F}$) at room temperature. The unknown, uniform displacement, V^* , of the line $y=B$ is solved for and the laminate CTE, $\bar{\alpha}_y$, is given by

$$\bar{\alpha}_y = \frac{V^*}{B\Delta T} \quad (3.31)$$

where B is the length of the modeled region (one-half of the crack spacing). The 272 element, 306 node finite element mesh shown in Fig. 10 is again used. The transverse crack density was varied by changing the y scale factor of the mesh. Each laminate was analyzed for several transverse crack densities ranging from 2 cracks/in. (0.79 cracks/cm) to 100 cracks/in. (39.4 cracks/cm). In addition, uncracked laminates were analyzed and the result compared to the classical lamination theory solution.

The variation of laminate CTE with crack density in cross-ply laminates is shown in Fig. 17. These same results are presented in the form of percent retention curves in Fig. 18. The curves for the quasi-isotropic laminates (Fig. 19) represent both actual changes and percent retention since the three quasi-isotropic laminates have the same CTE in the uncracked state. As expected, the finite element results show excellent agreement with classical lamination theory for all ten laminates in the uncracked state.

The cross-ply laminates exhibit a rather sharp drop in CTE at low crack densities (less than 25 cracks/in. (19.7 cracks/cm)). The percent retention curves of Fig. 18 predict a range of 35-76 percent reduction at a density of 25 cracks/in. (9.8 cracks/cm) and a range of 50-83 percent reduction at 50 cracks/in. (19.7 cracks/cm). Crack densities as high as 78 cracks/in. (30.7 cracks/cm) have been observed in quasi-isotropic T300/5208 graphite-epoxy laminates [8] and as high as 100 cracks/in. (39.4 cracks/cm) in graphite-polyimide [4]. The percent retention curves also show that the change in CTE is largest in the

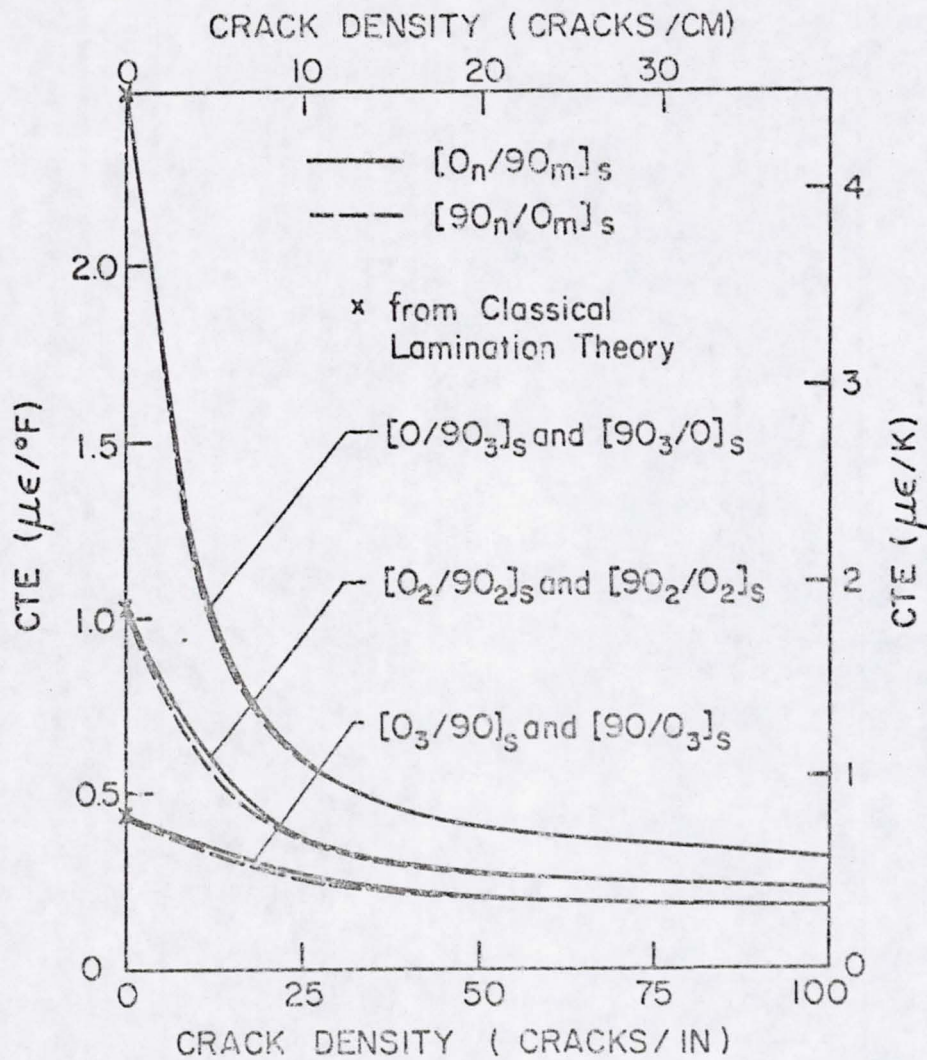


Fig. 17. CTE as a Function of Crack Density in Cross-Ply Laminates.

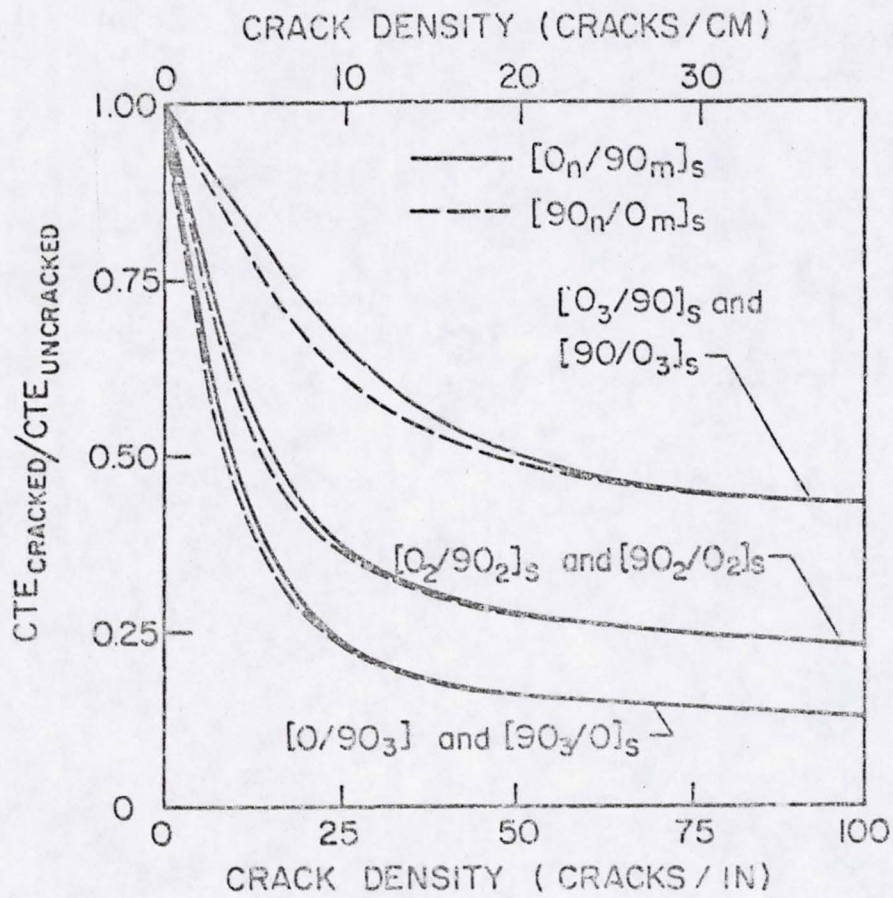


Fig. 18. Percent Retention of CTE in Cross-Ply Laminates.

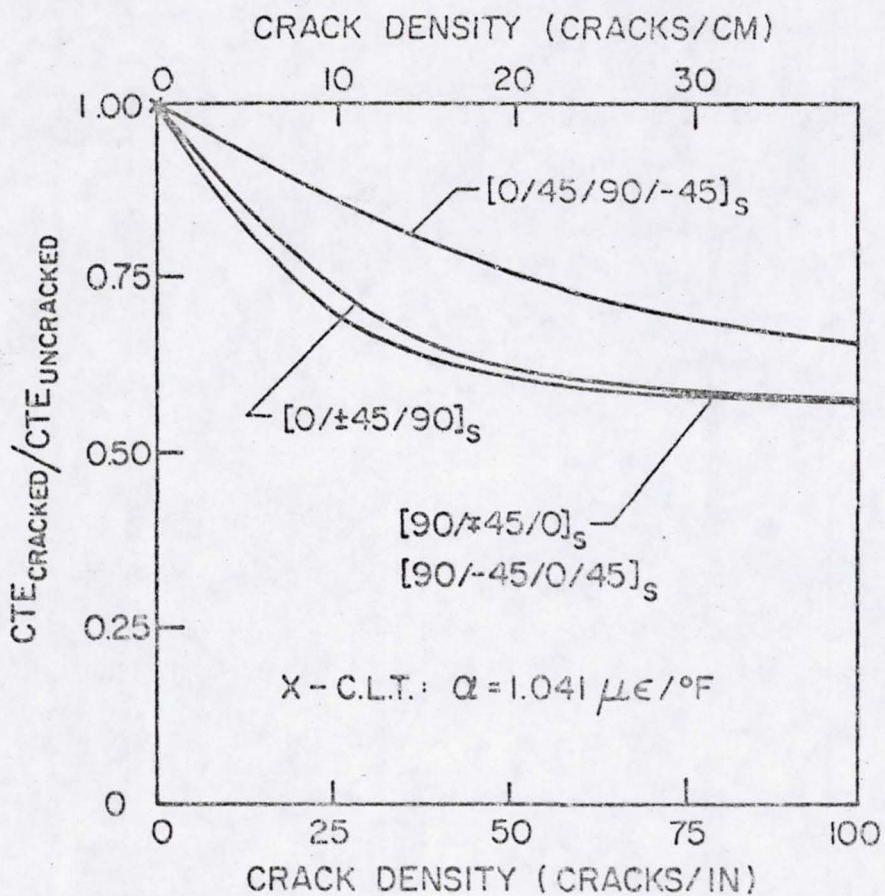


Fig. 19. Percent Retention of CTE in Quasi-Isotropic Laminates.

laminates with the highest percentage of 90° layers ($[0/90_3]_S$ and $[90_3/0]_S$). For the three pairs of laminates with the same percentage of 90° layer, the laminate with the 90° layers at the exterior ($[90_n/0_n]_S$) exhibit a slightly greater reduction in CTE than with the 90° layers together in the interior ($[0_n/90_m]_S$). This result is believed to be due to the additional freedom of the $[90_n/0_n]_S$ laminate to experience strain in the z direction (Fig. 8) in the vicinity of a transverse crack.

The results for the quasi-isotropic laminates (Fig. 19) show that the CTE decreases with increasing crack density, but at a much lower rate and to a lesser extent than the cross-ply laminates of Fig. 18. These differences are largely the result of the lower percentage of 90° layers in the laminate. However, as indicated in Fig. 19, the CTE retention is not controlled only by the percentage of 90° layers. It is also a function of the stacking sequence of the laminate. The laminates with the outer 90° layers or the two 90's adjacent at the midplane have only a 57 percent retention at 100 cracks/in. (39.4 cracks/cm) whereas the laminate with 90's interspersed between $\pm 45^\circ$ layers has a 65 percent retention at 100 cracks/in. This difference is due to the higher constraint in the thinner interior 90 layer. As in the cross-ply laminates, placing the 90° layers at the exterior of the laminate ($[90/\pm 45/0]_S$ and $[90/-45/0/45]_S$) results in a slightly greater reduction in CTE than when together at the interior ($[0/\pm 45/90]_S$). These results also clearly show that a lamination type theory which is independent of stacking sequence effects is not sufficient for analysis of this problem.

Chapter 4
EXPERIMENTAL PROGRAM

4.1 Material Specification

Five panels were used in this study, all from the same batch of prepreg material. The panels were fabricated using Narmco T300/5208 graphite-epoxy prepreg tape and cured according to the manufacturer's recommendations. All five panels were examined for flaws using a C-scan ultrasonic detector and were found to be of good quality.

Fiber volume determinations were made on all panels. The definition of a percent fiber volume used was:

$$V_f = \frac{\frac{W_f}{\rho_f}}{\frac{W_f}{\rho_f} + \frac{W_m}{\rho_m}} \times 100 \% \quad (4.1)$$

where W_f = weight of fiber
 W_m = weight of matrix
 ρ_f = density of fiber
 ρ_m = density of matrix

Using the relation $W_c = W_f + W_m$, where W_c = weight of composite sample, equation (4.1) may be expressed as

$$V_f = \frac{100}{\frac{\rho_f}{\rho_m} \left(\frac{W_c}{W_f} - 1 \right) + 1} \% \quad (4.2)$$

For T300/5208 the following values were used:

$$\begin{aligned} \rho_f &= 0.0636 \text{ lb/in}^3 && (1.76 \text{ g/cm}^3) \\ \rho_m &= 0.0459 \text{ lb/in}^3 && (1.27 \text{ g/cm}^3) \end{aligned}$$

Therefore, equation (4.2) becomes

$$V_f = \frac{100}{1.386 \left(\frac{W_c}{W_f} - 1 \right) + 1} \% \quad (4.3)$$

Thus a fiber volume determination requires weighing the composite sample (W_c), removing the matrix material using nitric acid digestion, and weighing the fiber (W_f). Fiber volumes for the five panels were determined to be within sixty-seven and seventy-three percent (Table 1).

4.2 Specimen Preparation

A total of twenty-four specimens were constructed, six from each cross-ply panel and three from each quasi-isotropic panel. All specimens were cut to $2.50 \pm .01$ in. ($6.35 \pm .025$ cm) squares. To enhance microscopic observation, two adjacent edges of each specimen were polished in the following manner. Saw marks were removed and the surface made planar using 600 grit paper. After cleaning, the specimen was polished on a metallographic wheel using the final abrasive, a 0.3 micron diamond paste solution. To avoid rounding the edges, the specimen was supported against a piece of aluminum angle while polishing. The supported specimen was rotated around the wheel in the

Table 1. Fiber Volumes of Test Panels

Laminate Configurations in Panel	Specimen 1	Specimen 2	Average
[0/90 ₃] _s [90/0 ₃] _s	68.7	68.8	68.75
[0 ₂ /90 ₂] _s [90 ₂ /0 ₂] _s	69.9	71.9	70.9
[0 ₃ /90] _s [90 ₃ /0] _s	72.6	71.8	72.2
[0/±45/90] _s [90/±45/0] _s	67.8	68.7	68.25
[0/45/90/-45] _s [90/-45/0/45] _s	72.4	72.0	72.2

opposite direction to its motion to avoid a directional bias in the polishing. The procedure required about one-half hour for each surface.

To identify the location of transverse cracks during microscopic observation, thin tape markings were placed in 0.2 in. (0.5 cm) intervals on the specimen surface along the two polished edges (Fig. 20). Such markings were visible as white humps on the specimen edge when viewed through the microscope.

Prior to thermal loading all specimens were dried for at least one week (168 hours) in a Hotpack vacuum oven at 30 in. Hg vacuum and 129°F (327K) and were stored in the chamber prior to testing and between thermal cycles.

4.3 Equipment

The development of transverse cracking during thermal loading was monitored through a 3 x 6 in. (7.6 x 15.2 cm) window on the side of an Applied Test Systems liquid nitrogen cooled environmental chamber (Fig. 21). An analog temperature controller used in conjunction with a shut down valve on the liquid nitrogen supply line provided control of the temperature and cooling rate of the chamber. The temperature of the chamber was monitored with a thermocouple bonded to the surface of a control specimen with silicone rubber and suspended directly above the test specimen.

Specimens were held in a rotating holder during testing to enable the viewing of either polished edge (Fig. 22). Using two nylon cords

ORIGINAL PAGE IS
OF POOR QUALITY

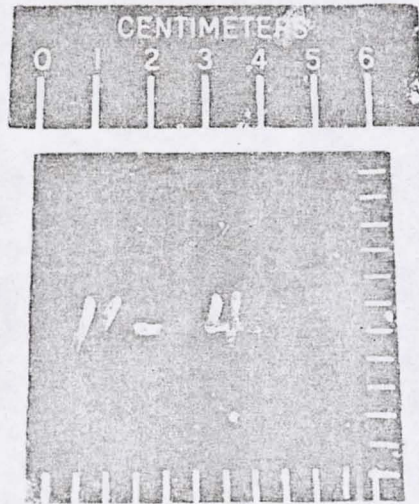


Fig. 20. Thermal Cycling Specimen.

ORIGINAL PAGE IS
OF POOR QUALITY

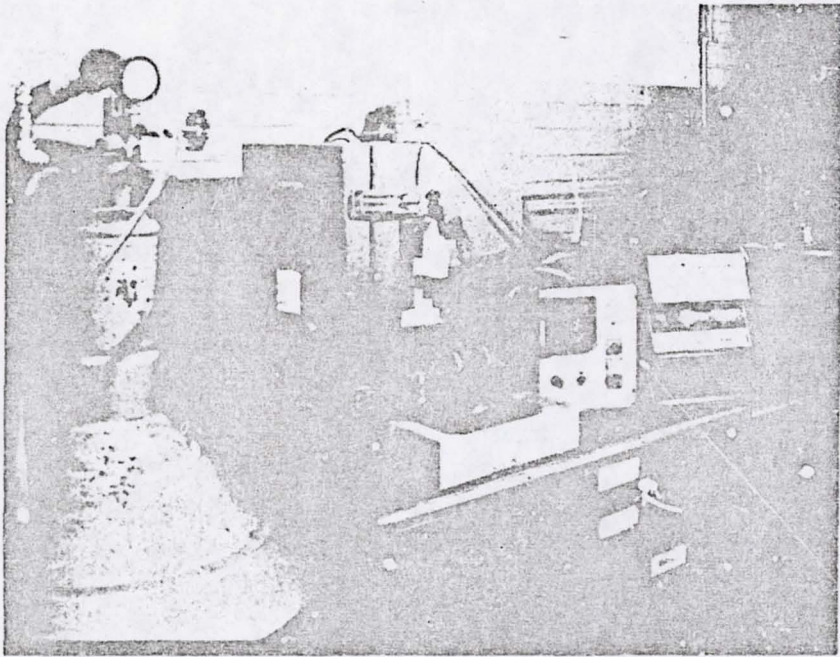


Fig. 21. Experimental Equipment.

ORIGINAL PAGE IS
OF POOR QUALITY

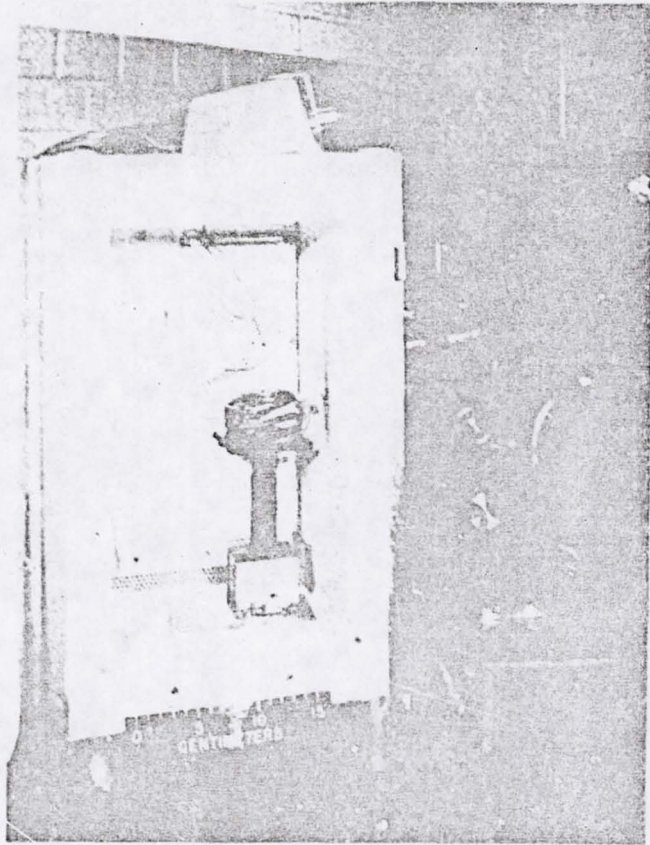


Fig. 22. Interior View of Environmental Chamber.

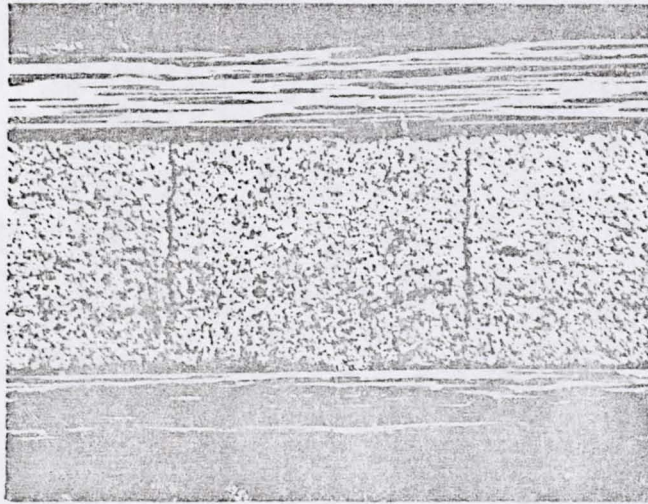
extending out through the top of the chamber, the specimen could be rotated without opening the chamber door.

A 75X microscope with a 2.1 in. (5.3 cm) focal length was used to detect transverse cracking during a test. In detecting cracking, the light source was directed nearly perpendicular to the specimen surface but at a slight angle to help exaggerate surface relief. After completing a thermal cycle, a Unitron microscope was used at higher magnifications (100-400X) to confirm cracking located during the test. Photography was also possible using a Polaroid camera attachment.

4.4 Initial Thermal Cycle Tests

Transverse cracking was monitored in 25°F (14K) increments during the initial cool down to -250°F (116K) beginning at 75°F (297K). A cooling rate of approximately 10°F (5.6K) per minute was used between examination temperatures, at which times the temperature was kept approximately constant. Specimens were tested individually due to the length of time required to carefully examine the two polished edges. Starting at a corner of the specimen, one edge was slowly traversed with the microscope and the location of cracks recorded with respect to the tape markings on the specimen. After completely viewing one edge, the specimen was rotated and the procedure repeated on the adjacent edge. Cracks were visible as thin lines, usually very straight and perpendicular to the top and bottom surface (Fig. 23). A complete test required from four to six hours.

ORIGINAL PAGE IS
OF POOR QUALITY



75X

Fig. 23. Transverse Cracking in a $[0_2/90_2]_S$ Laminate.

After the final examination at -250°F (116K), the specimen was slowly warmed to room temperature, removed from the chamber, and examined at higher magnifications (100-400X) to confirm the presence and location of cracks detected during the test.

4.5 Thermal Cycling Tests

Following the initial thermal cycle tests, fifteen specimens (three from each of the five panels) were thermally cycled between -250 and $+250^{\circ}\text{F}$ (116 and 394K). The initial cool down and return to room temperature was considered as the first thermal cycle. Subsequent thermal cycles consisted of heating from room temperature to 250°F (394K), cooling to -250°F (116K), and heating to room temperature all at a rate of approximately 10°F (5.6K) per minute. The specimens were exposed to a total of twenty thermal cycles. Transverse cracking was monitored with a Unitron microscope (100-400X) at the completion of the first, second, third, fourth, fifth, seventh, tenth, fifteenth, and twentieth cycle.

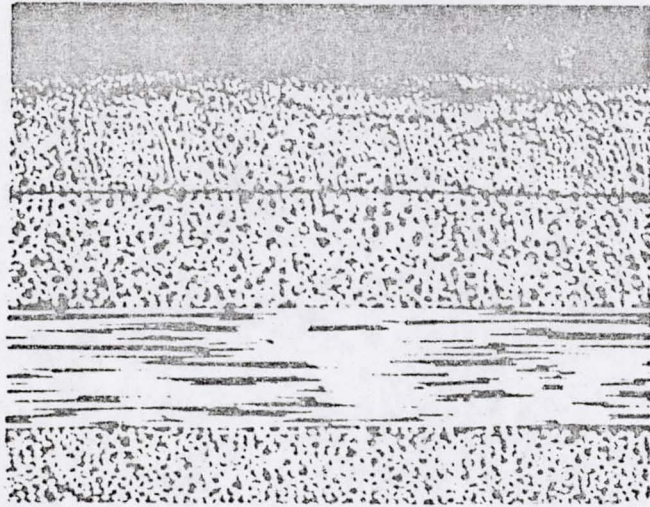
Chapter 5

EXPERIMENTAL RESULTS AND OBSERVATIONS

As described in sections 4.4 and 4.5, two types of tests were performed on the T300/5208 graphite epoxy specimens. Initial thermal cycle tests provided a knowledge of the temperature at which transverse cracking first occurred in a laminate and the crack density as a function of temperature. Thermal cycling tests provided a knowledge of crack density as a function of the number of cycles. In addition, several observations regarding the characteristics of transverse cracking were made while performing these tests. This chapter presents a discussion of all experimental results and related observations.

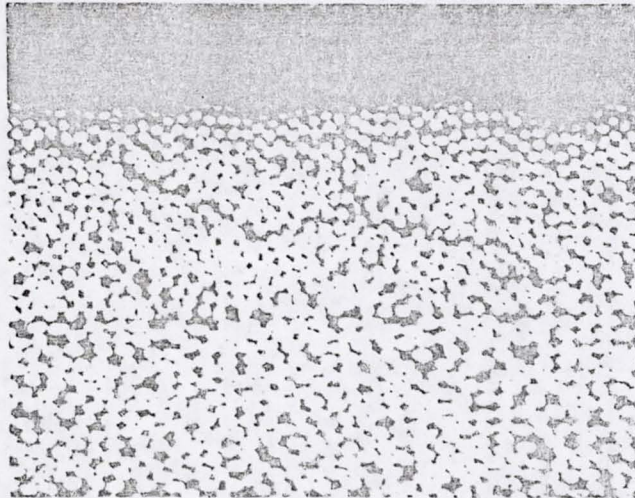
Prior to testing, all specimens were microscopically observed and found to be free of transverse cracks. The outer layers of the specimens cut from the two quasi-isotropic panels, however, were found to have large amounts of matrix damage present in the form of randomly directed crazing (Fig. 24). Consequently, an analysis of transverse cracking in the 90° layers of the $[90/\pm 45/0]_S$ and $[90/-45/0/45]_S$ laminate configurations was not possible. This damage was believed to have occurred either while cutting the specimens or during surface preparation.

Transverse crack densities reported are average densities over the length of the specimen (2.5 in. (6.35 cm)). Crack densities in the laminate configurations with two separate 90° layers ($[90/0_3]_S$, $[90_2/0_2]_S$, and $[90_3/0]_S$ laminates) are given as averages of the two layers.



150X

a) $[90/-45/0/45]_s$ Laminate



300X

b) $[90/+45/0]_s$ Laminate

Fig. 24. Outer 90° Layer Damage Present Prior to Testing in Quasi-Isotropic Laminates.

5.1 Initial Thermal Cycle Test Results

The temperatures at which transverse cracking was first observed in the cross-ply laminate configurations are shown in Table 2. During the initial cool-down from room temperature to -250°F (116K), four of the six cross-ply laminates experienced transverse cracking. A total of 13 of the 36 cross-ply specimen configurations exhibited transverse cracking. Of these 13 specimen configurations, cracks were observed during the test in only 8 specimen configurations; cracks were observed in the remaining 5 after the tests were completed and at higher magnifications.

A comparison of the three cross-ply laminate configurations with interior 90° layers ($[0/90_3]_s$, $[0_2/90_2]_s$, and $[0_3/90]_s$) is shown in Fig. 25. As the thickness of the 90° layer decreased from the $[0/90_3]_s$ laminate to the $[0_3/90]_s$ laminate, the thermal load required to produce transverse cracking decreased. This trend follows the classical lamination theory prediction (Chapter 3) and is a result of the corresponding increase in the 0° layer thickness which produces an increased constraint on the 90° layer and therefore an increased transverse normal stress, σ_2 , at a given thermal load.

A comparison of the temperatures of initial transverse cracking in the three cross-ply laminates with exterior 90° layers ($[90_3/0]_s$, $[90_2/0_2]_s$, and $[90/0_3]_s$) is shown in Fig. 26. Following classical lamination theory analysis, it was expected that transverse cracking would first occur in the $[90/0_3]_s$ laminate followed by the $[90_2/0_2]_s$ laminate and then the $[90_3/0]_s$ laminate. Although the $[90/0_3]_s$ laminate was the first to experience transverse cracking, the $[90_3/0]_s$ was the

Table 2

Temperature of Initial Transverse Cracking, °F (K)

Laminate Configuration	Specimen Number						Initial Cracking Temp.
	1	2	3	4	5	6	
$[0/90_3]_s$	NC	NC	NC	NC	NC	NC	NC
$[90/0_3]_s$	-50 (228)	UD	UD	NC	UD	NC	-50 (-228)
$[0_2/90_2]_s$	-200 (144)	NC	NC	UD	UD	-200 (144)	-200 (144)
$[90_2/0_2]_s$	NC	NC	NC	NC	NC	NC	NC
$[0_3/90]_s$	NC	NC	-175 (158)	NC	NC	NC	-175 (158)
$[90_3/0]_s$	-75 (214)	-175 (158)	-100 (200)	NC	-225 (130)	NC	-75 (214)

NC - No cracking.

UD - Cracking undetected during test, confirmed after test.

ORIGINAL PAGE IS
OF POOR QUALITY

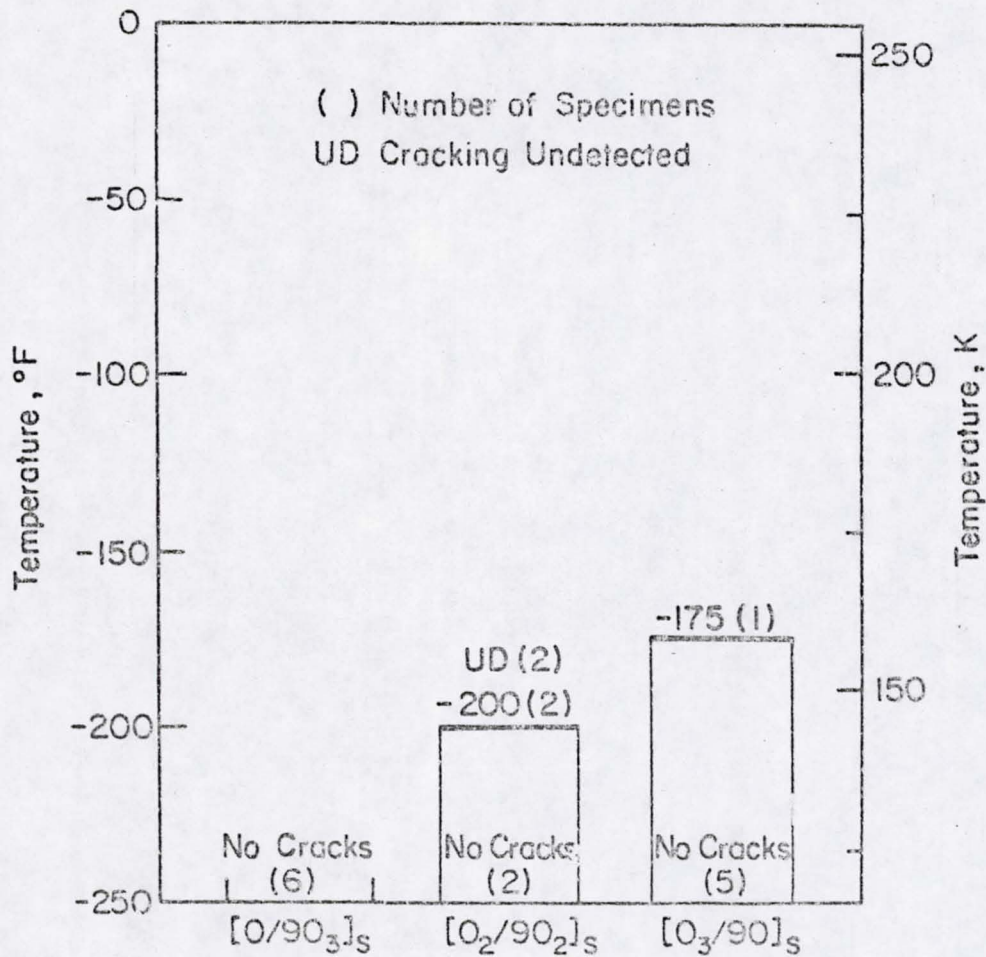


Fig. 25. Temperature of Initial Transverse Cracking in 90° Layer of $[0_n/90_m]_s$ Laminates.

ORIGINAL PAGE IS
OF POOR QUALITY

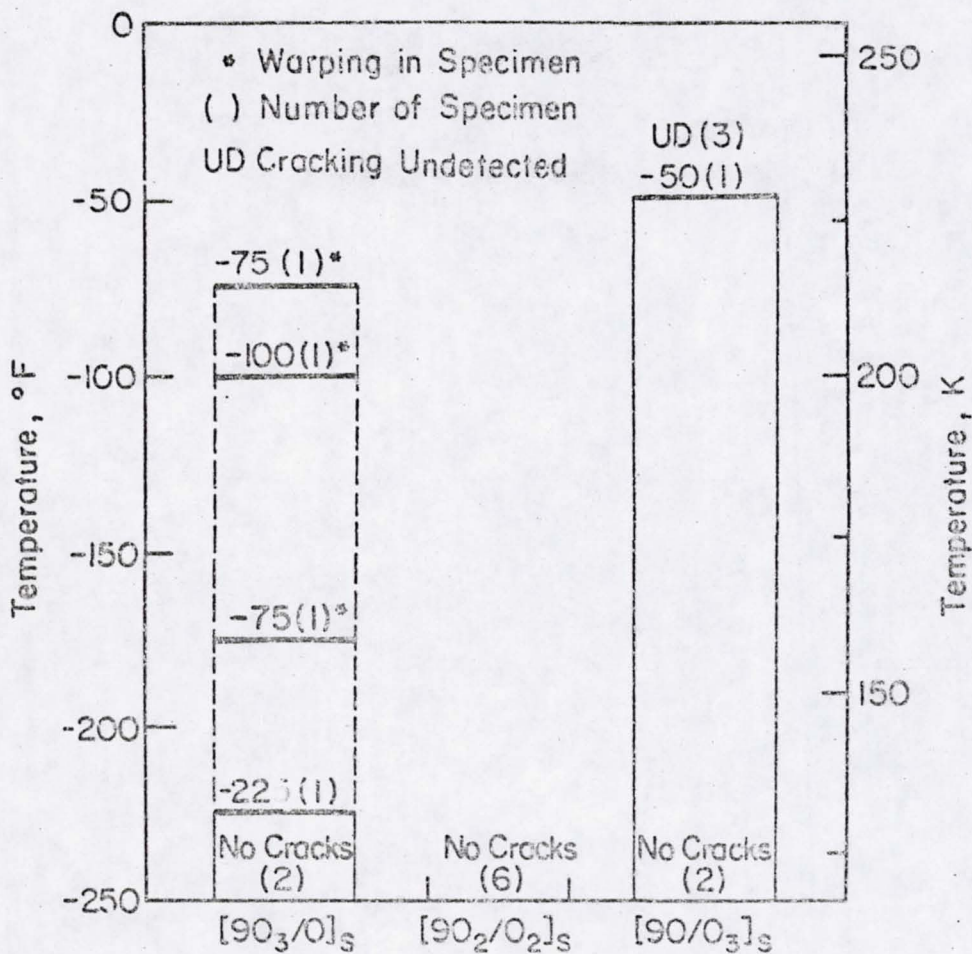


Fig. 26. Temperature of Initial Transverse Cracking
in 90° Layers of $[90_n/0_m]_s$ Laminates.

next to crack and the $[90_2/0_2]_S$ laminate remained crack-free for all tests. All transverse cracking in the $[90_3/0]_S$ laminate prior to -225°F (130K) occurred in specimens 1, 2, and 3 all of which experienced sudden, extensive transverse cracking with noticeable warping (Fig. 27) at increased thermal load levels (-200 , -175 , and -225°F , respectively). Microscopic observation revealed wide transverse cracks often accompanied with delaminations, primarily in the layer at the outside of the curvature (Fig. 28). Some fiber breakage in the adjacent 0° layer was also observed (Fig. 29).

While three $[90_3/0]_S$ laminate specimens experienced extensive transverse cracking and warping, the remaining three specimens tested were found to be more resistant to cracking and did not experience warping. This difference in behavior is believed to be a result of the position of the specimens in the panel from which they were cut. As shown in Fig. 30, specimens 1, 2, and 3 (those experiencing extensive cracking and warping) were cut from a portion of the panel adjacent to the edge after trimming off 0.5 in. (1.3 cm) whereas specimens 4, 5, and 6 (those more resistant to cracking) came from an interior portion of the panel. An investigation of the unused portion of the panel showed variations in the laminate thickness as far as 1.5 in. (3.8 cm) inward from the edge. Therefore, a thickness variation may have been present in specimens 1, 2, and 3. Although these specimens appeared to be uniform in thickness and symmetric under microscopic observations, it is believed that these variations were at least partially responsible for the observed behavior. Since the same specimens were used to study both

ORIGINAL PAGE IS
OF POOR QUALITY

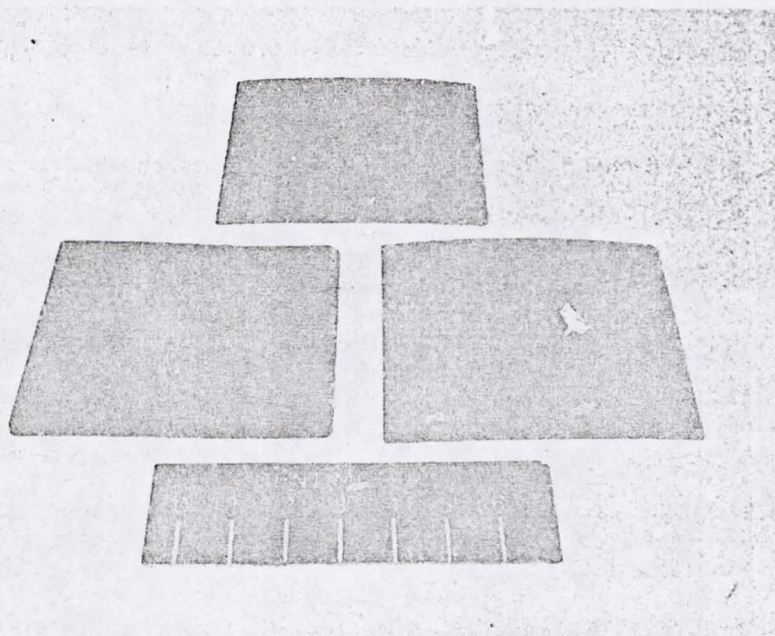
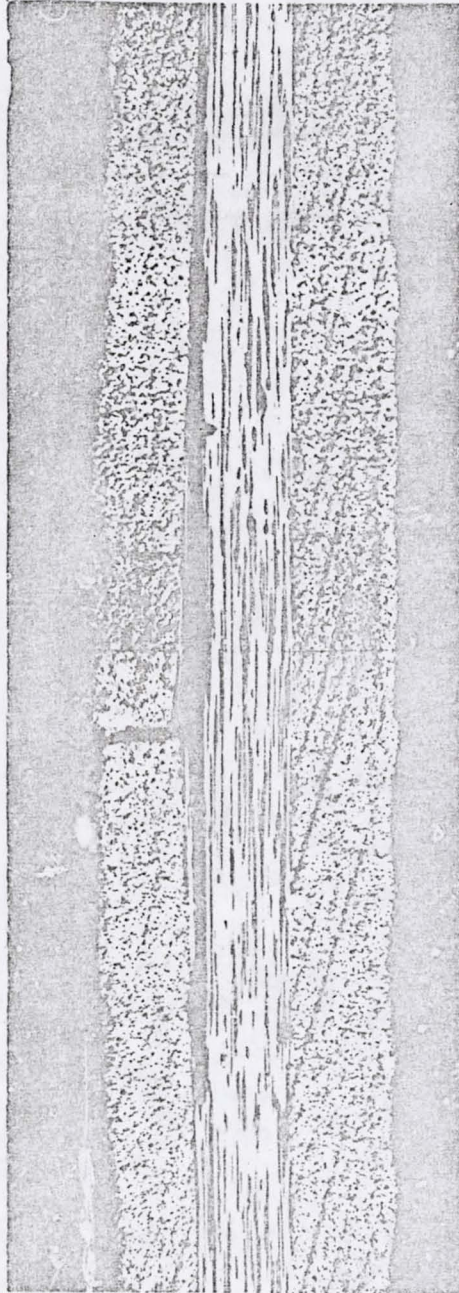


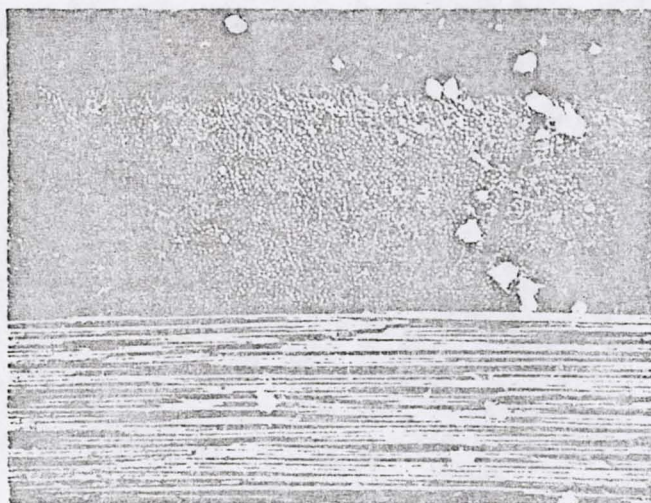
Fig. 27. Warping of $[90_3/0]_s$ Laminate Specimens
1, 2, and 3 Due to Thermal Loading.



50X

Fig. 28. Transverse Cracking and Delamination in
 $[90_3/0]_5$ Laminate (Specimen 2).

ORIGINAL FACE IS
OF POOR QUALITY



100..

Fig. 29. Fiber Breakage in Adjacent 0° Layer of $[90_3/0]_5$ Laminate (Specimen 2).

ORIGINAL PAGE IS
OF POOR QUALITY

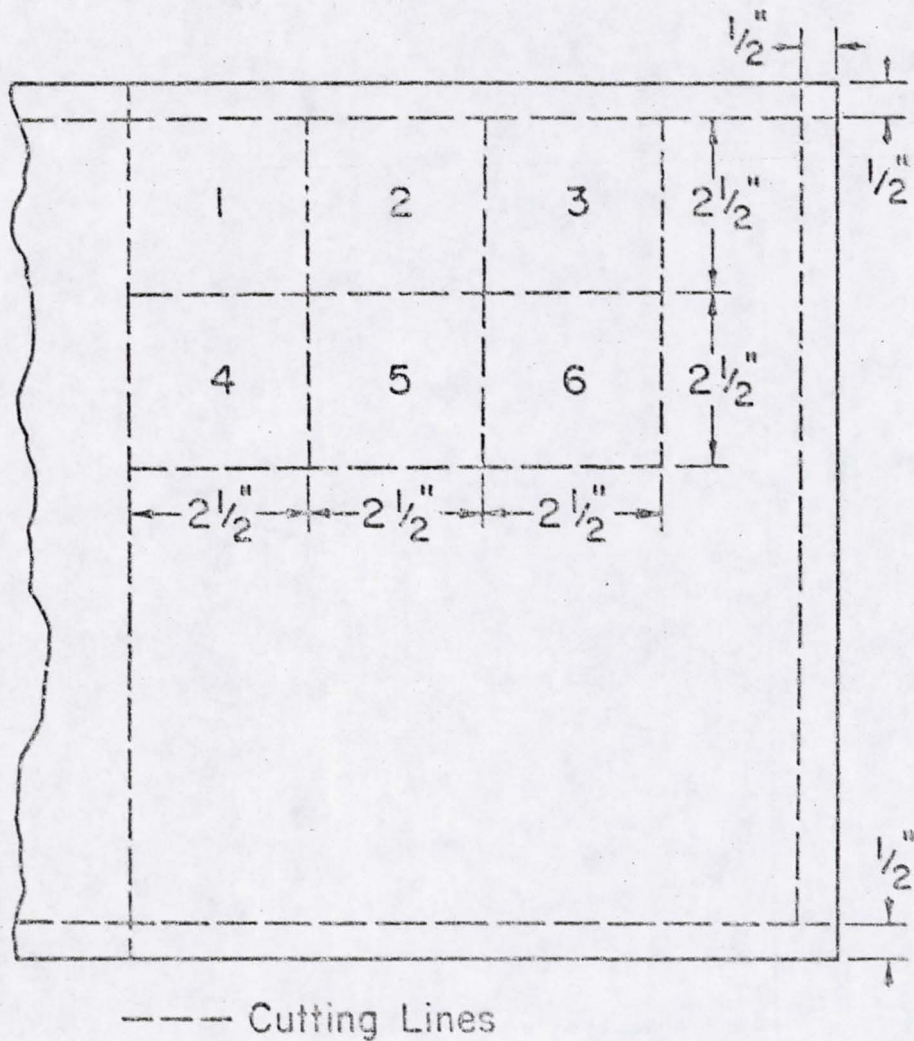


Fig. 30. Location of Test Specimens in $[0_3/90]_s$ and $[90_3/0]_s$ Laminate Panel.

the $[90_3/0]_5$ and $[0_3/90]_5$ laminates, some caution should be used when interpreting the $[0_3/90]_5$ laminate results, especially in the cyclic thermal tests where only specimens 1, 2, and 3 (those experiencing warping) were tested. Five of the six specimens, however, remained uncracked in the $[0_3/90]_5$ laminate configuration through the initial thermal cycle tests.

It is also noted that specimens 1, 2, and 3 used to study both the $[0/90_3]_5$ and $[90/0_3]_5$ laminates were cut from the edge of the panel after trimming off 0.5 in. (1.3 cm). However, no unusual behavior occurred from specimens 4, 5, and 6 which were cut from interior portions of the panel. All other specimens were cut from interior portions of the panels.

After the initial formation of transverse cracking was observed, additional cracking was reported under increasing thermal load in three cross-ply laminate configurations as shown in Table 3. At the completion of the initial cool down to -250°F (116K), all specimens were slowly warmed to room temperature and viewed under a microscope at higher magnifications. Numerous transverse cracks, undetected during the test, were observed in both the $[0_2/90_2]_5$ and $[90/0_3]_5$ laminates. Failure to detect cracks in the $[0_2/90_2]_5$ laminate was believed to be due to the small crack opening whereas slight rounding of the specimen edges during polishing made crack detection difficult in the thin $[0/90_3]_5$ laminate outer layers.

At the completion of the initial cool down, the highest crack density was present in the $[90_3/0]_5$ specimens with warping present

Table 3

Transverse Crack Density Versus Temperature
cracks/in. (cracks/cm)

Laminate Configur- ation	Temperature, °F (K)									Crack Density After Test
	-50 (228)	-75 (214)	-100 (200)	-125 (186)	-150 (172)	-175 (158)	-200 (144)	-225 (130)	-250 (116)	
$[0/90_3]_s$	-	-	-	-	-	-	-	-	-	-
$[90/0_3]_s$	0.0333 (0.131)	0.0333 (0.0131)	0.0667 (0.0262)	0.0667 (0.0262)	0.0667 (0.0262)	0.0667 (0.0262)	0.0667 (0.0262)	0.667 (0.0262)	0.0667 (0.0262)	0.233 (0.0919)
$[0_2/90_2]_s$	-	-	-	-	-	-	0.200 (0.0787)	0.200 (0.0787)	0.533 (0.210)	1.27 (0.499)
$[90_2/0_2]_s$	-	-	-	-	-	-	-	-	-	-
$[0_3/90]_s$ No Warping	-	-	-	-	-	-	-	-	-	-
$[90_3/0]_s$ No Warping	-	-	-	-	-	-	-	0.0667 (0.0262)	0.0667 (0.0262)	0.0667 (0.0262)
$[0_3/90]_s$ Warping	-	-	-	-	-	0.133 (0.0525)	0.133 (0.0525)	0.133 (0.0525)	0.133 (0.0525)	0.133 (0.0525)
$[90_3/0]_s$ Warping	-	0.0667 (0.0262)	0.467 (0.184)	0.667 (0.263)	0.800 (0.315)	1.67 (0.656)	2.20 (0.866)	3.33 (1.31)	3.33 (1.31)	3.40 (1.34)

(specimens 1, 2, and 3). With the exception of the $[0_2/90_2]_S$ laminate, all other laminates had a final crack density of less than 0.25 cracks/in. (0.10 cracks/cm) corresponding to an average of less than one crack per specimen. The location of transverse cracks appeared to be random throughout the initial cycle tests for all laminates and a uniform spacing was not attained in any specimen at the completion of one cycle of thermal loading.

5.2 Cyclic Thermal Test Results

After the initial cool down to -250°F (116K), specimens 1, 2, and 3 from each of the five panels were thermal cycled 20 times between -250 and 250°F (116 and 394K). The effects of the cyclic tests on transverse crack densities are shown in Table 4.

5.2.1 Cross-Ply Laminates

At the completion of 15 thermal cycles, transverse cracking was present in all six cross-ply configurations. Crack densities ranged from 8.27 cracks/in. (3.26 cracks/cm) in the $[0_3/90]_S$ laminate to 0.133 cracks/in. (0.052 cracks/cm) in the $[0/90_3]_S$ laminate. A comparison of the three cross-ply laminate configurations with interior 90° layers is shown in Fig. 31. As the thickness of the 90° layer decreased from the $[0/90_3]_S$ laminate to the $[0_3/90]_S$ laminate, the transverse crack density present at a given number of thermal cycles increased. As was the case with the initial thermal cycle test results for the same three laminates, this trend follows the classical lamination theory predictions of

Table 4
 Transverse Crack Density Versus Number of Thermal Cycles
 cracks/in. (cracks/cm)

Laminate Configuration	Number of Thermal Cycles, 250 to -250 °F (116 to 394 K)								
	1	2	3	4	5	7	10	15	20
$[0/90]_s$	-	-	-	-	-	-	-	0.133 (0.0525)	0.133 (0.0525)
$[90/0]_s$	0.400 (0.158)	1.27 (0.499)	1.60 (0.630)	2.47 (0.971)	2.60 (1.02)	2.87 (1.13)	3.60 (1.42)	4.07 (1.60)	4.07 (1.60)
$[0_2/90_2]_s$	1.07 (0.420)	1.33 (0.525)	1.73 (0.682)	1.73 (0.682)	1.87 (0.735)	2.00 (0.787)	2.53 (0.997)	3.20 (1.26)	3.20 (1.26)
$[90_2/0_2]_s$	-	-	-	-	-	-	0.133 (0.0525)	0.200 (0.0787)	0.200 (0.0787)
$[0_3/90]_s$	0.133 (0.0525)	1.733 (0.682)	2.27 (0.892)	2.93 (1.15)	3.07 (1.21)	5.73 (2.26)	6.00 (2.36)	8.27 (3.25)	8.27 (3.25)
$[90_3/0]_s$	3.33 (1.31)	4.33 (1.71)	4.33 (1.71)	4.33 (1.71)	4.33 (1.71)	4.60 (1.81)	4.67 (1.84)	4.67 (1.84)	4.73 (1.86)
$[0/\pm 45/90]_s$	-	-	-	-	-	-	0.133 (0.0525)	0.133 (0.0525)	0.267 (0.105)
$[90/\mp 45/0]_s$	N/A	N/A	N/A	N/A	N/A	N/A	N/A	N/A	N/A
$[0/45/90/-45]_s$	-	-	-	-	-	-	-	-	-
$[90/-45/0/45]_s$	N/A	N/A	N/A	N/A	N/A	N/A	N/A	N/A	N/A

N/A - Information Not Available Due to Damage Present Prior to Testing.

ORIGINAL PAGE IS
OF POOR QUALITY

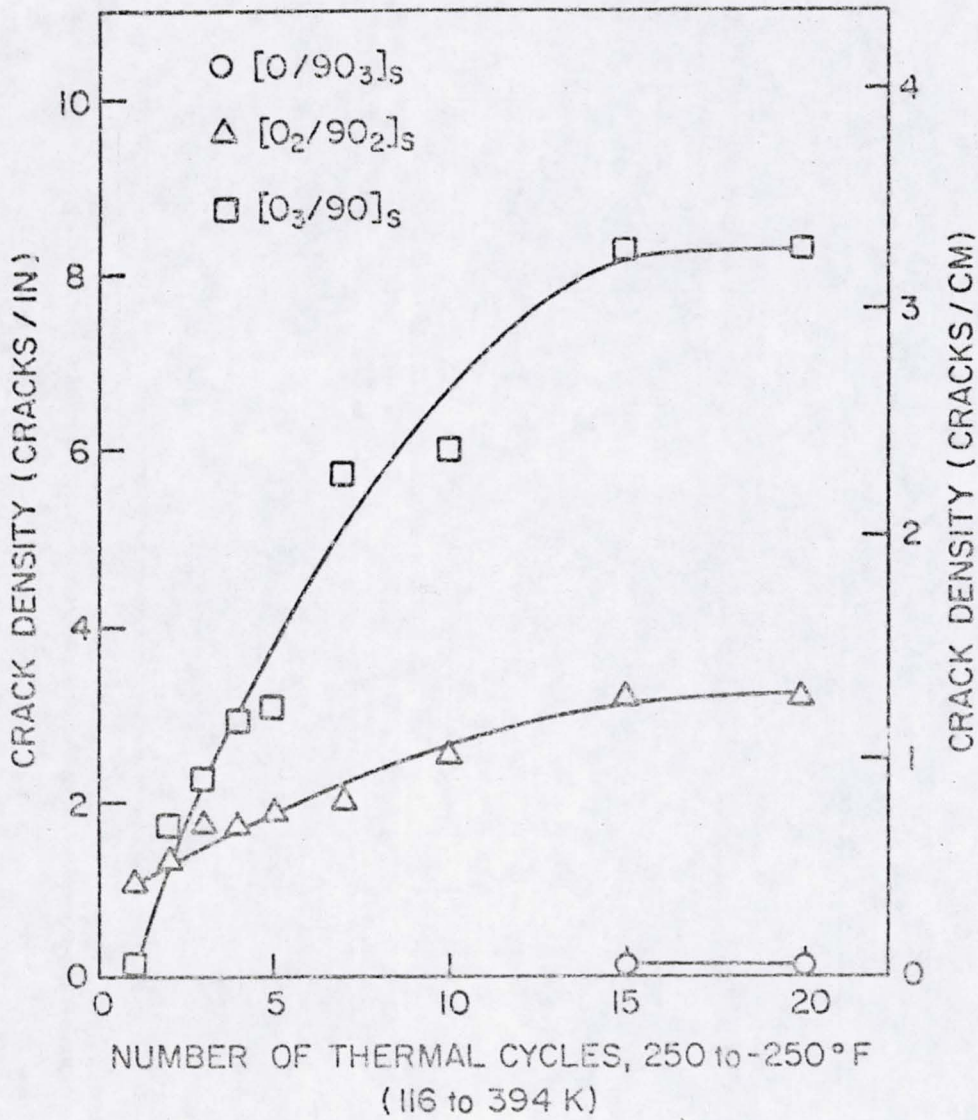


Fig. 31. Cyclic Thermal Test Results for $[0_n/90_m]_s$ Cross-Ply Laminates.

an increasing transverse normal stress, σ_2 , in the 90° layer with decreasing 90° layer thickness at a given thermal load. The differences in crack density increased with the number of thermal cycles up to 15 cycles at which point no additional cracking occurred. Throughout the thermal cycling, the location of transverse cracks still appeared to be quite random and without regular spacing.

A comparison of the three cross-ply laminates with exterior 90° layers is shown in Fig. 32. The $[90_3/0]_S$ laminate, which experienced extensive transverse cracking and warping in the initial cycle, showed a 42% increase in crack density after 20 cycles. This final crack density, however, was only 16% greater than the final density of the $[90/0_3]_S$ laminate, which was nearly crack free after the initial thermal cycle tests. Although predicted to have a higher σ_2 in the 90° layer at a given thermal load than the $[90_3/0]_S$ laminate, the $[90_2/0_2]_S$ laminate remained more resistant to transverse cracking. This may have been a result of the warping present in the $[90_3/0]_S$ specimens as discussed in the previous section. As was the case with the internal 90° layer cross-ply laminates, crack spacings were still irregular after 20 thermal cycles, suggesting that further transverse cracking may have occurred with additional thermal cycling.

An interesting comparison may be made between the crack densities in the $[0_3/90]_S$ and $[90/0_3]_S$ laminates (Fig. 33). In the uncracked state, lamination theory predicts σ_2 to be identical in the two laminates at a given thermal load since they have the same percentage of 0° and 90° layers. It might therefore be expected that the crack densi-

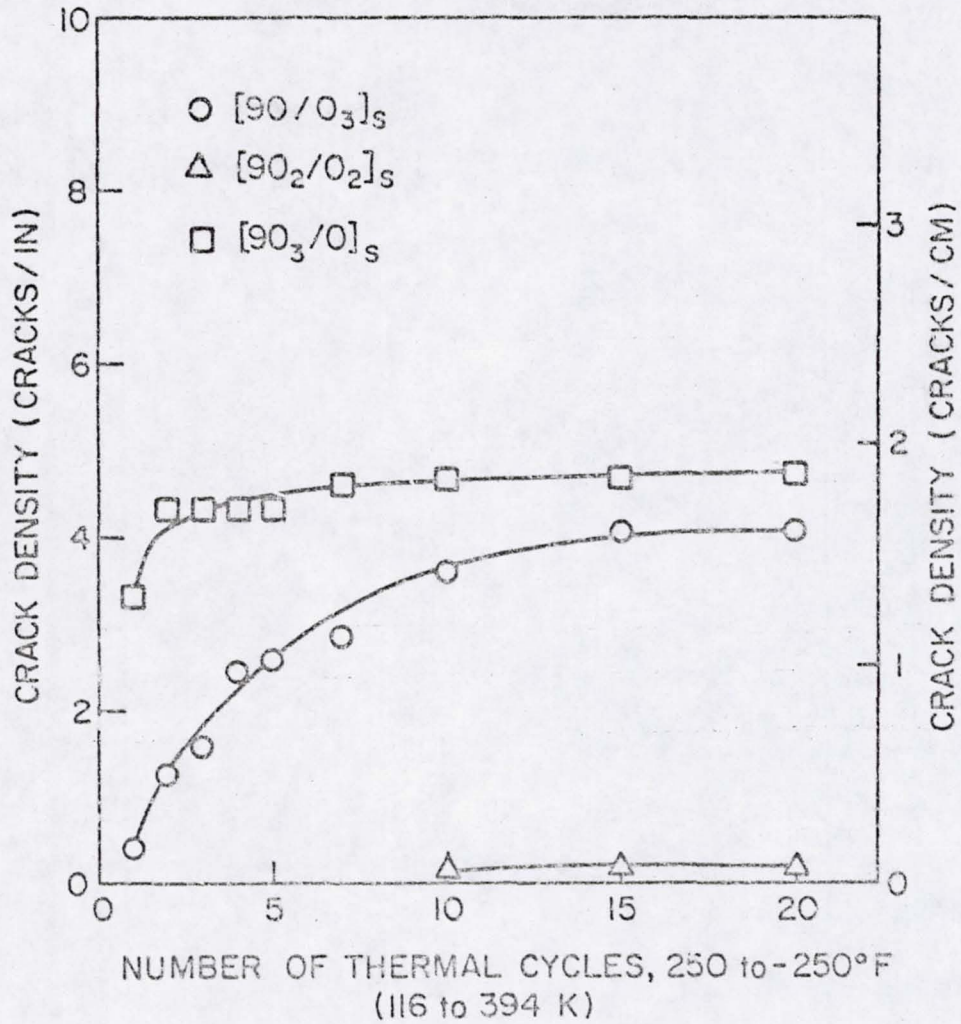
ORIGINAL PAGE IS
OF POOR QUALITY

Fig. 32. Cyclic Thermal Test Results for $[90_m/0_n]_s$ Cross-Ply Laminates.

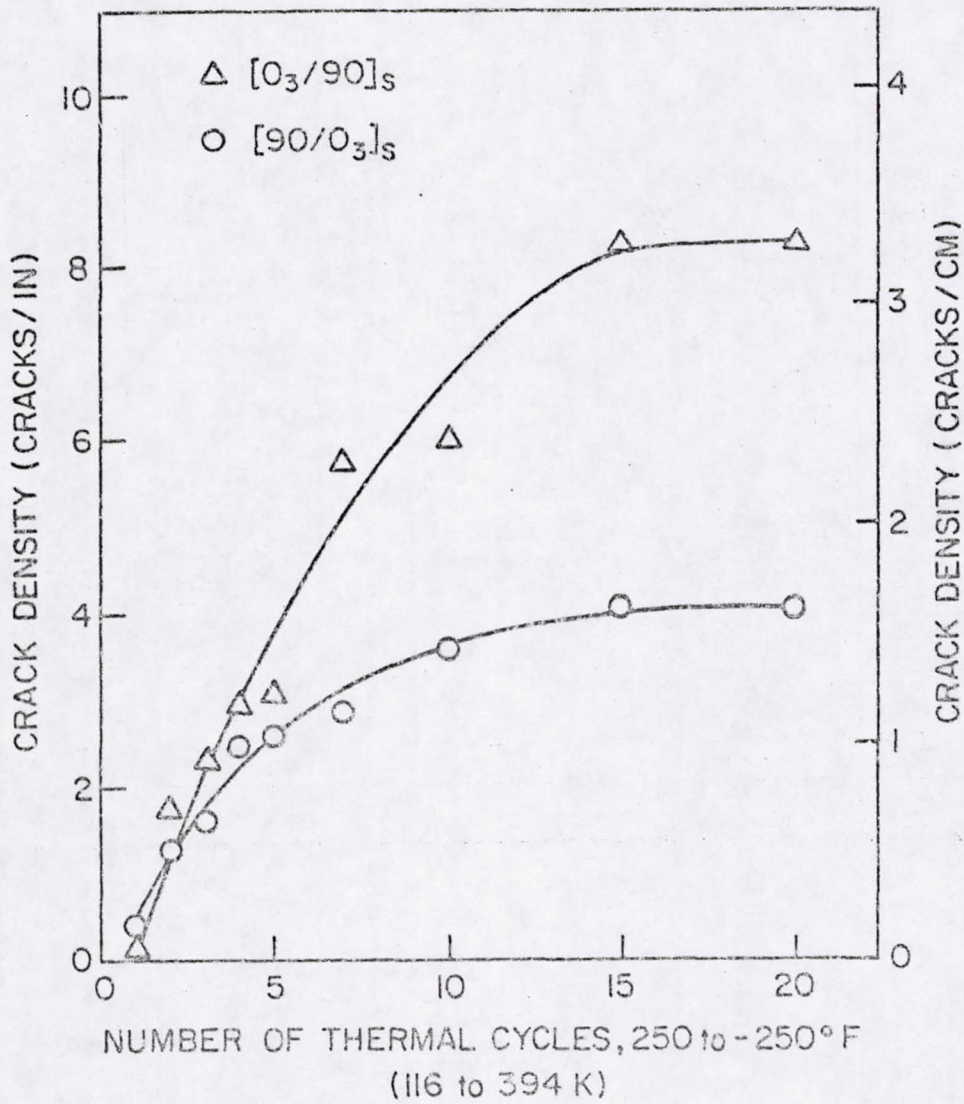
ORIGINAL PAGE IS
OF POOR QUALITY

Fig. 33. Comparison of $[0_3/90]_s$ and $[90/0_3]_s$ Laminate Cyclic Thermal Test Results.

ties would be approximately equal after cyclic loading. After 5 thermal cycles, however, the crack density in the $[0_3/90]_5$ laminate was approximately twice that in the $[90/0_3]_5$, indicating an influence of the laminate stacking sequence on transverse cracking. This difference in crack densities may possibly be understood by considering an equal number of critical flaws producing transverse cracking to be present in the 90° layers of the two laminates per unit volume. A flaw in the $[0_3/90]_5$ laminate would produce a transverse crack extending completely across the 90° layer whereas a transverse crack produced in the $[90/0_3]_5$ laminate would be present in only one of the two exterior 90° layers separated by the 0° layer. The resulting average crack density present in the $[0_3/90]_5$ laminate would be twice that present in the $[90/0_3]_5$ laminate, a fact which agrees with the cyclic thermal test results after five thermal cycles.

Similar reasoning suggests that the transverse crack density present in the $[0_2/90_2]_5$ laminate should be twice that present in the $[90_2/0_2]_5$ laminate. Through 20 thermal cycles, however, the crack density present in the $[0_2/90_2]_5$ laminate was over an order of magnitude greater than in the $[90_2/0_2]_5$ laminate. Considering that such a trend developed in the $[0_3/90]_5$ and $[90/0_3]_5$ laminates only after 5 thermal cycles and that the 90° layers are at a higher state of stress, at a given thermal load, than in the $[0_2/90_2]_5$ and $[90_2/0_2]_5$ laminates, it is suggested that this trend may have developed if more thermal cycles were considered.

A similar comparison of the $[0/90_3]_S$ and $[90_3/0]_S$ laminates is difficult since the $[90_3/0]_S$ laminate specimens used were those which experienced extensive transverse cracking and warping in the initial thermal cycle tests. It is believed that the trend of twice the crack density present in the laminate with an interior 90° layer might only be seen after further thermal cycling, since the state of stress in the 90° layers at a given thermal load is the lowest of all the cross-ply laminates studied.

5.2.2 Quasi-Isotropic Laminates

As previously discussed, analysis of transverse cracking in the outer layers of the quasi-isotropic panels ($[90/\mp 45/0]_S$ and $[90/-45/0/45]$ laminates) was not possible due to extensive matrix damage present prior to testing. The $[0/\pm 45/90]_S$ laminate experienced limited transverse cracking beginning after ten cycles. No cracking was reported in the $[0/45/90/-45]_S$ laminate or in any of the $+45^\circ$ or -45° layers of any laminate. While the quasi-isotropic laminates were found to be generally resistant to transverse cracking, a slight increase in resistance was exhibited when the stacking sequence was changed from $[0/\pm 45/90]_S$ to $[0/45/90/-45]_S$ resulting in a thinner 90° layer.

5.3 Correlation with Analytical Studies

5.3.1 Determination of In Situ Transverse Strength

Experimental results for the initial temperature of transverse cracking along with a classical lamination theory analysis (Section

3.2.1) may be used to determine the in situ transverse strength, σ_2^{ult} , of the laminates investigated. In making these determinations, the experimentally determined temperature of initial transverse cracking in a laminate is input into a classical lamination theory analysis and the resulting transverse stress in the 90° layer (σ_2^{ult}) determined. Results for the six cross-ply laminates are shown in Fig. 34. All cross-ply laminates exhibit an in situ transverse strength, σ_2^{ult} , at least 1.9 times greater than the uniaxial transverse strength $Y_t(T)$. Some specimens from all six laminates remained uncracked at -250°F (116K), indicating that σ_2^{ult} may be somewhat greater than the maximum values designated by dashed lines in Fig. 34.

A 90° layer thickness effect on σ_2^{ult} may be seen in the $[0_n/90_m]_s$ cross-ply laminates. As the thickness of the 90° layer decreases, σ_2^{ult} increases. This result is in agreement with ref. [34] and may be a result of the corresponding increase in the constraint imposed by an increasing thickness of adjacent 0° layers. A similar thickness effect was not evident in the $[90_n/0_m]_s$ cross-ply laminates.

Since all four quasi-isotropic laminates remained uncracked throughout the initial cool down to -250°F , only a lower limit for σ_2^{ult} may be determined. At -250°F , $\sigma_2^{ult} = 2.66 Y_t(T)$ in the 90° layers of the four quasi-isotropic laminates.

In determining in situ strength using experimental results and a classical lamination theory analysis, it is noted that finite length specimens with free edges were used in the experimental study whereas

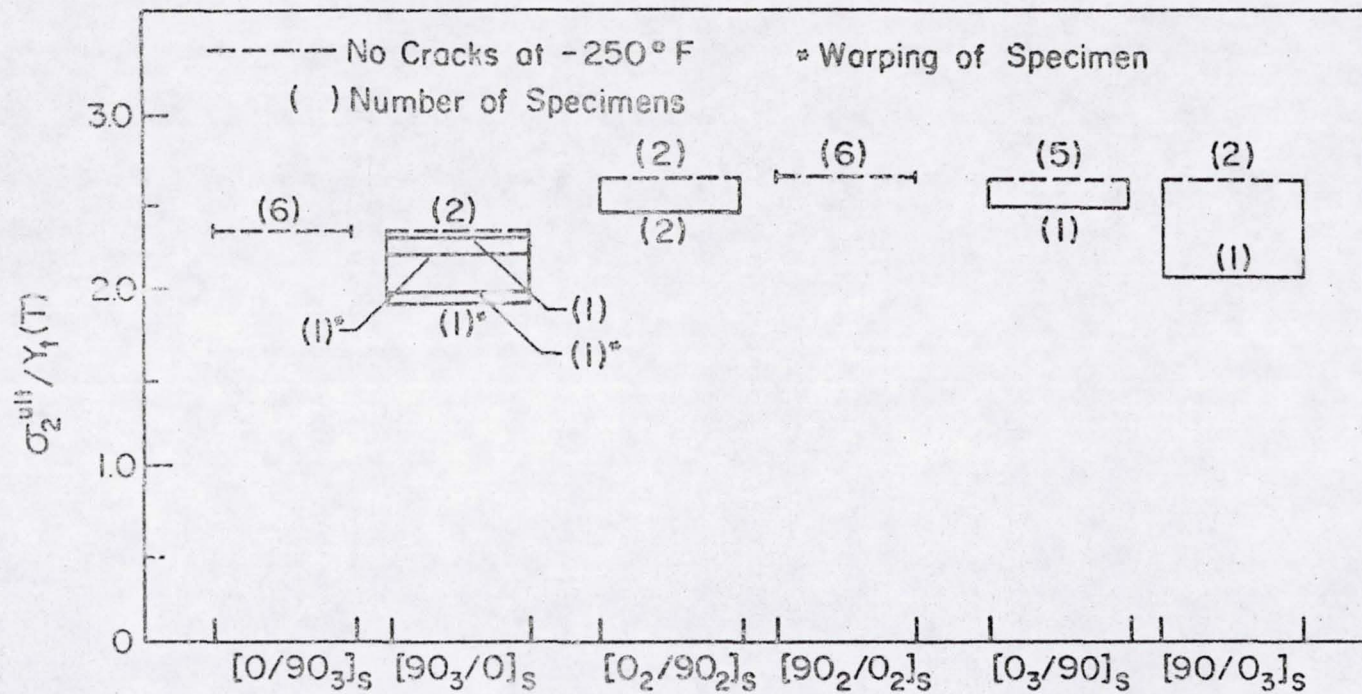


Fig. 34. In Situ Transverse Strength of 90° Layers in Cross-Ply Laminates.

classical lamination theory assumes infinite length laminates. Nagarkar and Herakovich [32] studied finite width composite laminates and found the thermal stress, σ_2 , in the 90° layer of a $[0/90]_c$ T300/5208 laminate to be 26 percent greater at the free edge than in the interior portion of the laminate. For a $[90/0]_s$ laminate, σ_2 at the free edge was 16% greater than in the interior. Therefore, the temperature of initial transverse cracking may correspond to a crack forming at the free edge of the specimen whereas the stress predicted with classical lamination theory is the lower value present in the interior of the specimen. Thus, the in situ transverse strength, σ_2^{ult} , may be even greater than predicted.

5.3.2 Crack Spacing in $[0_2/90_2]_s$

A comparison of the crack spacing observed experimentally (section 5.1) and predicted analytically (section 3.3.3) for the $[0_2/90_2]_s$ laminate during the initial cool down to -250°F (116K) is shown in Fig. 35. The uniform crack spacings predicted with a finite element analysis (0.09 in. at -200°F and 0.045 in. at -250°F) are in great contrast to the sparse, randomly located transverse cracking observed experimentally. As shown in Fig. 36, transverse crack spacing was still non-uniform throughout the specimen after 20 thermal cycles. However, some localized regions had developed approximately uniform crack spacings which approached the predicted spacing. It is believed that the predicted uniform crack spacing may have developed throughout the length of the specimen with additional thermal cycling.

C-2

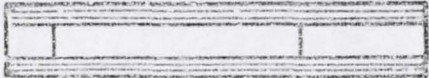
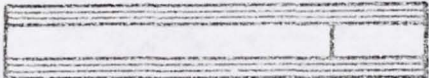

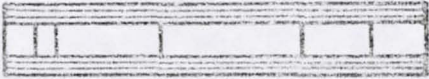
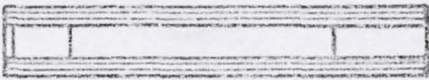

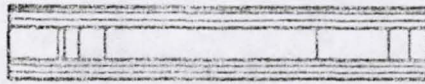
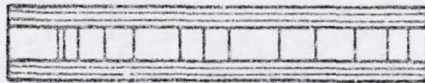
Temp. °F (K)	Experimental Results	Analytical Predictions
-200 (144)	 Specimen 1  Specimen 6	
-250 (116)	 Specimen 1  Specimen 6	

Fig. 35. Transverse Cracking During Thermal Loading in $[0_2/90_2]_5$ Laminate.

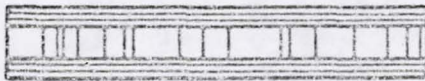
ORIGINAL PAGE IS
OF POOR QUALITY



1 Cycle



5 Cycles



10 Cycles



20 Cycles

Fig. 35. Transverse Cracking During Thermal Cycling
in $[0_2/90_2]_S$ Laminate, Specimen 1.

5.4 Observations

During both the initial thermal cycle tests and cyclic thermal tests, all transverse cracks were found to be fully propagated across the thickness of the 90° layer upon first detection. The location of the initial transverse cracks appeared to be random, favoring neither the end nor the midpoint of the specimen. Transverse cracks tended to avoid resin rich regions, and as shown in Fig. 37, generally changed direction to follow the edge of the region rather than pass through it.

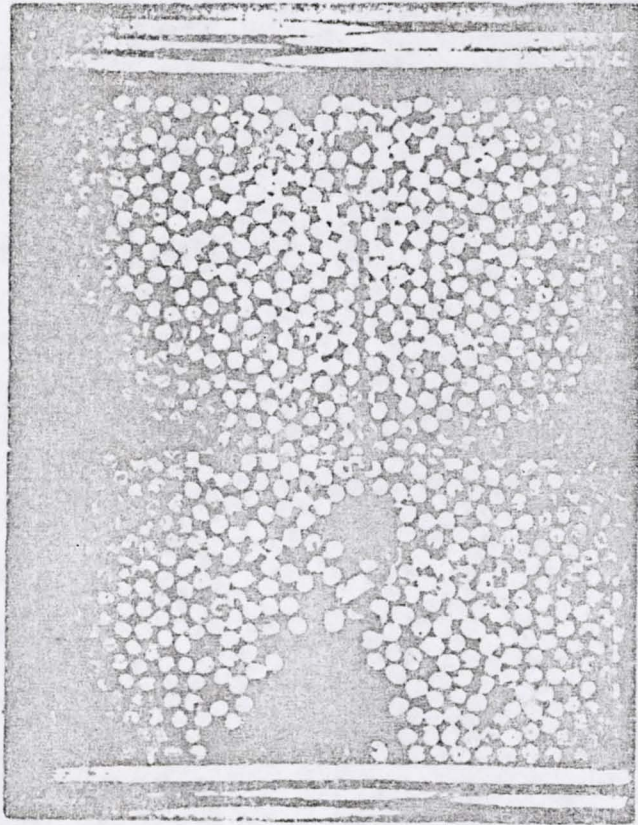
As may be seen in Fig. 38, transverse cracking involved fiber splitting in addition to matrix cracking. Generally, fiber splitting provided for a straight crack path, seldom meandering from its previous direction. Fiber splitting was observed in all laminates exhibiting transverse cracking.

Transverse cracks were seen to vary in width across the 90° layer, tapering when approaching an adjacent layer as shown in Fig. 38. Such tapering was present in all laminates exhibiting cracking and indicates the constraint placed on the cracked 90° layer by the adjacent layer.

The presence of delaminations accompanying transverse cracks was observed in the $[90_3/0]_5$ laminate specimens experiencing warping as previously discussed (Fig. 28). Such delaminations generally followed the interface between adjacent layers, but as shown in Fig. 29, sometimes fiber breakage occurred in the adjacent 0° layer. Delaminations were sometimes found to grow in length with progressive thermal cycling.

Some transverse cracks in the cross-ply laminates with interior 90° layers were seen to branch into two distinct cracks as shown in

ORIGINAL PAGE IS
OF POOR QUALITY



400X

Fig. 37. Transverse Cracking Around a Resin Rich
Region in a $[0_2/90_2]_5$ Laminate.

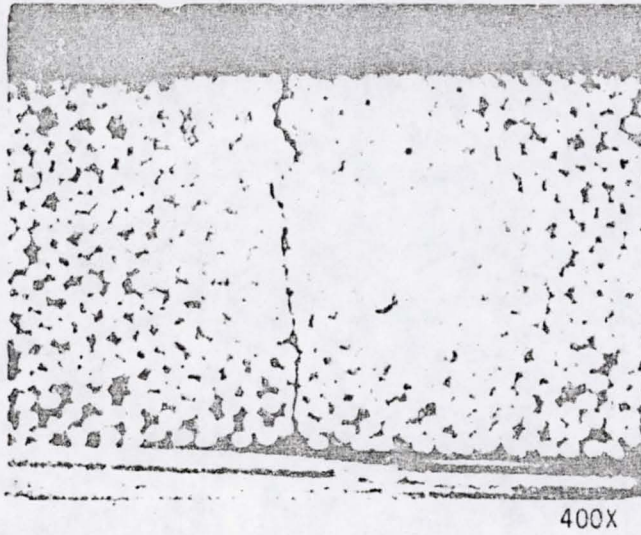
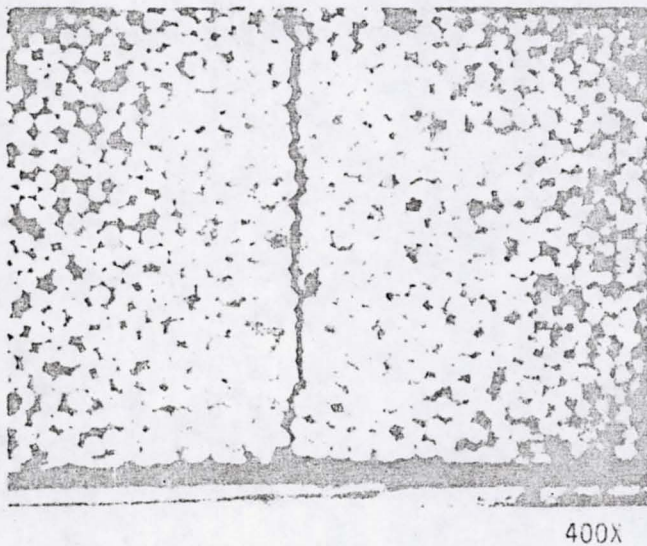
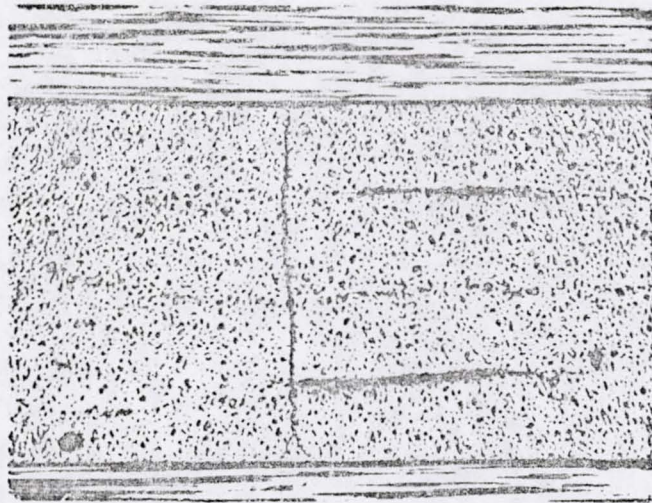
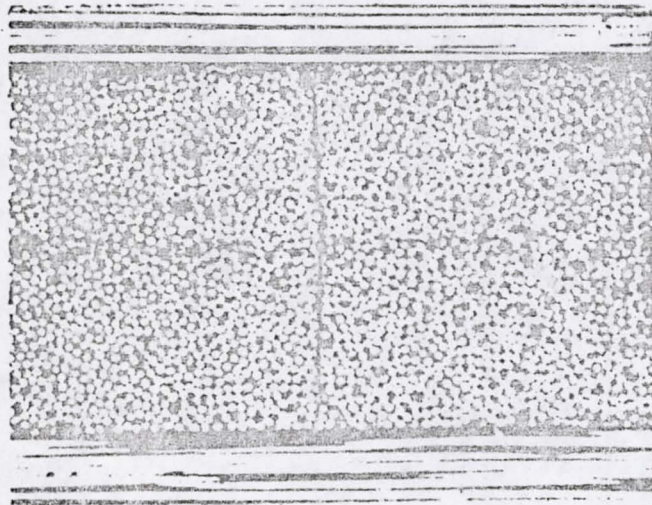
ORIGINAL PAGE IS
OF POOR QUALITYa) $[90/0_3]_5$ Laminateb) $[0_2/90_2]_5$ Laminate

Fig. 38. Fiber Splitting and Transverse Crack Tapering.

Fig. 39. Generally, the point at which the branching occurred was only a few fiber diameters from the adjacent 0° layer. No crack branching was seen in any of the remaining laminates investigated.



100X

a) $[0_2/90_2]_S$ Laminate

200X

b) $[0_3/90]_S$ Laminate

Fig. 39. Transverse Crack Branching.

Chapter 6

CONCLUSIONS

This study has investigated the characteristics of thermally-induced transverse cracks, both experimentally and analytically, in T300/5208 graphite-epoxy laminates. Of particular interest was the determination of the temperature at which transverse cracks initially form, the state of stress in the vicinity of a transverse crack, the initial equilibrium transverse crack spacing, the formation of additional transverse cracking under increased thermal load and under thermal cycling, and the influence of transverse cracking on the laminate CTE. The following conclusions may be drawn as a result of this study:

1. The T300/5208 laminates studied in this investigation are free of cracks after curing.
2. Four of the six cross-ply laminates experience transverse cracking during the initial cool down to -250°F (116K) whereas all quasi-isotropic laminates remain crack free.
3. Increasing the percentage of the 90° layer in the $[0_n/90_m]_s$ laminate results in an increased thermal load required to produce transverse cracking.
4. The in situ transverse strength of the 90° layer is more than 1.9 times greater than the transverse strength of the unidirectional 90° material.
5. The initial equilibrium transverse crack spacing in the $[0_2/90_2]_s$ laminate is quite random and much greater than the uniform crack spacing predicted analytically.

6. A through the thickness gradient in the transverse tensile stress is present in the cracked 90° layer, decreasing in magnitude with distance from the transverse crack and resulting in a higher stress near the adjacent constraining layer than in the interior portion of the 90° layer.

7. The initial equilibrium transverse crack spacing predicted in the $[0_2/90_2]_5$ laminate with a generalized plane strain finite element analysis corresponds well to that predicted with a modified shear-lag analysis.

8. All six cross-ply laminates as well as the $[0/\pm 45/90]_5$ quasi-isotropic laminate exhibit transverse cracking following 20 thermal cycles between 250 and -250°F (116 and 394K).

9. A uniform transverse crack spacing is not present in any of the laminates studied following 20 thermal cycles, but the uniformity of crack spacing increases with increasing thermal cycles.

10. The cross-ply laminates exhibit a rather sharp drop in laminate CTE at low crack densities (less than 50 cracks/in. (19.7 cracks/cm)).

11. The quasi-isotropic laminates exhibit a decrease in laminate CTE with increasing crack density, but at a much lower rate and to a lesser extent than the cross-ply laminates.

12. While transverse cracking was able to be detected in a majority of the laminates with a $75\times$ microscope, higher magnification is needed to confirm the presence of cracks in all laminates studied.

REFERENCES

1. Bailey, J. E. and Parvizi, A., "On Fiber Debonding Effects and the Mechanism of Transverse-Ply Failure in Cross-Ply Laminates of Glass Fiber/Thermoset Composites," J. Materials Science, Vol. 16, 1981, pp. 649-659.
2. Bailey, J. E., Curtis, P. T., and Parvizi, A., "On the Transverse Cracking and Longitudinal Splitting Behavior of Glass and Carbon Fiber Reinforced Epoxy Cross Ply Laminates and the Effect of Poisson and Thermally Generated Strain," Proc. Royal Soc. (London), Ser. A, Vol. 366, 1979, pp. 599-623.
3. Garrett, K. W. and Bailey, J. E., "Multiple Transverse Fracture in 90° Cross-Ply Laminates of a Glass Fiber-Reinforced Polyester," J. Materials Science, Vol. 12, 1977, pp. 157-168.
4. Mills, J. S., Herakovich, C. T. and Davis, J. G., "Transverse Microcracking in Celion 6000/PMR-15 Graphite-Polyimide," Virginia Polytechnic Institute and State University, VPI-E-79-35, December 1979.
5. Crossman, F. W. and Wang, A. S. D., "The Dependence of Transverse Cracking and Delamination on Ply Thickness in Graphite/Epoxy Laminates," Symposium on Damages in Composite Materials: Basic Mechanisms, Accumulation, Tolerance and Characterization, Bel Harbour, Florida, 1980.
6. Parvizi, A., Garrett, K. W. and Bailey, J. E. "Constrained Cracking in Glass Fiber-Reinforced Epoxy Cross-Ply Laminates," J. Materials Science, Vol. 13, 1978, pp. 195-201.
7. Reifsnider, K. L. and Highsmith, A., "Characteristic Damage States: A New Approach to Representing Fatigue Damage in Composite Laminates," Materials, Experimentation and Design in Fatigue. London: Westbury House, 1981. pp. 246-260.
8. Kriz, R. D., Stinchcomb, W. W. and Tenney, D. R., "Effects of Moisture, Residual Thermal Curing Stresses and Mechanical Load on the Damage Development in Quasi-Isotropic Laminates," Virginia Polytechnic Institute and State University, VPI-E-80-5, February 1980.
9. Spain, R. G., "Thermal Microcracking of Carbon Fiber/Resin Composites," Composites, Vol. 2, March 1971, pp. 33-37.
10. Chamis, C. C., "Residual Stresses in Angle Plieed Laminates and Their Effects on Laminate Behavior," NASA TM 78835, April 1978.

11. Hahn, H. T. and Pagano, N. J., "Curing Stresses in Composite Laminates," J. Composite Materials, Vol. 9, January 1975, pp. 91-107.
12. Weitsman, Y., "Residual Thermal Stresses Due to Cool-Down of Epoxy Resin Composites," J. Applied Mechanics, Vol. 46, No. 3, September 1979, pp. 563-567.
13. Daniel, I. M. and Liber, T., "Effect of Laminate Construction on Residual Stresses in Graphite/Polyimide Composites," Experimental Mechanics, Vol. 17, No. 1, January 1977, pp. 21-25.
14. Bowles, D. W., "The Effects of Microcracking on the Thermal Expansion of Graphite-Epoxy Composites," Large Space Systems Technology - 1981, NASA CP-2215, November, 1981.
15. Casswell, T. G., "Transverse Microcracking of T300/5208 Graphite-Epoxy Due to Thermal Loading," Senior Project, Dept. of Engineering Science and Mechanics, Virginia Polytechnic Institute and State University, July 1982.
16. Camahort, J. L., Rennhack, E. H., and Coons, W. C., "Effects of Thermal Cycling Environment on Graphite/Epoxy Composites," Environmental Effects on Advanced Composite Materials, ASTM STP 602, American Society for Testing and Materials, 1976, pp. 37-49.
17. Fahmy, A. A. and Cunningham, T. G., "Investigation of Thermal Fatigue in Fiber Composite Materials," NASA CR-2641, July 1976.
18. Berman, L. D., "Reliability of Composite Zero-Expansion Structures for Use in Orbital Environment," Composite Reliability, ASTM STP 580, American Society for Testing and Materials, 1975. pp. 288-297.
19. Parvizi, A. and Bailey, J. E., "On Multiple Transverse Cracking in Glass Fiber Epoxy Cross-Ply Laminates," J. Materials Science, Vol. 13, 1978, pp. 2131-2136.
20. Plunkett, R., "Damping in Fiber Reinforced Laminated Composites at High Strain," J. Composite Materials, Vol. 14 Supplement, 1980, pp. 109-117.
21. Stevens, G. T. and Lupton, A. W., "Some Factors Controlling Transverse Cracking in Cross-Ply Laminates," J. Materials Science, Vol. 12, March 1977, pp. 1706-1708.
22. Wang, A. S. D. and Crossman, F. W., "Initiation and Growth of Transverse Cracks and Edge Delaminations in Composites Laminates. I: An Energy Method," J. Composites Materials, Vol. 14 Supplement, 1980, pp. 71-87.

23. Crossman, F. W., Warren, W. J., Wang, A. S. D. and Law, G. E., Jr., "Initiation and Growth of Transverse Cracks and Edge Delaminations in Composite Laminates. II: Experimental Correlation," J. Composite Materials, Vol. 14 Supplement, 1980, pp. 88-106.
24. Rybicki, E. F., Schmueser, D. W. and Fox, J., "An Energy Release Rate Approach for Stable Crack Growth in the Free Edge Delamination Problem," J. Composite Materials, Vol. 11, October 1977, pp. 470-487.
25. Bowles, D. E., "The Effect of Microcracks on Composite Thermal Expansion," to be published.
26. Milkovich, S. and Herakovich, C. T., "Temperature Dependence of Elastic and Strength Properties of T300/5208 Graphite-Epoxy," VPI-E-83-9, Virginia Polytechnic Institute and State University, Blacksburg, VA, May 1983.
27. Private communication with Dr. Ronald D. Kriz, Fracture and Deformation Division, National Bureau of Standards, Boulder, Colorado.
28. Short, J. S., Hyer, M. W., Post, D., Bowles, D. E., Tompkins, S. S., "Development of a Priest Interferometer for Measurement of Thermal Expansion of Graphite-Epoxy in the Temperature Range 116-366K," VPI-E-82-18, Virginia Polytechnic Institute and State University, Blacksburg, VA, September, 1982.
29. Bowles, D. E., Post, D., Herakovich, C. T., Tenney, D., "Moire Interferometry for Thermal Expansion of Composites," Experimental Mechanics, Vol. 21, No. 12, pp. 441-447, Dec. 1981.
30. Brooks, E. W., Jr., Herakovich, C. T., Post, D., Hyer, M. W., "Advances in Moire Interferometry for Thermal Response of Composites," VPI-E-82-4, Virginia Polytechnic Institute and State University, Blacksburg, VA, March, 1982.
31. Stein, P. A., Undergraduate Student, Engineering Science and Mechanics, VPI & SU, unpublished data.
32. Nagarkar, A. P. and Herakovich, C. T., "Nonlinear Temperature Dependent Failure Analysis of Finite Width Composite Laminates," VPI-E-79-36, Virginia Polytechnic Institute and State University, Blacksburg, VA, December, 1979.
33. Chamis, C. C. and Sullivan, T. L. "In Situ Strength: An Initial Assessment," NASA TM-73771, March, 1978.
34. Flaggs, D. L. and Kural, M. H., "Experimental Determination of the In Situ Transverse Lamina Strength in Graphite/Epoxy Laminates," J. Composite Materials, Vol. 16, March 1982. pp. 103-116.

35. Tsai, S. W., "Strength Characteristics of Composite Materials," NASA CR-224, April, 1965.
36. Pagano, N. J. and Hahn, H. T., "Evaluation of Composite Curing Stresses," Composite Materials: Testing and Design (Fourth Conference), ASTM STP 617, American Society for Testing and Materials, 1977, pp. 317-329.
37. Private communication with Mr. D. E. Bowles.
38. Jones, R. M., Mechanics of Composite Materials, Scripta Book Company, Washington, DC, 1975.
39. Buczek, M. B., Herakovich, C. T., "Finite Element Models for Predicting Crack Growth Characteristics in Composite Materials," VPI-E-82-29, Virginia Polytechnic Institute and State University, Blacksburg, VA, October, 1982.
40. Branca, T. R. "Creep of a Uniaxial Metal Matrix Composite Subjected to Axial and Normal Lateral Loads," TAM Report 341, Univ. Illinois, June, 1971.
41. Crane, D. A. and Adams, D. F., "Finite Element Micromechanical Analysis of a Unidirectional Composite Including Longitudinal Shear Loading," Report UWME DR-001-101-1, Univ. Wyoming, February 1981.

APPENDIX A

T300/5208 Graphite-Epoxy Properties

Table A.1 Material Property Coefficients for T300/5208 Graphite-Epoxy

Second Order Least Squares Fit Coefficients to be used in the Equation:

$$\text{Property (T)} = C_0 + C_1T + C_2T^2 \quad (T \text{ in } ^\circ\text{F})$$

Property	C_0	C_1	C_2	Reference
E_1 (Psi)	2.13×10^7	-5.57×10^2	2.32×10^2	26
E_2, E_3 (Psi)	1.63×10^6	-4.10×10^2	2.68×10^0	26,27
G_{12}, G_{13} (Psi)	1.06×10^6	-6.00×10^2	-1.22×10^0	26
G_{23} (Psi)	4.87×10^5	-	-	32
ν_{12}, ν_{13}	3.43×10^{-1}	-5.65×10^{-4}	1.22×10^{-7}	26
ν_{23}	4.90×10^{-1}	-	-	32
x_T (Psi)	2.01×10^5	1.05×10^2	1.36×10^{-2}	26
y_T (Psi)	4.04×10^3	-1.73×10^{-1}	1.17×10^{-2}	26
α_1 ($\epsilon/^\circ\text{F}$)	-1.24×10^{-7}	1.34×10^{-11}	5.45×10^{-12}	28
α_2 ($\epsilon/^\circ\text{F}$)	1.18×10^{-5}	1.35×10^{-8}	2.07×10^{-11}	29,30,31

ORIGINAL PAGE IS
OF POOR QUALITY

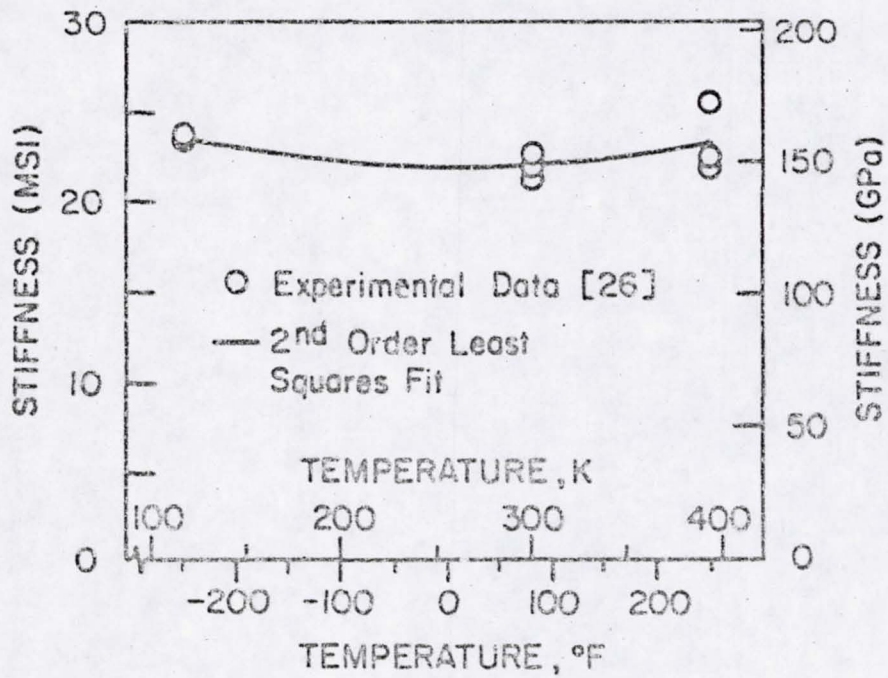


Fig. A.1. E_1 Temperature Dependence.

ORIGINAL PAGE IS
OF POOR QUALITY

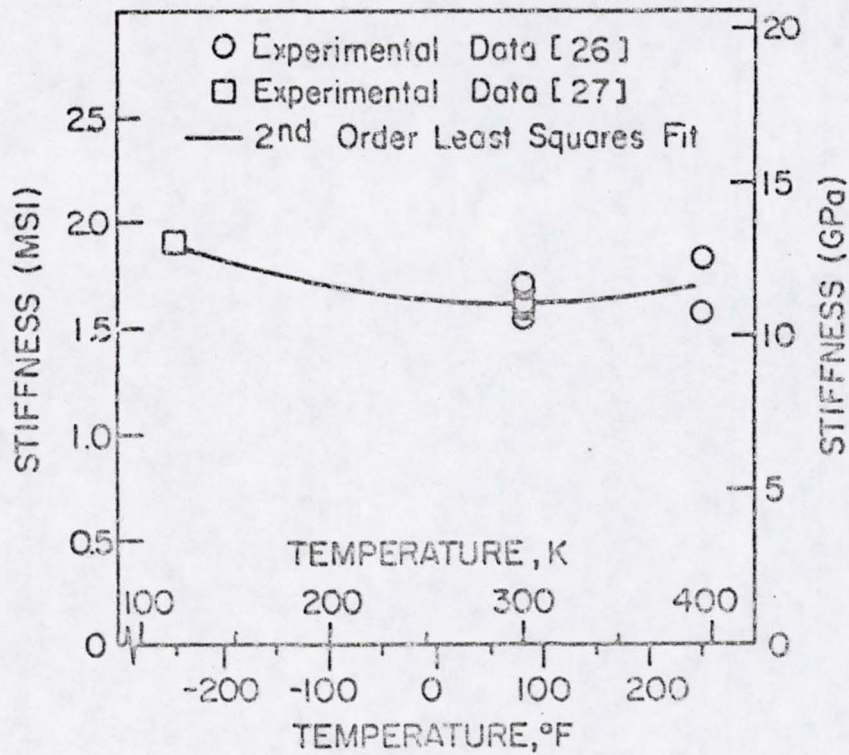
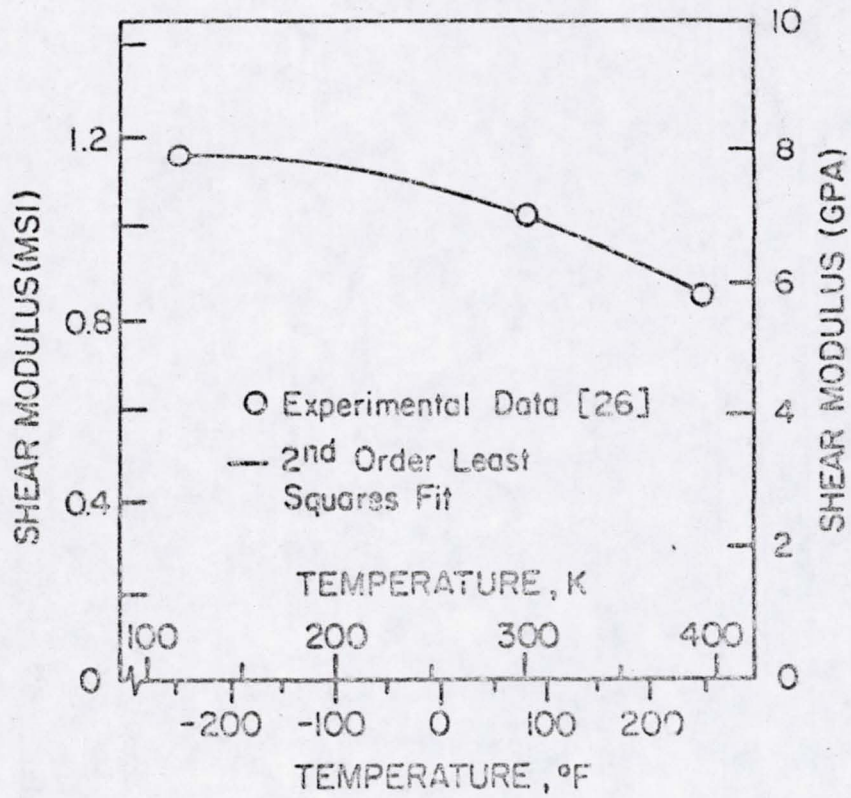
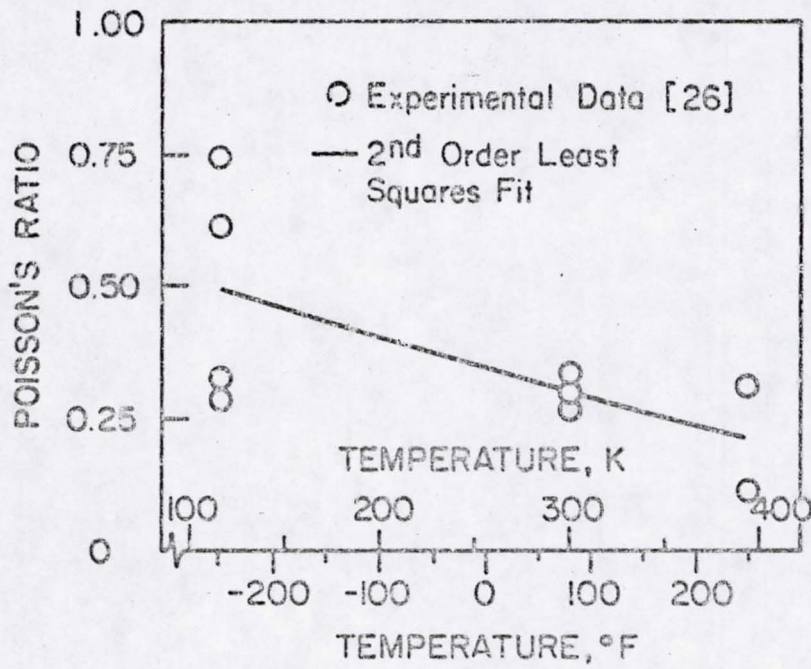


Fig. A.2. E_2 Temperature Dependence.

ORIGINAL PAGE IS
OF POOR QUALITYFig. A.3. G_{12} Temperature Dependence.

ORIGINAL PAGE IS
OF POOR QUALITYFig. A.4. ν_{12} Temperature Dependence.

ORIGINAL PAGE IS
OF POOR QUALITY

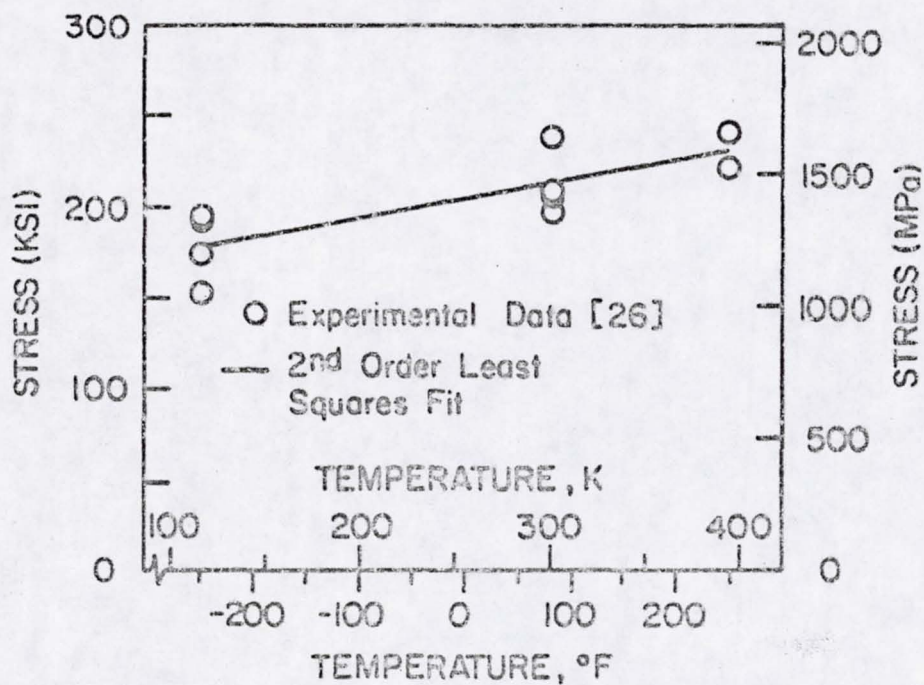


Fig. A.5. Axial Strength Temperature Dependence.

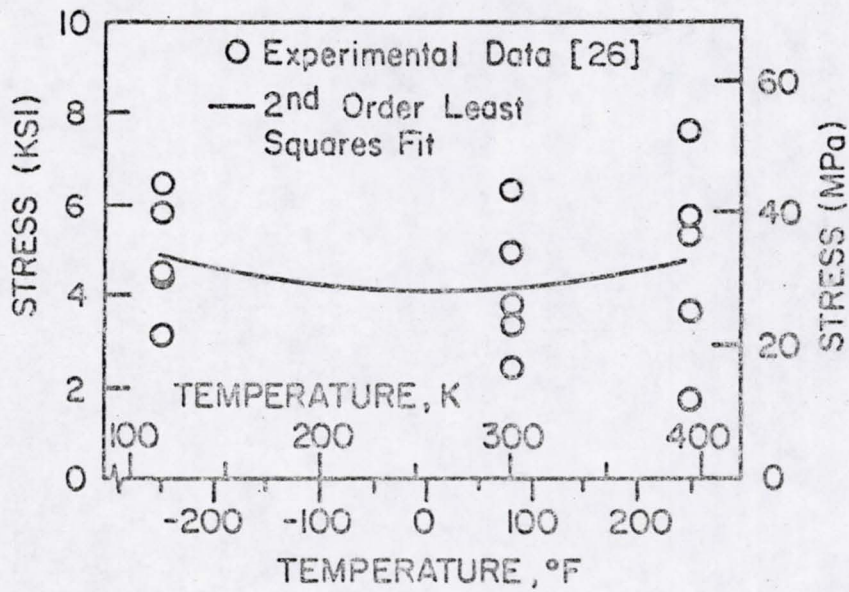


Fig. A.6. Transverse Strength Temperature Dependence.

ORIGINAL PAGE IS
OF POOR QUALITY

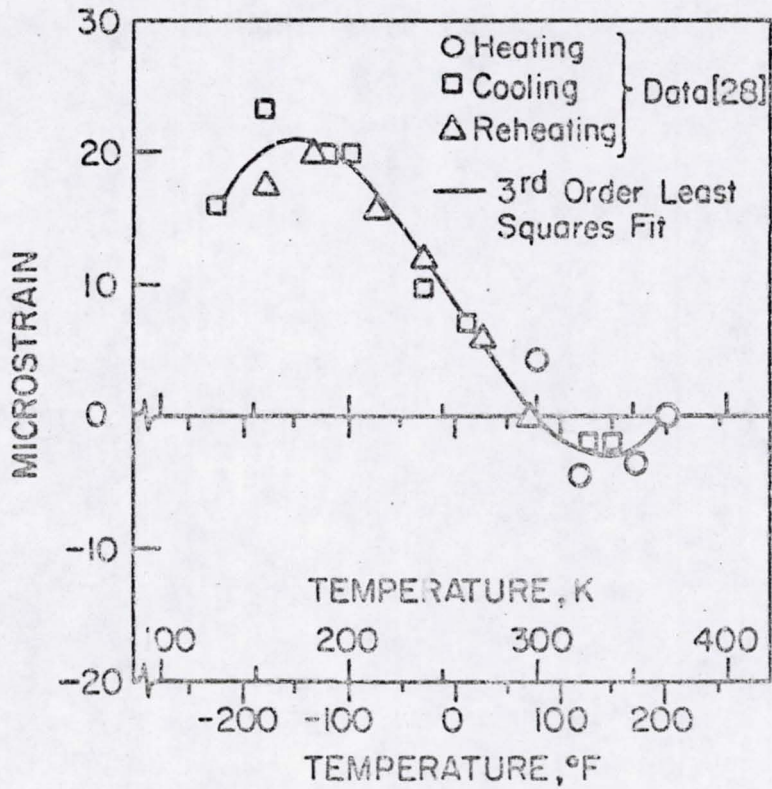


Fig. A.7. Axial Thermal Expansion Temperature Dependence.

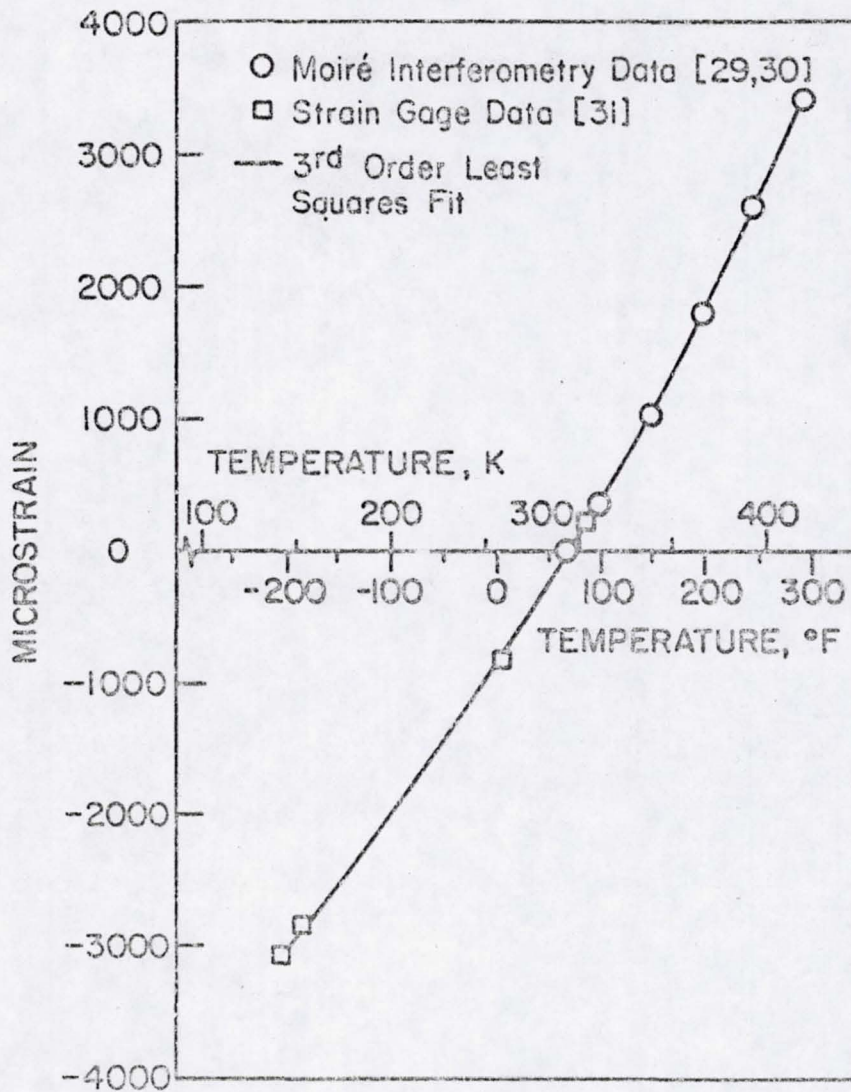
ORIGINAL PAGE IS
OF POOR QUALITY

Fig. A.8. Transverse Thermal Expansion Temperature Dependence.

APPENDIX B

Constrained Displacement Finite Element Solutions

The process of constraining displacements requires a technique of systematically modifying the global stiffness matrix and the global force vector of the finite element solution. Branca [40] and Crane and Adams [41] have illustrated the modifications required. However, it does not appear that a rigorous development of the procedure has been presented. Of particular interest is the question of a unique solution while permitting an arbitrary choice of the constrained node used in the solution. This appendix addresses this question in a rigorous manner by considering the variational formulation of the anisotropic, thermo-elastic, generalized plane strain finite element analysis.

The principle of virtual work may be written

$$\delta(U + V) = 0 \quad (\text{B.1})$$

where

$U \equiv$ stored strain energy

$V \equiv$ potential of applied loads

Equation (B.1) can be written

$$\delta\left[\frac{1}{2} \int_R (\sigma \cdot \bar{\epsilon}) dR - \sum_{i=1}^N Q_i q_i\right] \quad (\text{B.2})$$

where

$\bar{\epsilon} \equiv$ mechanical strain

$Q_i \equiv$ applied nodal forces

$q_i \equiv$ nodal displacements

$N \equiv$ number of nodes

$R \equiv$ region of interest.

Assuming superposition of thermal and mechanical strains, the strain-displacement relations in the material coordinate system for a temperature change ΔT are:

$$\begin{pmatrix} \epsilon_{xx} \\ \epsilon_{yy} \\ \epsilon_{zz} \\ \gamma_{yz} \\ \gamma_{xz} \\ \gamma_{xy} \end{pmatrix} = \begin{pmatrix} u_{,x} - \alpha_x \Delta T \\ v_{,y} - \alpha_y \Delta T \\ w_{,z} - \alpha_z \Delta T \\ v_{,z} + w_{,y} \\ u_{,z} + w_{,x} \\ u_{,y} + v_{,x} - \alpha_{xy} \Delta T \end{pmatrix} \quad (B.3)$$

Where $\alpha_x, \alpha_y, \alpha_{xy}, \alpha_z$ are the nonzero coefficients of thermal expansion of individual layers. Using elemental displacements of the form

$$u = \sum_{i=1}^N \phi_i(y,z) U_i + \epsilon_x x$$

$$v = \sum_{i=1}^N \phi_i(y,z) V_i$$

$$w = \sum_{i=1}^N \phi_i(y,z) W_i$$

where

$\phi_i(y,z) \equiv$ element shape functions

$U_i, V_i, W_i \equiv$ nodal displacements

ϵ_x \equiv total uniform x strain

N = number of nodes per element

The strain displacement relations become

$$\{\bar{\epsilon}\} = [B]\{q\} + \{\epsilon_0\} \quad (B.4)$$

where

[B] \equiv matrix of element shape function derivatives,

$$\{\epsilon_0\} = \left\{ \begin{array}{c} \epsilon_{xx} - \alpha_x \Delta T \\ -\alpha_y \Delta T \\ -\alpha_z \Delta T \\ 0 \\ 0 \\ -\alpha_{xy} \Delta T \end{array} \right\}$$

and it is assumed that lamina are in x-y planes. The constitutive relation in global coordinates can be written

$$\{\sigma\} = [\bar{C}]\{\bar{\epsilon}\} \quad (B.5)$$

combining (B.4) and (B.5),

$$\{\sigma\} = [\bar{C}][B]\{q\} + \{\bar{\sigma}_0\} \quad (B.6)$$

Substituting Eqns. (B.4) and (B.6) into Eqn. (B.2) yields

$$\delta \left[\frac{1}{2} \int_R ([B]\{q\} + \{\epsilon_0\})^T [C] ([B]\{q\} + \{\epsilon_0\}) dR - \{q\}^T \{Q\} \right] = 0 \quad (B.7)$$

At this point, we consider a one element example (Fig. B1). For this example, the quantity $[B]\{q\}$ may be written

$$[B]\{q\} = \begin{bmatrix} 0 & 0 & 0 & 0 & 0 & 0 & 0 & 0 & 0 \\ 0 & \psi_{1,y} & 0 & 0 & \psi_{2,y} & 0 & 0 & \psi_{3,y} & 0 \\ 0 & 0 & \psi_{1,z} & 0 & 0 & \psi_{2,z} & 0 & 0 & \psi_{3,z} \\ 0 & \psi_{1,z} & \psi_{1,y} & 0 & \psi_{2,z} & \psi_{2,y} & 0 & \psi_{3,z} & \psi_{3,y} \\ \psi_{1,z} & 0 & 0 & \psi_{2,z} & 0 & 0 & \psi_{3,z} & 0 & 0 \\ \psi_{1,y} & 0 & 0 & \psi_{2,y} & 0 & 0 & \psi_{3,y} & 0 & 0 \end{bmatrix} \begin{Bmatrix} U_1 \\ V_1 \\ W_1 \\ U_2 \\ V_2 \\ W_2 \\ U_3 \\ V_3 \\ W_3 \end{Bmatrix} \quad (B.8)$$

Next, the v displacements of nodes 2 and 3 are constrained ($V_2 = V_3$). Under this constraint, either V_2 or V_3 may be expressed in terms of the other displacement, reducing the number of independent displacements by one. A combination of terms is then possible in $[B]$ and $\{Q\}$. Selecting V_2 as the "master" displacement representing all constrained displacements yields

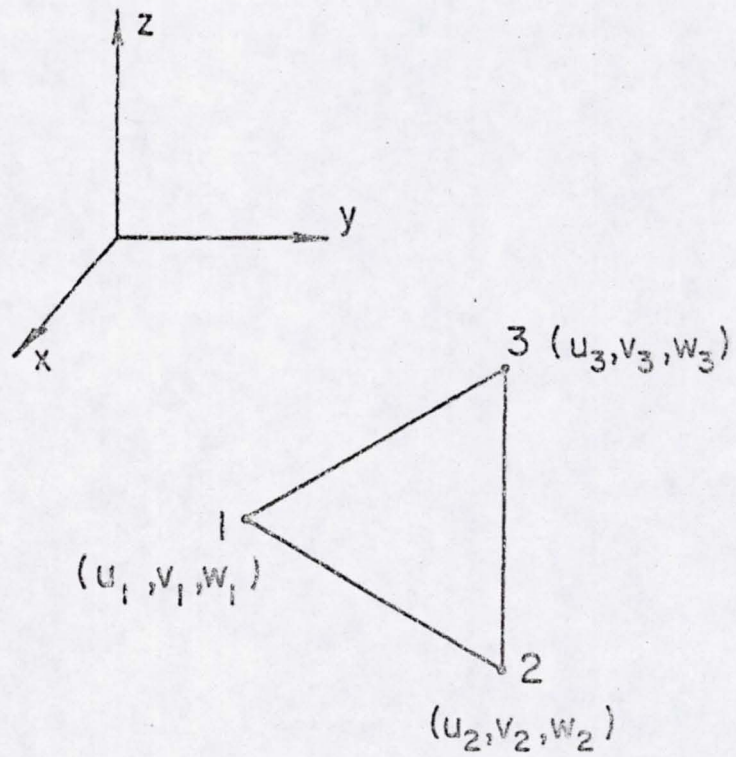
ORIGINAL PAGE IS
OF POOR QUALITY

Fig. B.1 One Element Finite Element Example.

$$[B^*][q^*] = \begin{bmatrix} 0 & 0 & 0 & 0 & 0 & 0 & 0 & 0 \\ 0 & \psi_{1,y} & 0 & 0 & (\psi_{2,y} + \psi_{3,y}) & 0 & 0 & 0 \\ 0 & 0 & \psi_{1,z} & 0 & 0 & \psi_{2,z} & 0 & \psi_{3,z} \\ 0 & \psi_{1,z} & \psi_{1,y} & 0 & (\psi_{2,z} + \psi_{3,z}) & \psi_{2,y} & 0 & \psi_{3,y} \\ \psi_{1,z} & 0 & 0 & \psi_{2,z} & 0 & 0 & \psi_{3,z} & 0 \\ \psi_{1,y} & 0 & 0 & \psi_{2,y} & 0 & 0 & \psi_{3,y} & 0 \end{bmatrix} \begin{Bmatrix} u_1 \\ v_1 \\ w_1 \\ u_2 \\ v_2 \\ w_2 \\ u_3 \\ w_3 \end{Bmatrix} \quad (B.9)$$

$$\text{and } \{Q^*\} = \begin{Bmatrix} Q_1 \\ Q_2 \\ Q_3 \\ Q_4 \\ Q_5 + Q_8 \\ Q_6 \\ Q_7 \\ Q_9 \end{Bmatrix}$$

With the constraint $V_2 = V_3$ imposed, we proceed to take the first variation of the modified equation (7)

$$\int_R [B^*]^T [\bar{C}] [B^*] dR \{q^*\} + \int_R [B^*]^T [\bar{C}] \{\epsilon_0\} dR - \{Q^*\} = 0 \quad (B.10)$$

The resulting set of equations has one less equation than before imposing the constraint. Assembling Eqn. (B.10) in a more conventional form

$$[K^*]\{q^*\} = \{F^*\}$$

where

$$[K^*] = \int_R [B^*]^T [\bar{C}] [B^*] dR$$

and

$$\{F^*\} = \{Q^*\} - \int_R [B^*]^T [\bar{C}] \{\epsilon_0\} dR \quad (B.11)$$

A comparison of the modified quantities $[K^*]$ and $\{F^*\}$ with the original quantities $[K]$ and $\{F\}$ suggests a series of systematic modifications, convenient to the existing computer code, to accommodate constrained displacements. Again, consider the one element example shown in Fig. B.1 with the V_2 and V_3 displacements constrained. Before applying the constraint, the governing finite element equations are of the form

$$\begin{bmatrix} K_{11} & K_{12} & K_{13} & K_{14} & K_{15} & K_{16} & K_{17} & K_{18} & K_{19} \\ K_{12} & K_{22} & K_{23} & K_{24} & K_{25} & K_{26} & K_{27} & K_{28} & K_{29} \\ K_{13} & K_{23} & K_{33} & K_{34} & K_{35} & K_{36} & K_{37} & K_{38} & K_{39} \\ K_{14} & K_{24} & K_{34} & K_{44} & K_{45} & K_{46} & K_{47} & K_{48} & K_{49} \\ K_{15} & K_{25} & K_{35} & K_{45} & K_{55} & K_{56} & K_{57} & K_{58} & K_{59} \\ K_{16} & K_{26} & K_{36} & K_{46} & K_{56} & K_{66} & K_{67} & K_{68} & K_{69} \\ K_{17} & K_{27} & K_{37} & K_{47} & K_{57} & K_{67} & K_{77} & K_{78} & K_{79} \\ K_{18} & K_{28} & K_{38} & K_{48} & K_{58} & K_{68} & K_{78} & K_{88} & K_{89} \\ K_{19} & K_{29} & K_{39} & K_{49} & K_{59} & K_{69} & K_{79} & K_{89} & K_{99} \end{bmatrix} \begin{Bmatrix} U_1 \\ V_1 \\ W_1 \\ U_2 \\ V_2 \\ W_2 \\ U_3 \\ V_3 \\ W_3 \end{Bmatrix} = \begin{Bmatrix} F_1 \\ F_2 \\ F_3 \\ F_4 \\ F_5 \\ F_6 \\ F_7 \\ F_8 \\ F_9 \end{Bmatrix} \quad (B.12)$$

When displacements V_2 and V_3 are constrained, the fifth and eighth columns of $[K]$ are added together term by term and the sum entered as either the fifth or eighth column, depending on which displacement is chosen as the master displacement. The other column is modified by placing zeros in all entries. Next, the fifth and eighth rows are added term by term and the sum placed as the fifth row. The eighth row is modified by placing a zero in all entries except a one on the main diagonal. Similarly in the force vector, the sum of the fifth and eighth entry is placed as the fifth entry and a zero is placed as the eighth entry. The final form appears as

$$\begin{bmatrix}
 K_{11} & K_{12} & K_{13} & K_{14} & (K_{15}+K_{18}) & K_{16} & K_{17} & 0 & K_{19} \\
 K_{12} & K_{22} & K_{23} & K_{24} & (K_{25}+K_{28}) & K_{26} & K_{27} & 0 & K_{29} \\
 K_{13} & K_{23} & K_{33} & K_{34} & (K_{35}+K_{38}) & K_{36} & K_{37} & 0 & K_{39} \\
 K_{14} & K_{24} & K_{34} & K_{44} & (K_{45}+K_{48}) & K_{46} & K_{47} & 0 & K_{49} \\
 (K_{15}+K_{18}) & (K_{25}+K_{28}) & (K_{35}+K_{38}) & (K_{45}+K_{48}) & (K_{55}+K_{58}+K_{58}+K_{88}) & (K_{56}+K_{68}) & (K_{57}+K_{78}) & 0 & (K_{59}+K_{89}) \\
 K_{16} & K_{26} & K_{36} & K_{46} & (K_{56}+K_{68}) & K_{66} & K_{67} & 0 & K_{69} \\
 K_{17} & K_{27} & K_{37} & K_{47} & (K_{57}+K_{78}) & K_{67} & K_{77} & 0 & K_{79} \\
 0 & 0 & 0 & 0 & 0 & 0 & 0 & 1 & 0 \\
 K_{19} & K_{29} & K_{39} & K_{49} & (K_{59}+K_{89}) & K_{69} & K_{79} & 0 & K_{99}
 \end{bmatrix}
 \begin{Bmatrix}
 U_1 \\
 V_1 \\
 W_1 \\
 U_2 \\
 V_2 \\
 W_2 \\
 U_3 \\
 V_3 \\
 W_3
 \end{Bmatrix}
 =
 \begin{Bmatrix}
 F_1 \\
 F_2 \\
 F_3 \\
 F_4 \\
 F_5+F_8 \\
 F_6 \\
 F_7 \\
 0 \\
 F_9
 \end{Bmatrix}$$

or

$$[K^*]\{U^*\} = \{F^*\} \quad (B.13)$$

Displacement V_3 may have been chosen as the master displacement in which case the combining of terms would have occurred in row and column eight. The solutions obtained when using different master displacements

are identical, making the choice arbitrary. Since the modified stiffness matrix, $[K^*]$ in Eqn. (B.13) remains symmetric, the solution procedure is unaffected. Although not evident in the one element example considered, the modifications made in the stiffness matrix $[K]$ may produce a greater bandwidth in $[K^*]$, requiring that the bandwidth be recomputed after such modifications. For multiple element cases, the modifications may be made on the assembled global stiffness matrix rather than modifying the affected element matrices separately.

APPENDIX C

Composite Laminate Finite Element-Two-Dimensional-Constrained Displacements (CLFE2DC)

Input Data Sequence

<u>Cards 1 & 2 (20A4)</u>		<u>Title Cards</u>
<u>Column</u>		<u>Contents</u>
1-80	Title	
<u>Card 3 (16I5)</u>		<u>Master Control Card</u>
<u>Column</u>		<u>Contents</u>
1-5	NEM	Number of Elements
6-10	NODS	Number of Node Points
11-16	NPE	Number of Nodes Per Element
	= 4 4 Node	Linear Elements
	= 8 8 Node	Serendipity Elements
	= 9 9 Node	Lagrangian Elements
16-20	NANG	Number of Different Angles
21-25	NSDF	Number of Specified Nodal Displacements
26-30	NSBF	Number of Specified Nodal Forces
31-35	NCON	Number of Constrained Displacements
36-40	NPLOT	Plot Option
	= 0	none
	= 1	undeformed plot only
	= 2	deformed plot only
	= 3	both undeformed and deformed
41-45	NT1	Dump file for displacements
	= 0	no dump
	≠ 0	dumps displacements to unit NT1
46-50	NT2	Dump file for strains, stresses, and strain energies
	= 0	no dump
	≠ 0	dumps to unit NT2
51-55	NCHECK	Data Check Option (NE. 0 - Data Check Only)
<u>Card 4 (8D10.5)</u>		<u>Scale Factors</u>
<u>Column</u>		<u>Contents</u>
1-10	SCAY	Y-Nodal Coordinate Scale Factor
11-20	SCAZ	Z-Nodal Coordinate Scale Factor
<u>Card 5 (16I5)</u>		<u>Printer Control Card</u>
<u>Column</u>		<u>Contents</u>
1-5	KEY(1)	Key for Printing Element Data
6-10	KEY(2)	Key for Printing Nodal Data

11-15	KEY(3)	Key for Printing Specified Nodal Displacements
16-20	KEY(4)	Key for Printing Specified Nodal Forces
21-25	KEY(5)	Key for Printing Displacements
26-30	KEY(6)	Key for Printing Strains, Stresses and Strain Energies Per Unit Volume

(If KEY(1) .NE. 0 - Print)

If NPLOT .EQ. 0 skip Card 6 and go to Card 7

<u>Card 6</u>	(8E10.5)	Plotter Control Card
	<u>Column</u>	<u>Contents</u>
	1-10	PYSCL Plot Y-Scale Factor
	11-20	PZSCL Plot Z-Scale Factor
	21-30	VMAX Maximum Allowable V-Displacement
	31-40	WMAX Maximum Allowable W-Displacement

<u>Card 7</u>	(3(6X, D14.7))	E ₁₁ Material Property Card
	<u>Column</u>	<u>Contents</u>
	7-20	Constant term, A
	27-40	Linear term, B
	47-60	Quadratic term, C

$$E_{11} = A + BT + CT^2$$

<u>Card 8</u>	(3(6X, D14.7))	E ₂₂ Material Property Card
<u>Card 9</u>	(3(6X, D14.7))	E ₃₃ Material Property Card
<u>Card 10</u>	(3(6X, D14.7))	G ₂₃ Material Property Card
<u>Card 11</u>	(3(6X, D14.7))	G ₁₃ Material Property Card
<u>Card 12</u>	(3(6X, D14.7))	G ₁₂ Material Property Card
<u>Card 13</u>	(3(6X, D14.7))	NU ₂₃ Material Property Card
<u>Card 14</u>	(3(6X, D14.7))	NU ₁₃ Material Property Card
<u>Card 15</u>	(3(6X, D14.7))	NU ₁₂ Material Property Card
<u>Card 16</u>	(3(6X, D14.7))	Alpha 11 Material Property Card
<u>Card 17</u>	(3(6X, D14.7))	Alpha 22 Material Property Card
<u>Card 18</u>	(3(6X, D14.7))	Alpha 33 Material Property Card
<u>Card 19</u>	(8D10.5)	Angle Data Card
	<u>Column</u>	<u>Contents</u>
	1-10	Ang(1) Angle No. 1 (In Degrees)

11-15	Ang(2)	Angle No. 2 (in Degrees)
.	.	.
.	.	.
.	.	.
.	Ang(NANG)	Angle No. NANG (in Degrees)

Card 20 (5X,1515)		Element Data Card(s)
Column		Contents
1-5	Blank	(Can Put Element Numbers in for Reference)
6-10	IANG(N)	Angle Number of Element N
11-15	NOD(N,1)	Node #1 of Element N
16-20	NOD(N,2)	Node #2 of Element N
21-25	NOD(N,3)	Node #3 of Element N
26-30	NOD(N,4)	Node #4 of Element N
		(continue through NOD(N,NPE) for NPE > 4.)
31-35	ISTRS(N,1)	Stress and Strain Output Code for Element N.
		= 0 - None
		= 1 - Side 1
		= 2 - Side 2
		= 3 - Side 3
		= 4 - Side 4
		= 5 - Center
		= 6 - "Node 1"
		= 7 - "Node 2"
		= 8 - "Node 3"
		= 9 - "Node 4"

36-40	ISTRS(N,2)
41-45	ISTRS(N,3)

.

.

.

71-75	ISTRS(N,9)
-------	------------

*Repeat Card 20 NEM Times

Card 21 (5X,2D10.5)		Nodal Data Card(s)
Column		Contents
1-5	Blank	(Can Put Node Numbers in for Reference)
6-15	Y(N)	Y-Coordinate of Node N
16-25	Z(N)	Z-Coordinate of Node N

*Repeat Card 21 NODS Times #

*If NSDF .EQ. 0 - Skip Card 22 and Go on to Card 23

Card 22 (2I5,D10.5)		Specified Nodal Degree of Freedom Card(s)
Column		Contents
1-5	ND	Node Number of Specified D.O.F.
6-10	IDR	Direction of Specified D.O.F.
		(1 = u, 2 = v, and 3 = w)

11-20 VBDF(N) Specified Displacement Value

*Repeat Card 22 NSDF Times

* If NSBF .EQ. 0 - Skip Card 23 and Go on to Card 24

Card 23 (215,D10.5)		Specified Modal Force Card(s)
Column		Contents
1-5	ND	Node Number of Specified Force
6-10	IDR	Direction of Specified Force (1 = u, 2 = v, 3 = w)
11-20	VBSF(N)	Specified Boundary Force Value

*Repeat Card 23 NSBF Times

*If NCON .EQ. 0 - Skip Card 24 and Go on to Card 25

Card 24 (215) Specified Constrained Displacement Card(s)		Contents
Column		Contents
1-5	ND	Node Number of Specified Constrained Displacement
6-10	IDR	Direction of Specified Constrained Displacement (1 = u, 2 = v, and 3 = w)

*Repeat Card 24 NCON Times

Card 25 (3(6X,D14.7))		Normal Strain and Temperature Load Card
Column		Contents
7-20	EPSX	Applied Normal, (X-Direction), Strain
27-40	TFREI	Stress Free Temperature
47-60	TEMP	Analysis Temperature

-End-

END

DATE

FILMED

DEC 12 1983